OUKA
The University of Osaka
Institutional Knowledge Archive

Title	High-Density GaAs/(GaAs)m(AlAs)n Quantum Wires Grown on (775) B-Oriented GaAs Substrates by Molecular Beam Epitaxy
Author(s)	Higashiwaki, Masataka
Citation	大阪大学, 1998, 博士論文
Version Type	VoR
URL	https://doi.org/10.11501/3144057
rights	
Note	

The University of Osaka Institutional Knowledge Archive : OUKA

https://ir.library.osaka-u.ac.jp/

The University of Osaka



Thesis

High-Density GaAs/$(GaAs)_m(AlAs)_n$ Quantum Wires Grown on (775)B-Oriented GaAs Substrates by Molecular Beam Epitaxy

Masataka Higashiwaki

OSAKA UNIVERSITY

Graduate School of Engineering Science

Department of Physical Science

Toyonaka Osaka

January 1998

Thesis

High-Density GaAs/$(GaAs)_m(AlAs)_n$ Quantum Wires Grown on (775)B-Oriented GaAs Substrates by Molecular Beam Epitaxy

Masataka Higashiwaki

OSAKA UNIVERSITY

Graduate School of Engineering Science

Department of Physical Science

Toyonaka Osaka

January 1998

ABSTRACT

High-density and highly uniform GaAs corrugation naturally formed on a (775)B-oriented GaAs surface grown at a substrate temperature (T_s) of 670°C by molecular beam epitaxy (MBE) was found by atomic force microscope (AFM) observation. The lateral period and vertical amplitude of the GaAs corrugation were decided precisely to be 12 nm and 1.2 nm by cross-sectional transmission electron microscopy observation, respectively, and it was found that extremely high-density quantum wires (QWRs) (8×10^5 QWRs/cm^{-1}) were realized due to the lateral confinement effect of carriers by well width modulation in a quantum well (QW) with a corrugated AlAs-on-GaAs upper interface and a flat GaAs-on-AlAs lower interface grown on the (775)B GaAs substrate. The (775)B GaAs surface is flat for $T_s \leq 580$°C and is corrugated for $T_s \geq 640$°C in contrast with the flat surface observed for AlAs layers grown for T_s=540–700°C. Moreover, it was confirmed that the (775)B GaAs substrate is most suitable for fabrication of QWR structures by AFM and photoluminescence (PL) measurements.

Using the GaAs corrugation, GaAs/AlAs, GaAs/$(GaAs)_2(AlAs)_2$ and GaAs/$(GaAs)_4(AlAs)_2$ QWRs were grown on (775)B GaAs substrates. The PL peak from the GaAs/$(GaAs)_4(AlAs)_2$ QWRs at 14 K showed large polarization anisotropy [$P = (I_{\parallel} - I_{\perp})/(I_{\parallel} + I_{\perp}) = 0.19$]. FWHM of the PL peak was as small as 15 meV at λ=692 nm, which is the smallest ever observed for self-organized GaAs/AlGaAs QWRs. Uniformity of the GaAs/$(GaAs)_4(AlAs)_2$ QWRs was comparable to the best uniformity for GaAs/AlGaAs QWRs achieved in GaAs/AlGaAs V-groove QWRs, GaAs/AlGaAs T-QWRs and GaAs/AlGaAs tilted T-QWRs fabricated with the most precise controllability and high uniformity of MBE and metalorganic chemical vapor deposition. The PL intensity from the GaAs/$(GaAs)_4(AlAs)_2$ QWRs was almost as large as that from a GaAs/$(GaAs)_4(AlAs)_2$ QW grown on a (100) GaAs substrate simultaneously. Furthermore, the one-dimensionality of the GaAs/$(GaAs)_4(AlAs)_2$ QWRs was confirmed not only by the PL polarization dependence but also by temperature dependences of PL FWHM, PL intensity and PL decay time. These results indicate that the GaAs/$(GaAs)_4(AlAs)_2$ QWRs on the (775)B GaAs substrate meet all requirements for application to QWR lasers, i.e., high one-dimensionality, high density, high uniformity, high crystal quality, high reproducibility and easy device fabrication.

Finally, GaAs/$(GaAs)_4(AlAs)_2$ GRIN-SCH QWR lasers were grown on (775)B GaAs substrates, and stripe-geometry lasers were fabricated. The (775)B QWR lasers oscillated at room temperature (RT) under a condition of pulsed current, and this is the first time for self-organized QWRs to oscillate at RT. The threshold currents of the (775)B QWR lasers were smaller than those of simultaneously grown (100) QW lasers. The threshold current density of the QWR laser on the (775)B GaAs substrate was as low as 2.8 kA/cm^2, which is a good result for QWR lasers next to the V-groove QWR laser.

Contents

Table of Contents 1

1 Introduction 5

1.1 Introduction 5

1.2 (775)B-oriented surface 9

1.3 This work 10

2 Experimental Equipments 13

2.1 Molecular beam epitaxy : MBE 13

2.1.1 MBE 13

2.1.2 Substrate preparation before MBE growth 14

2.2 Measurements 16

2.2.1 Atomic force microscopy : AFM 16

2.2.2 Transmission electron microscopy : TEM 17

2.2.3 Photoluminescence : PL 19

3 GaAs/AlAs Quantum Wires 21

3.1 Structural estimation of GaAs corrugation 21

3.1.1 Surface AFM observation 21

3.1.2 Cross-sectional TEM observation 23

3.2 PL properties 26

3.3 Summary 31

4 Growth Modes of GaAs and AlAs on (775)B GaAs Substrate 33

4.1 AFM observation of GaAs surfaces 33
4.2 TEM observation of $GaAs/(GaAs)_5(AlAs)_5$ QWRs structure 39
4.3 Summary 42

5 $GaAs/(GaAs)_2(AlAs)_2$ Quantum Wires **43**
5.1 Sample structure 43
5.2 PL properties 47
5.3 Theoretical analysis 51
5.4 Summary 55

6 $GaAs/(GaAs)_4(AlAs)_2$ Quantum Wires **57**
6.1 Sample structure 57
6.2 PL properties at low temperature 60
6.3 Temperature dependence of PL properties 66
6.4 Temperature dependence of exciton lifetime 71
6.5 Summary 78

7 Growth Mode of GaAs on High-Index GaAs Substrates around (775)B Plane **81**
7.1 Surface AFM observation 81
7.2 PL properties 85
7.3 Summary 89

8 $GaAs/(GaAs)_4(AlAs)_2$ Quantum Wire Laser **91**
8.1 Si and Be doping properties 91
8.2 Sample structure 96
8.3 PL properties 98
8.4 Device process 101
8.5 Laser characteristics 104
8.6 Summary 110

9 Conclusions **111**

Acknowledgment **115**

References **117**

Publication list **123**

A Detection of size fluctuation from PL linewidth **127**

B Polarization of luminescence from QWR **129**

Chapter 1

Introduction

1.1 Introduction

Recently, a main material of semiconductor devices is Si, however, III-V compound semiconductors have been widely investigated because of their suitable physical properties for high speed electronics transistors and optical devices. GaAs, which is the main material used in this study, shows good properties as follows.

1. GaAs has the direct band gap and thus can be applied to light emitting devices, which cannot be made by Si.

2. Electron mobility in GaAs is about six times larger than that in Si at room temperature.

The advance of crystal growth techniques of semiconductor, such as molecular beam epitaxy (MBE) and metalorganic chemical vapor deposition (MOCVD), enabled us to fabricate heterostructures in the atomic scale. As a result, various kinds of devices have been developed with III-V compound semiconductors, e.g., high electron mobility transistor (HEMT)[1,2], resonant tunneling diode (RTD)[3,4], quantum well (QW) laser[5–7]. Recently, modulated semiconductor devices are widely used in all over the world, and satellite broadcasting, portable phones and optical communication turn to be common with the use of HEMTs and QW lasers. In future, modulated semiconductor devices with much

higher performance must be needed, and thus, developments of these devices are making progress now.

In this decade, more advanced quantum structures, such as quantum wire (QWR) and quantum dot (QD), have attracted because of their superior optical and electrical properties[8–14]. In case of a QWR (QD), carriers are confined in the region less than *de Brogie* wavelength of electron in two directions (in three directions), i.e., the carriers are quantized in a wire-like structure (in a dot-like structure). Hence, QWR and QD correspond to the one-dimensional (1D) and the zero-dimensional (0D) systems, respectively. As a result, their density of states (DOS) become sharper than that of the two-dimensional (2D) system in a QW as shown in Fig. 1.1. Novel optical properties, such as a narrower gain spectrum, a higher differential gain[13], an increased binding energy of exciton[15,16] and an enhanced optical nonlinearity[17] are expected theoretically for QWRs, which lead to superior performances of QWR lasers as follows.

1. Reduced temperature sensitivity of threshold current[9]

   Temperature dependence of threshold current of semiconductor lasers is ascribed to thermal spreading of injected carriers over a wide energy range of states. In case of a QWR laser, however, the temperature effect is suppressed since DOS of the QWR has a sharp peak structure and is a decreasing function as increasing temperature.

2. Modulation bandwidth[10,12]

   Higher DOS at the QWR subbands results in a larger peak gain compared to QW for the same carrier concentration, with a corresponding increase in the differential gain dg/dN. The limit to the direct modulation bandwidth of semiconductor laser is set by the relaxation oscillation frequency f_r, which is given by $f_r = \frac{1}{2\pi}[(dg/dN)P_0\tau_{ph}^{-1}]^{1/2}$, where P_0 is the photon density in the cavity of laser and τ_{ph} is the photon lifetime in the cavity[18]. Hence, the larger differential gain due to the sharp 1D DOS leads to the increase of modulation bandwidth of the QWR laser.

3. Low threshold current[14]

   Compared with a QW laser, a larger part of carriers confined in a QWR laser

contributes to lasing due to its sharp 1D DOS, which leads to low threshold current (in the μA range).

Such improved device characteristics would make QWR lasers useful in various optoelectronic applications involving integration of lasers with low power electronics or high-density laser arrays, e.g., optical computer interconnects, image processing and optical computing.

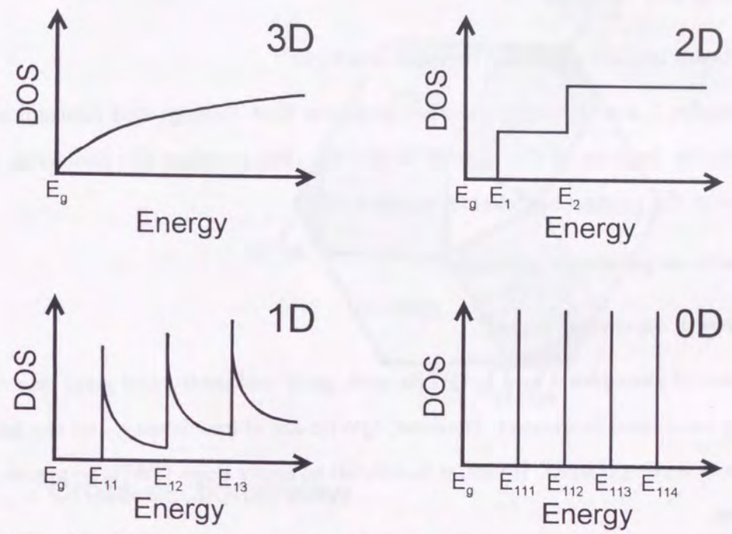

Figure 1.1: Density of states of n-dimensional systems (n: integer, 0–3).

The realization of useful QWR lasers, however, requires the development of QWR heterostructures meeting several constraints[19]. Such heterostructures should not only exhibit well resolved quasi-1D subbands, but also should be compatible with high optical gain, efficient charge carrier injection and low-loss optical cavity design in order to yield the expected improvements in laser performance. Well resolved quasi-1D subband structure is accomplished if the energy level broadening in a QWR due to size fluctuation is much smaller than its subband separation ΔE. In addition, $\Delta E \geq k_B T$ is necessary in order to minimize thermal population of higher order subbands (k_B: Boltzman constant, T: temperature). Defect-free QWR structures are also required to maintain long carrier

lifetimes and high quantum efficiency for high optical gain. Moreover, efficient capture of the injected carriers into a QWR active region followed by fast relaxation into the ground states is important to attain threshold at sufficiently low injection current levels. Furthermore, high-density QWRs, tight optical waveguides and low-loss optical cavities are required for increasing the optical mode gain and for reducing the threshold gain.

Up to today, a lot of studies have been reported about the fabrication of QWRs and their properties, and typical studies and their problems are as follows.

1. Etching and regrowth[20]

2. Ion-beam implantation and thermal treatment[21]

   Examples 1 and 2 have conclusive problems that damage and contamination are inevitable because of the process in the air. For avoiding the problems, methods without the process in the air are contrived.

3. Growth on patterned substrates[22-27]

4. Regrowth on cleaved edges[28]

   In case of examples 3 and 4, QWRs with good uniformity and good size controllability have been fabricated. However, QWRs are of low density, and the fabrication process is complicated. Hence, it is difficult to apply these QWRs to practical QWR lasers.

5. Natural formation using particular crystal growth modes

   - Fractional superlattice and Serpentine superlattice[29,30]
   - Self-organized multi-atomic steps on vicinal and high-index surfaces[31-33]

   Example 5 is considered to be the closest to practical device applications since high-density QWRs can be obtained without complicated process. Most QWRs in this technique, however, are lack of uniformity at the present stage.

GaAs QWRs grown on (775)B-oriented GaAs substrates are classified into example 5, however, the (775)B QWRs have superior properties compared with other QWRs, particularly at the point of density and uniformity.

1.2 (775)B-oriented surface

Figure 1.2 shows a schematic illustration of crystal orientation of a (775)B GaAs surface. The (775)B plane is oriented 8.5°-off from a (111)B surface toward a (110) surface. Incidentally, "A" signifies the surface terminated by Ga, and "B" corresponds to the surface terminated by As.

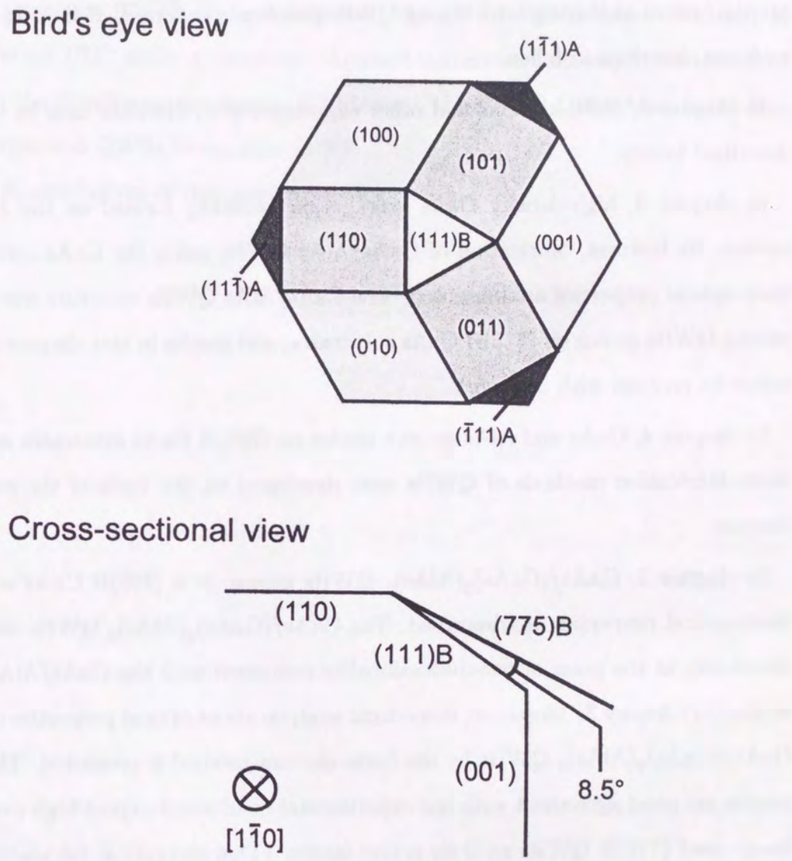

Figure 1.2: Schematic illustration of crystal orientation of a (775)B surface and around a (111)B surface.

1.3 This work

In this thesis, GaAs QWRs using self-organized corrugation on (775)B GaAs surfaces are described. These QWRs are naturally formed in a thin GaAs/$(GaAs)_m(AlAs)_n$ QW with a corrugated AlAs-on-GaAs interface and a flat GaAs-on-AlAs interface and show high potential for application to QWR lasers. The self-organized (775)B QWRs were found in this study for the first time. Especially, density and size uniformity of the (775)B QWRs are the best or at the top level among QWRs previously reported. Following this chapter, each one describes as follows.

In chapter 2, MBE systems and other experimental equipments used in this work are described briefly.

In chapter 3, high-density GaAs corrugation naturally formed on the (775)B GaAs surface, its features, fabrication of GaAs/AlAs QWRs using the GaAs corrugation and their optical properties are presented. The GaAs/AlAs QWRs structure was the first one among QWRs grown on (775)B GaAs substrates, and results in this chapter made up our minds to proceed with this work.

In chapter 4, GaAs and AlAs growth modes on (775)B GaAs substrates are described. Some fabrication methods of QWRs were developed on the basis of the results in this chapter.

In chapter 5, GaAs/$(GaAs)_2(AlAs)_2$ QWRs grown on a (775)B GaAs substrate and their optical properties are described. The GaAs/$(GaAs)_2(AlAs)_2$ QWRs were improved drastically at the point of one-dimensionality compared with the GaAs/AlAs QWRs described in Chapter 3. Moreover, theoretical analysis about optical properties of the (775)B GaAs/$(GaAs)_2(AlAs)_2$ QWRs by the finite element method is presented. The calculated results are good agreement with the experimental results and expect high performance of lasers used (775)B QWRs as their active layers. (This theoretical calculation was done by Assoc. Prof. M. Ogawa in Kobe University, not by the author.)

In chapter 6, GaAs/$(GaAs)_4(AlAs)_2$ QWRs grown on a (775)B GaAs substrate and their various photoluminescence (PL) properties are described. The GaAs/$(GaAs)_4(AlAs)_2$ QWRs have extremely high uniformity which is the top level in all QWRs reported and

meet all requirements for application to QWR lasers, i.e., high uniformity, high density, high optical quality and simple fabrication process.

In chapter 7, growth modes of GaAs layers and optical properties of GaAs/$(GaAs)_4(AlAs)_2$ QWs (QWRs) on misoriented (111)B GaAs substrates are presented. The results indicate that (775)B GaAs substrates are most suitable for fabrication of QWRs at the point of uniformity.

In chapter 8, it is described about stripe-geometry GaAs/$(GaAs)_4(AlAs)_2$ GRIN-SCH QWR lasers grown on (775)B GaAs substrates. The (775)B QWR lasers oscillated at room temperature (RT) under a condition of pulsed current and showed lower threshold currents than the simultaneously grown (100) lasers. The (775)B QWR laser is the first one for self-organized QWRs to oscillate at RT.

In chapter 9, conclusions of this work are given.

Chapter 2

Experimental Equipments

In this chapter, experimental equipments and techniques used in this study are described.

2.1 Molecular beam epitaxy : MBE

2.1.1 MBE

MBE is one of crystal growth methods in ultra high vacuum. Growth procedure is very simple as follows. Solid sources for crystal growth, such as Ga, Al, In, As and dopants, are heated in effusion cells and evaporate. The crystal growth occurs by irradiating the evaporated molecular beams to a clean and heated surface of a substrate. Thickness of the growth film is determined by the growth time, and the growth time is controlled by mechanical shutters.

Figure 2.1 shows (a) a photograph and (b) a schematic illustration in a growth chamber of Nissin RB-2001G MBE system, which was the main machine used in this work. This MBE system consists of two chambers (a growth chamber and a load-lock chamber) and pumping systems. The growth chamber of the MBE system is always evacuated by an ion getter pump (ANELVA PIC-400IP) and a Ti sublimation pump, even during MBE growth, and is equipped with a liquid nitrogen shroud. The pressure in the growth chamber is kept below 1×10^{-10} Torr. Group III and V fluxes are measured by a beam flux monitor with a nude ion gauge at the growth position. Growth temperature is monitored with an

optical pyrometer, and the temperature is collected by melting points of Al (660°C) and InSb (525°C). Reflection high-energy electron diffraction (RHEED) and quadrupole mass spectrometer (QMS; ANELVA AQA-360) are equipped in the growth chamber and used for *in situ* monitoring.

Another MBE system was also used in this study (VG80-H). This MBE system was only used for the growth of GRIN-SCH lasers in Chapter 8. The VG80-H MBE system is almost the same as the Nissin RB-2001G except having three chambers, which are an entry chamber, a preparation chamber and a growth chamber, respectively.

2.1.2 Substrate preparation before MBE growth

GaAs substrates used in this study were prepared before MBE growth as follows.

1. Degreasing
   (a) Cleaving a GaAs substrate for MBE growth into a proper size.
   (b) Degreasing the substrate with boiled trichloroethylene for 3 min (3 times).
   (c) Cleaning the substrate with methanol in an ultrasonic bath for 3 min (3 times).
   (d) Rinsing the substrate with distilled water (10 times).
2. Clean etching
   (a) Putting the substrate in a solution of H_2SO_4:H_2O = 5:2.
   (b) Etching the substrate using a sulfuric acid etchant (H_2SO_4:H_2O_2:H_2O = 5:1:1) kept at a temperature of about 100°C for 1 min.
   (c) Rinsing the substrate with distilled water (10 times).
   (d) Blowing water on a surface of the substrate with N_2 gas.
   (e) Baking the substrate at a temperature of 200°C on a hot plate for 1–2 hours.

Then, the GaAs substrate was mounted on a Mo holder by indium, and it was degassed in the Load-lock chamber at 350°C for 30 minutes. Finally, the substrate was thermally cleaned at a substrate temperature of 650°C for 15 minutes in As_4 atmosphere (10^{-6} Torr) just before MBE growth in the growth chamber.

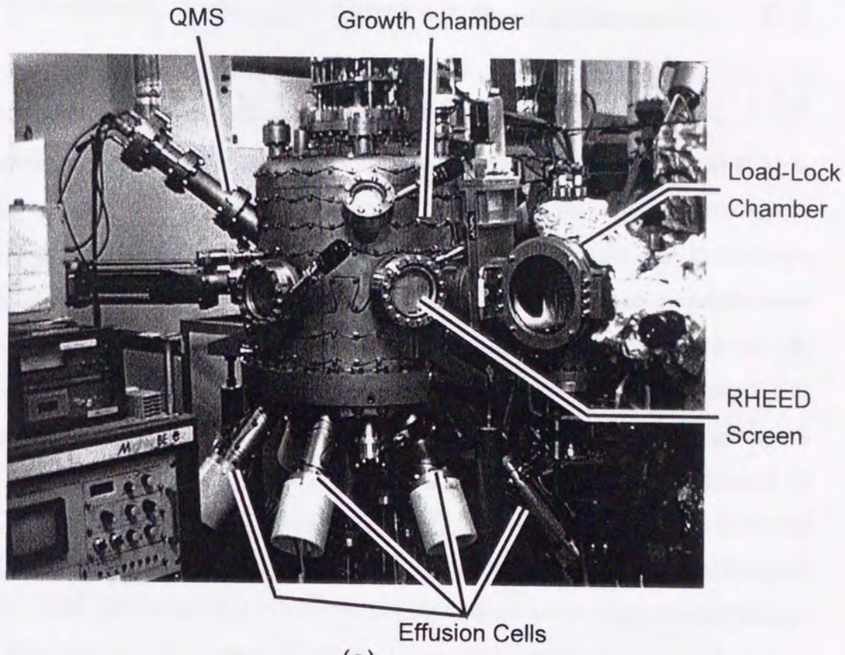

Figure 2.1: (a) Photograph of Nissin RB-2001G MBE system. (b) Schematic illustration in the MBE growth chamber.

2.2 Measurements

2.2.1 Atomic force microscopy : AFM

AFM is a very useful instrument to observe a surface of semiconductor film with an error of less than one atomic layer. This is the method that a cantilever is kept close to a sample surface and a three-dimensional picture of the sample surface is described by measuring *van der Waals* force and/or repulsive force between the sample surface and the cantilever. Figure 2.2 shows a schematic illustration of an AFM instrument used in this study (Digital instruments Nanoscope III), and AFM measurements were done with a tapping mode. The tapping-mode means a method that measures the repulsive force by touching at the sample surface softly with a vibrating cantilever. The vibration of cantilever which shows Z-axis is measured by detecting a reflected laser beam at the back of cantilever with a photo-detector. X-axis and Y-axis are also controlled by scanning on the sample surface.

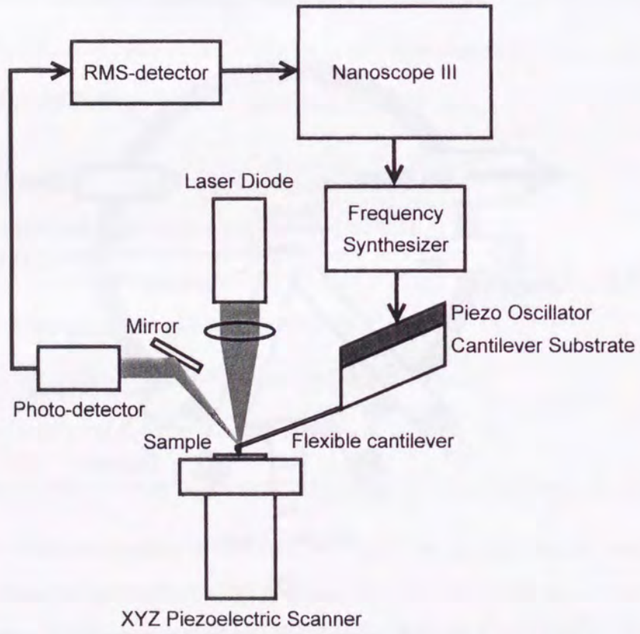

Figure 2.2: Schematic illustration of AFM system (Digital Instrument Nanoscope III).

2.2.2 Transmission electron microscopy : TEM

TEM is one of electron microscopes, which has the highest resolving power now. The mechanism is as follows. First, electron beam with the power of several kV is irradiated into a thinned sample. A large part of the electron beam passes through the sample, however, a small part of the beam is scattered by atoms elastically and inelastically. In these scattering, interference between inelastical scattered electrons is reduced due to the gap of wavelength, as a result, there is no contribution to lattice image. On the other hand, new spherical waves by elastical collision interfere in the sample. As a result, the spherical waves follow the law of Bragg, which is obtained as

$$d \sin\theta = n\lambda \ ,$$

where d is the interval between crystal planes, θ is the angle between crystal planes and the reflected wave, n is the integral number and λ is the wavelength of the electron beam, respectively. TEM observation is a work that we select one or some of the Bragg reflected waves and focus them on the screen. There are three typical methods as follows.

1. **Bright-field image:** This is the method that transmitted waves through a sample directly are focused on a screen. Regular parts in the sample turn to be bright, and irregular parts by absorption or scattering of electronic waves turn to be dark as shown in Fig. 2.3 (a).

2. **Dark-field image:** This is the method that one of diffracted waves which are Bragg-reflected by a specific crystal plane is selected and focused on the screen. As its name, bright parts in the bright-field image turn to be dark, and dark parts are observed bright in opposite as shown in Fig. 2.3 (b).

3. **Lattice image:** This is the method that a precise structure of a sample is able to be observed in the atomic scale. Electrons which are Bragg-reflected at each crystal plane in the sample are focused at the point behind an objective lens as shown in Fig. 2.3 (c). Gathering of intersections between diffracted waves and the focused surface corresponds to the diffracted image of electrons. This diffracted electron image is the Fourier transformed image of the crystal lattice in the incident

direction of electrons. In case that the electron waves go ahead still more, they interfere each other because of overlaps of their paths, as a result, a new interfered image appears by each diffracted spot. This image is equal to a Fourier transformed image by components of diffracted waves. In consequence, the last interference image corresponds to a reproduction of a real atomic arrangement (distribution of potential) since the arrangement of atoms in the sample is Fourier-transformed twice.

Cross-sectional TEM observations in this work were joint research projects with Sano Laboratory in Kwansei-Gakuin University. The TEM apparatus used in this work was a JEM-2000FX2 with 200 keV acceleration voltage. We chose the lattice image method with picking up the [200] reflection selectively for emphasizing contrast between GaAs and AlAs. The TEM apparatus was operated by Mr. Higuchi, Mr. Morimoto and Ms. Honda, who were members of Sano Laboratory.

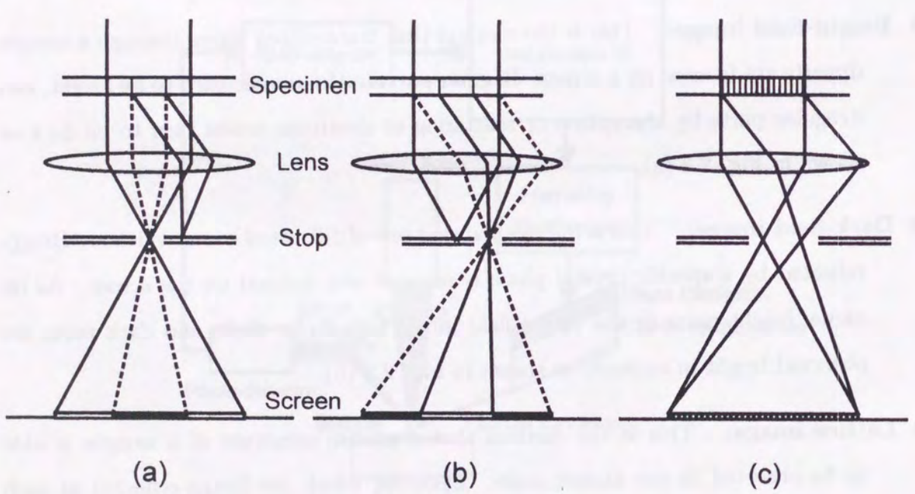

Figure 2.3: Schematic illustrations of principles of (a) bright-field image, (b) dark-field image and (c) lattice image.

2.2.3 Photoluminescence : PL

PL is one of optical analyses with highest sensitivity, and it is very useful since samples are not damaged in the observation. In this work, PL measurements were done to decide size uniformity from PL linewidth (see *Appendix A*), one-dimensionality from PL polarization (see *Appendix B*), temperature dependences of PL linewidth and intensity (see Section 6.3) and PL decay time (see Section 6.4) and crystal quality of QWRs from PL intensity, respectively.

Figure 2.4 shows a schematic illustration of the PL system of Hiyamizu Laboratory. A sample was cooled directly by a He-Gas cryostat, and a temperature of the sample was measured by a thermocouple close to the sample, and the temperature can be controlled from 10 K to room temperature. The excitation source was a He-Cd laser with λ=325 nm, and the laser beam was focused on the sample surface in a diameter of about 200 μm. PL spectrum from the sample was observed by a monochromator and a photomultiamplifier, and PL signals through a lock-in-amplifier were recorded by a personal computer.

PL results in Chapter 3 were observed by the system of KUBOTA Corporation. Samples were placed in liquid helium during observation, and the excitation source was Ar^+ laser with λ=514.5 nm.

The time-resolved PL measurement to estimate exciton lifetimes was done using an instrument of ATR Adaptive Communications Research Laboratories, and details of the measurement and a block diagram of the time-resolved PL system are given in Chapter 6.

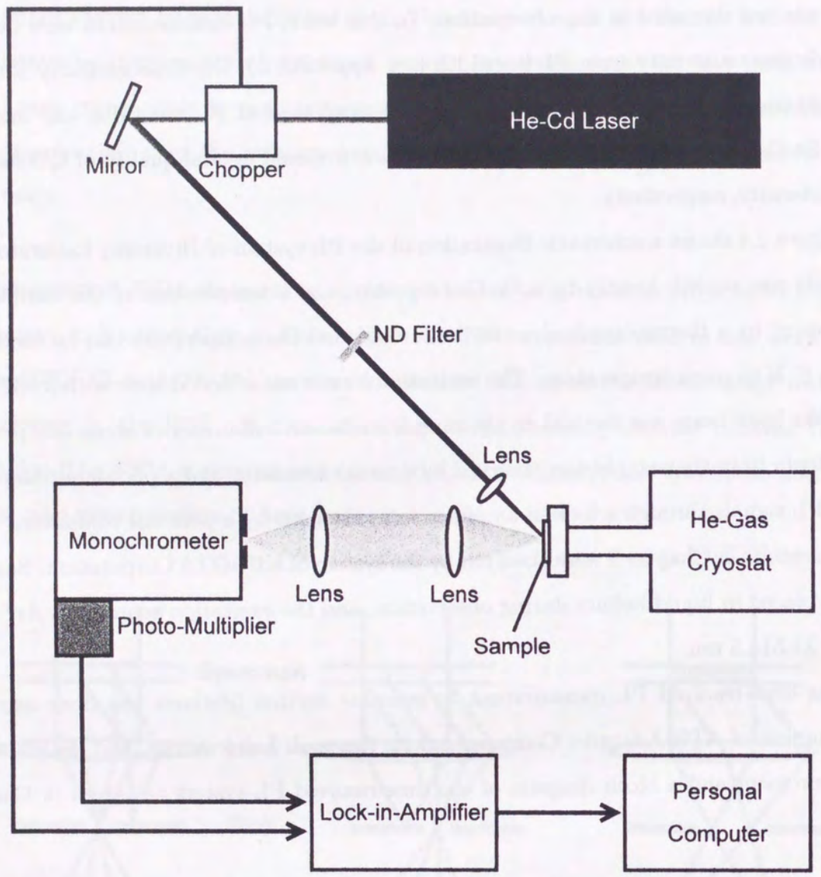

Figure 2.4: Schematic illustration of PL system of Hiyamizu Laboratory.

Chapter 3

GaAs/AlAs Quantum Wires

For the application of QWRs to devices, high-density and highly uniform QWRs are indispensable. In this chapter, structural estimations of high-density corrugation naturally formed on (775)B GaAs surfaces and optical properties of high-density GaAs/AlAs QWRs using the (775)B GaAs corrugation are reported. The study in this chapter was the start point of the work related to the (775)B QWRs.

3.1 Structural estimation of GaAs corrugation

For surface AFM and cross-sectional TEM observations, a 15-period GaAs(5 nm)/AlAs(5 nm) superlattice (SL) structure was grown on a GaAs(200 nm)/AlAs(200 nm) buffer layer (800 nm in total) on a (775)B GaAs substrate by MBE at a substrate temperature (T_s) of 670°C. V/III pressure ratio was 10 (16) for GaAs (AlAs), and growth rates were 1 μm/h for both GaAs and AlAs. A schematic illustration of the GaAs(5 nm)/AlAs(5 nm) SL structure is shown in Fig. 3.1.

3.1.1 Surface AFM observation

Figure 3.2 shows a surface morphology of a 5-nm-thick GaAs layer, which corresponds to the top layer of the GaAs(5 nm)/AlAs(5 nm) SL, observed by AFM. Regular corrugation with extremely straight step edges in the [1$\bar{1}$0] direction can be seen. From the AFM image, the lateral period and vertical amplitude of the corrugation were approximately 12

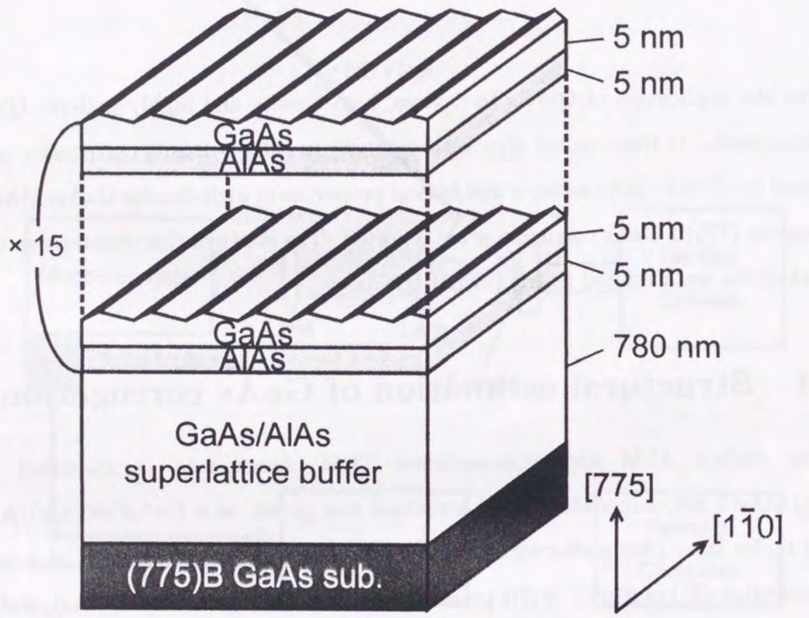

Figure 3.1: Schematic illustration of a GaAs(5 nm)/AlAs(5 nm) superlattice structure grown on a (775)B GaAs substrate.

nm and approximately 1 nm, respectively. Although similar corrugation has often been observed for GaAs and AlGaAs grown on vicinal (110) GaAs substrates[31] and vicinal (100) GaAs substrates[32], the corrugation on the (775)B surface is of much shorter period (1/5–1/10 of that previously reported[31,32]), in addition, it is very uniform. Almost the same corrugation as shown in Fig. 3.2 was also observed on the surface of a GaAs layer grown on the (775)B GaAs substrate at T_s=640°C, but it was not observed at T_s=580°C. Temperature dependence of surface morphology of GaAs layers grown on (775)B GaAs substrates is given in the next chapter in detail. Surface corrugation like the (775)B one has lately considerable attention since corrugation can be applied to fabrication of QWRs without a process of substrate. Then, cross-sectional TEM observation was done to confirm structural features of the GaAs(5 nm)/AlAs(5 nm) SL and to decide exact shapes and sizes of the GaAs corrugation.

3.1.2 Cross-sectional TEM observation

Figure 3.3 shows (a) a TEM micrograph of the ($\bar{1}$10) cross section of the GaAs(5 nm)/AlAs(5 nm) SL and (b) its schematic illustration. A regular corrugation can be seen on an AlAs-on-GaAs interface with a period of 12 nm [interface (A) in Fig. 3.3 (b)] in contrast to a flat GaAs-on-AlAs interface [interface (B) in Fig. 3.3 (b)]. The corrugated interface consists of a (111)B terrace with a length of 8 nm and a (441)B microfacet with a length of 4.2 nm. The lateral period and vertical amplitude of the corrugation are decided to be 12 nm and 1.2 nm, respectively. It is expected that the regularly corrugated AlAs-on-GaAs interface and the flat GaAs-on-AlAs interface result in a regular modulation of the well width of the AlAs/GaAs/AlAs QW grown on the (775)B GaAs substrate, in consequence, QWRs can be obtained for the case of the QW with reduced well width.

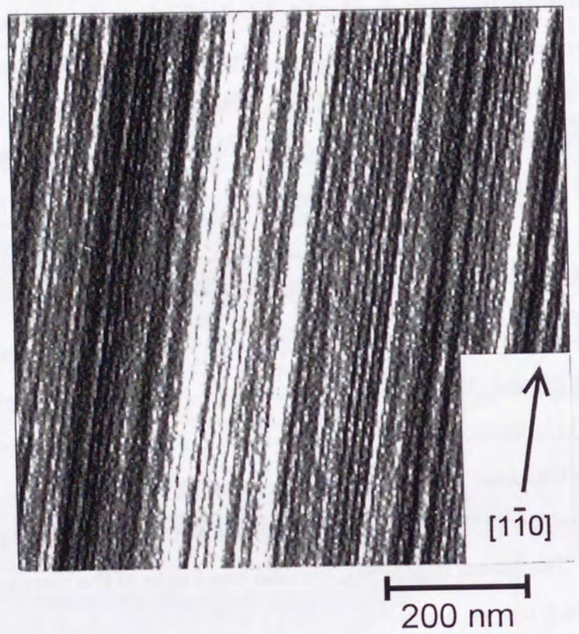

Figure 3.2: Surface morphology of a 5-nm-thick GaAs surface as the top layer of the GaAs(5 nm)/AlAs(5 nm) superlattice grown on the (775)B GaAs substrate observed by AFM.

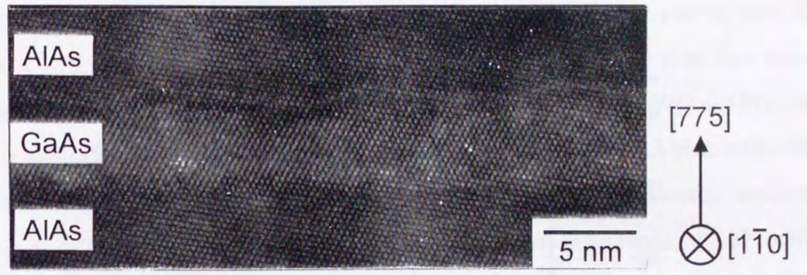

(a)

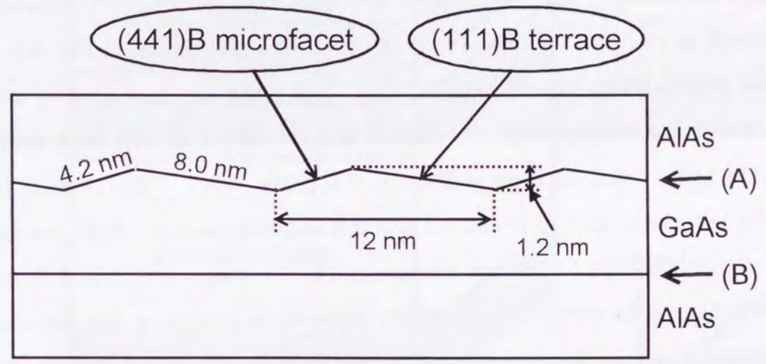

(b)

Figure 3.3: (a) TEM micrograph of the ($\bar{1}$10) cross section of the GaAs(5 nm)/AlAs(5 nm) superlattice grown on the (775)B GaAs substrate. (b) Schematic illustration of a GaAs/AlAs QW with a corrugated AlAs-on-GaAs interface and a flat GaAs-on-AlAs interface.

3.2 PL properties

In order to form GaAs/AlAs QWR structures using the interface corrugation, GaAs/AlAs QWs with well widths of L_w=10.5, 6.3, 4.3 and 3.3 nm as shown in Fig. 3.4 were grown on a GaAs/AlAs buffer layer (800-nm thick) on the (775)B GaAs substrate and on a (411)A GaAs substrate simultaneously at T_s=670°C. The AlAs barrier layers of the QWs were 17-nm thick. The (411)A substrate was used as a reference sample with extremely flat interfaces even grown at high temperatures[34,35]. The layer thicknesses are those observed for the (411)A substrate, i.e., they are average well widths for (775)B QWs. The numbers of QWs were 1 (L_w=10.5 nm), 4 (6.3 nm), 8 (4.3 nm) and 32 (3.3 nm), respectively.

PL spectra at 4.2 K from the QWs on the (775)B substrate for two different polarization directions are shown in Fig. 3.5. The PL spectrum with the polarization parallel to the [1$\bar{1}$0] direction, i.e., the direction of lines of the surface corrugation in Fig. 3.2, and that with the perpendicular polarization on the (775)B plane are illustrated by a solid line and a dotted line, respectively. The sample was excited by an Ar^+ laser with a power of 10 mW and a beam diameter of 200 μm. PL peaks at 801, 777, 746 and 715 nm are from the QWs with L_w=10.5, 6.3, 4.3 and 3.3 nm, respectively. With decreasing well width, the polarization anisotropy increases. The PL peak (λ=715 nm) from the 3.3-nm QWs exhibits the strongest polarization dependence, indicating that one-dimensional confinement of carriers becomes more effective with decreasing L_w due to the corrugation of the AlAs-on-GaAs interface while the other one remains flat.

FWHM of the PL peak (λ=715 nm) from the 3.3-nm QWs on the (775)B substrate is as small as 15 meV at 4.2 K, which compares favorably with those of previously reported QWRs, e.g., 23 meV at 10 K[31], 25 meV at 20 K[32]. This result indicates that very uniform formation of QWRs is realized on the (775)B substrate. Another advantage of the present QWRs formed on the (775)B substrate is that an extremely high density of QWRs [1/(12 nm) = 8×10^5 cm^{-1}] can be realized, which is almost five times higher than that of self-organizing AlAs/GaAs/AlGaAs QWRs on vicinal (100) GaAs substrates[32] and is one order of magnitude higher than that of GaAs/AlGaAs QWRs on vicinal (110)

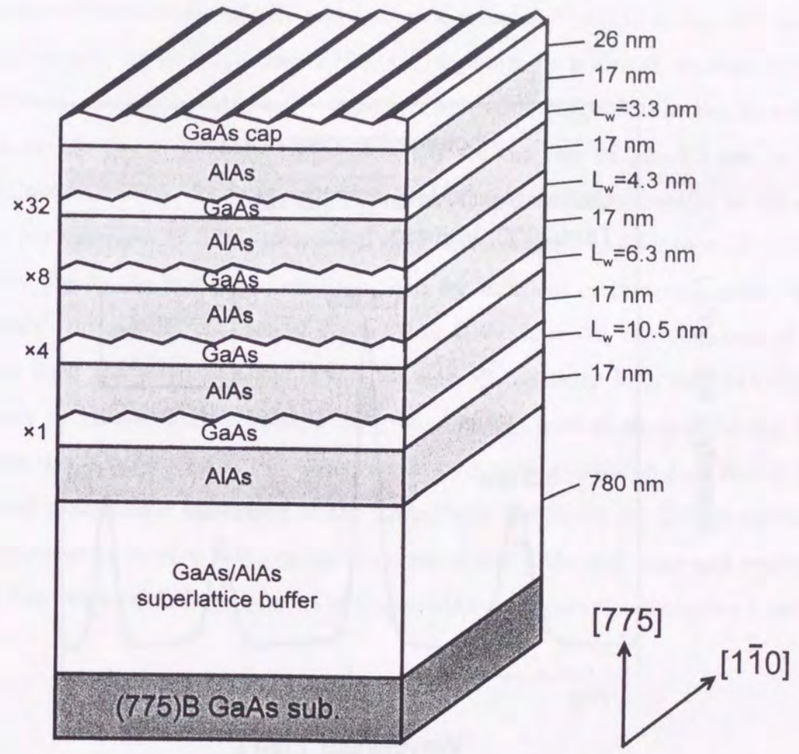

Figure 3.4: Schematic illustration of a GaAs/AlAs QWs (QWRs) structure grown on the (775)B GaAs substrate at T_s=670°C.

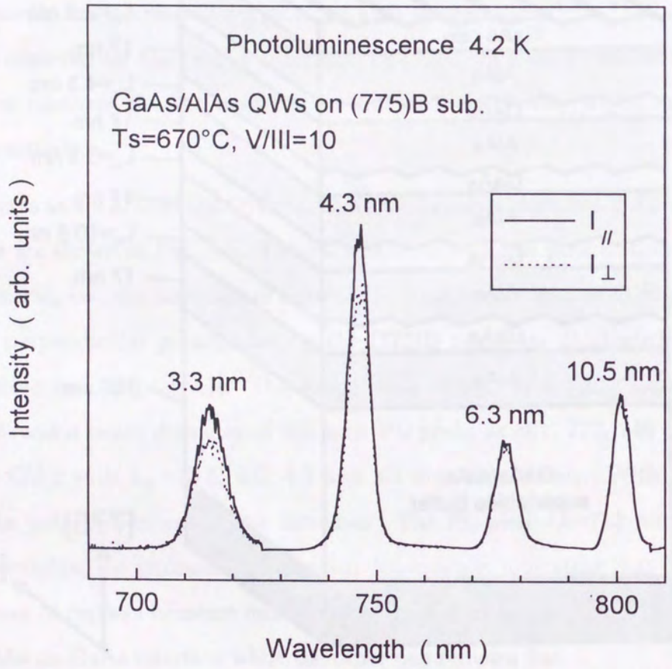

Figure 3.5: Polarization dependence of PL spectra (4.2 K) from GaAs/AlAs QWs grown on the (775)B GaAs substrate.

GaAs substrates[31]. The PL intensity from the GaAs/AlAs QWRs on the (775)B substrate was almost the same as that from the QWs on the (411)A substrate, indicating that the QWRs on the (775)B substrate had high optical quality.

The degrees of polarization, $P \equiv (I_{\parallel} - I_{\perp})/(I_{\parallel} + I_{\perp})$, for the (775)B and (411)A samples are plotted as a function of well width in Fig. 3.6. As $L_{\rm w}$ decreases, the degree of polarization increases monotonically and reaches a value of $P = 0.11$ at $L_{\rm w}$=3.3 nm for the (775)B sample, while in the case of the (411)A sample, it is almost constant around zero and even the largest value is $P = 0.03$. This result suggests that the formation of QWRs occurs in the $[1\bar{1}0]$ direction, especially for the case of $L_{\rm w}$=3.3 nm, on the (775)B substrate, because PL from a QWR is preferentially polarized parallel to the wire direction (see *Appendix B*). This rather small value of the degree of polarization ($P = 0.11$) is probably due to the well layer being too thick for sufficient carrier confinement with the interface corrugation. In case of GaAs/AlAs QWs, however, the thickness of the GaAs well layer is limited to about 3 nm, because PL intensity from the GaAs/AlAs QW greatly decreases. This is because the ground energy level of electrons in the QW approaches the X-band edge of the AlAs barrier layer with decreasing $L_{\rm w}$. Hence, this rather small polarization anisotropy of the GaAs/AlAs QWRs on the (775)B substrate will be improved by further reducing the thickness of the GaAs well layer and replacing the AlAs barriers with AlGaAs barriers or GaAs/AlAs short-period superlattice barriers.

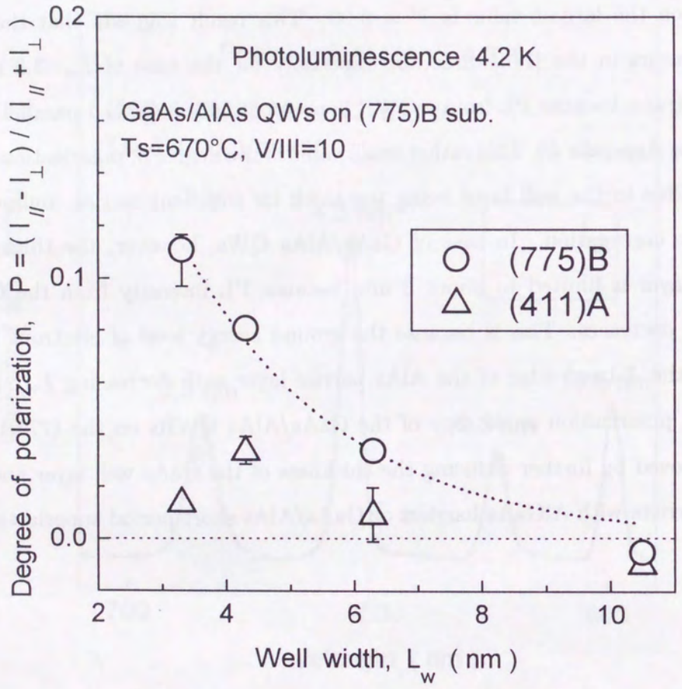

Figure 3.6: Degrees of polarization, $P = (I_{\parallel} - I_{\perp})/(I_{\parallel} + I_{\perp})$, for GaAs/AlAs QWs grown on (775)B and (411)A GaAs substrates as a function of well width $L_{\rm w}$.

3.3 Summary

GaAs/AlAs QWRs were naturally formed in a thin GaAs/AlAs QW ($L_{\rm w}$=3.3 nm) with a regularly corrugated AlAs-on-GaAs interface and a flat GaAs-on-AlAs interface grown on a (775)B GaAs substrate by MBE. It was observed by TEM that the lateral period and vertical amplitude of the interface corrugation are 12 nm and 1.2 nm, respectively. AFM observation revealed that the corrugation of a GaAs surface is very regular and uniform. The PL peak at λ=715 nm from the QWRs with a cross section of about 12×3 nm^2 showed a polarization degree of $P = (I_{\parallel} - I_{\perp})/(I_{\parallel} + I_{\perp})$=0.11 and a very small FWHM of 15 meV at 4.2 K. This FWHM value is much smaller than those (20–40 meV) reported so far for self-organizing QWRs[31,32], indicating highly uniform formation of the QWRs. Extremely high density of QWRs (8×10^5 cm^{-1}) was also realized, and the PL intensity from the QWRs was almost the same as that of GaAs/AlAs QWs grown on a (411)A substrate, implying that the present QWRs have considerable potential for application to optical devices.

Chapter 4

Growth Modes of GaAs and AlAs on (775)B GaAs Substrate

This chapter describes surface morphologies of GaAs and AlAs layers grown on (775)B GaAs substrates as a function of growth temperature and layer thickness. According to results reported in this chapter, GaAs/$(GaAs)_m(AlAs)_n$ QWRs presented in Chapter 5, 6 and 8 were designed.

4.1 AFM observation of GaAs surfaces

Experimental conditions were as follows. In MBE growth, substrate temperatures were changed from 540°C to 640°C. V/III pressure ratio was 9 (14) for GaAs (AlAs), and growth rates were 0.5–1.0 μm/h for both GaAs and AlAs layers. The substrates were rotated at a rate of 30–60 rpm. Immediately after the MBE growth of GaAs or GaAs/AlAs layers was concluded, all samples were cooled to room temperature under As_4 atmosphere, and they were taken out from the MBE growth chamber for observation of their surface morphologies by AFM in N_2 gas atmosphere.

Figure 4.1 shows AFM images of surface morphologies of 500-nm-thick GaAs layers grown on (775)B GaAs substrates at T_s=540, 560, 580, 610 and 640°C. The GaAs surfaces are flat for T_s=540-580°C (step heights of the surface are less than 0.3 nm) [(a)–(c)]. However, the surface is slightly corrugated for T_s=610°C (d), and regular surface corru-

gation is clearly observed for T_s=640°C (e). Step edges of the corrugation run straight in the [1$\bar{1}$0] direction. The lateral period (L_p) of the surface corrugation of the GaAs layer grown at T_s=640°C is approximately 35 nm, and the step heights (H_s) are approximately 4 nm, respectively. The AlAs layer always shows a flat surface for T_s=540–670°C.

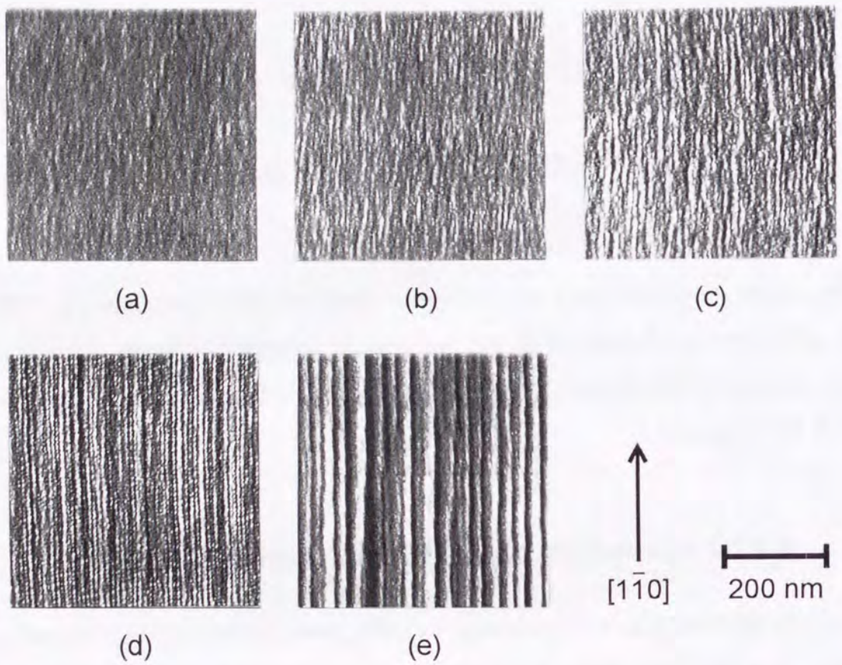

Figure 4.1: Surface AFM images of 500-nm-thick GaAs layers grown on (775)B GaAs substrates by MBE at (a) T_s=540°C, (b) 560°C, (c) 580°C, (d) 610°C and (e) 640°C.

Following the temperature dependence, thickness dependence of L_p and H_s of the surface corrugation of GaAs layers grown on the (775)B GaAs substrates at T_s=640°C were studied. Two buffer layers with flat surfaces and interfaces were used in this study; a GaAs(1.5 nm)/AlAs(1.5 nm) superlattice structure (10 periods) on a 500-nm-thick GaAs(50 nm)/AlAs(50 nm) superlattice grown at T_s=550°C (type A), and a GaAs layer (500 nm) grown at T_s=550°C (type B). It is notable that the results discussed below are not related to the buffer layer because GaAs and AlAs surfaces grown on (775)B GaAs

substrates are always flat for T_s=550°C. After the growth of buffer layers, the substrate temperature was increased to 640°C, and the samples were kept at T_s=640°C for a minute under As_4 atmosphere (10^{-6} Torr). Then, GaAs layers of 0.3, 0.6, 1.2, 1.8, 2.4 and 4.8 nm in thickness were grown on the type A buffer layers, and 10-, 50- and 250-nm-thick GaAs layers were grown on the type B buffer layers. Figure 4.2 shows AFM images of surface morphologies of the GaAs layers with thicknesses of (a) 1.2 nm, (b) 4.8 nm, (c) 50 nm and (d) 250 nm. Regular surface corrugation is visible on all GaAs layers.

L_p of the surface corrugation of the GaAs layers is plotted as a function of layer thickness d_{GaAs} in Fig. 4.3. In the region of $d_{GaAs}\leq$4.8 nm, L_p and H_s are almost constant (approximately 12 nm and approximately 1 nm, respectively), and the shapes of the surface corrugation are similar. To the author's knowledge, formation of such uniform corrugation in the early stage of growth has not yet been reported. As d_{GaAs} increases, both L_p and H_s increase, and finally L_p and H_s saturate at approximately 35 nm and approximately 4 nm, respectively, for $d_{GaAs}\geq$200 nm. The size-increasing feature and saturation behavior of L_p and H_s similar to the corrugation observed on the (775)B GaAs substrates was observed and explained for GaAs layers grown on vicinal (100) GaAs surfaces[38–40]. The constant L_p and H_s during the early stage of growth, however, to the author's knowledge, were observed in this study for the first time, and the reported simulation models[38–40] do not explain the constant L_p and H_s during the early stage of growth.

The GaAs layer grown on the (775)B GaAs substrate at T_s=550°C exhibited a flat surface, but the surface corrugation of L_p=12 nm was formed by thermal annealing at T_s=640°C under As_4 atmosphere (10^{-6} Torr). Figure 4.4 shows surface AFM images of the 1.5-nm-thick top GaAs layers of the GaAs(1.5 nm)/AlAs(1.5 nm) superlattice structures (a) before and (b) after thermal annealing at T_s=640°C. The feature size of the surface corrugation after thermal annealing is almost the same as those of the thin GaAs layers with d_{GaAs}=0.3–4.8 nm grown at T_s=640°C. It should be noted that the feature size of the surface corrugation does not change with the thickness of GaAs layers for annealing experiments. Formation of the surface corrugation with multi-atomic steps due to rearrangement of atoms on the surface during thermal annealing was reported on a vicinal (100) GaAs surface[41]. However, the reason for L_p to be 12 nm for this (775)B surface is

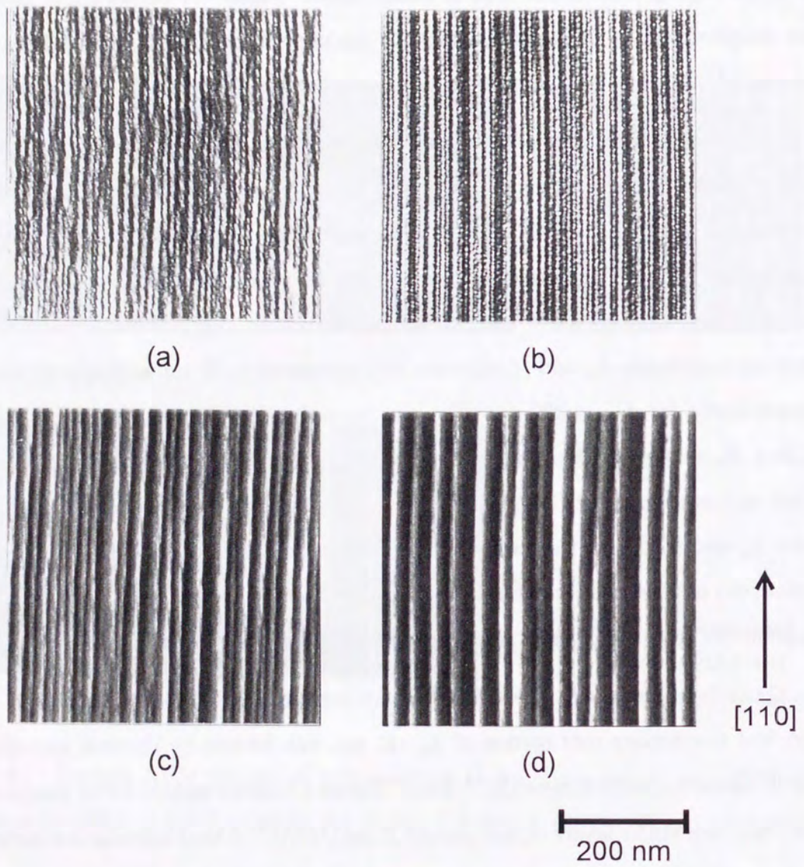

Figure 4.2: Surface AFM images of GaAs layers of various thicknesses d_{GaAs} grown on (775)B GaAs substrates at T_{s}=640°C by MBE. (a) d_{GaAs}=1.2 nm, (b) d_{GaAs}=4.8 nm, (c) d_{GaAs}=50 nm and (d) d_{GaAs}=250 nm.

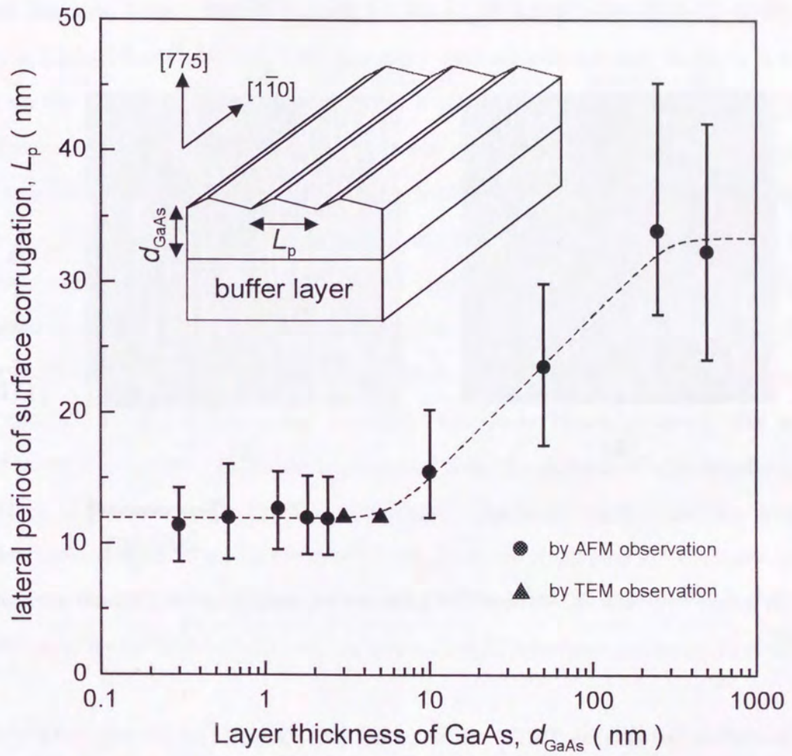

Figure 4.3: GaAs layer thickness (d_{GaAs}) dependence of lateral period (L_{p}) of surface corrugation of GaAs layer grown at T_{s}=640°C on (775)B GaAs substrates.

not clear at present.

Continuity of the straight step edges along the [1$\bar{1}$0] direction was improved with increasing d_{GaAs}. The average length of the straight step edges was approximately 250 nm for d_{GaAs}=0 nm, which is the sample only thermally annealed, but became more than 1 μm for d_{GaAs}=4.8 nm and more than 10 μm for d_{GaAs}=250 nm.

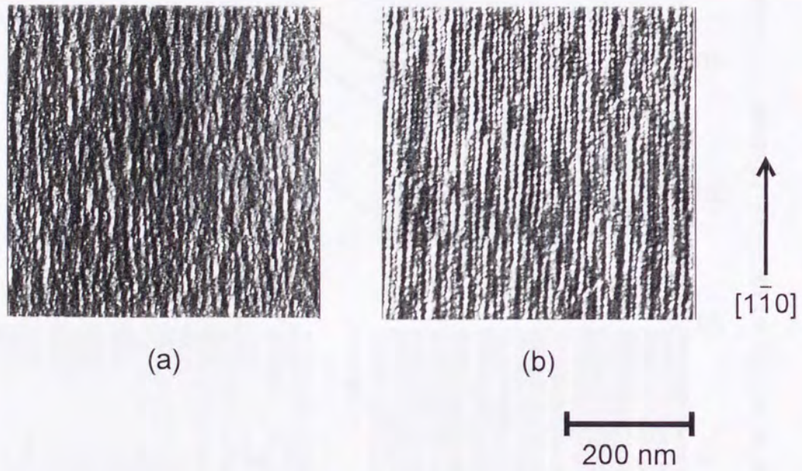

Figure 4.4: AFM images of GaAs surfaces (a) before and (b) after thermal annealing at T_s=640°C.

4.2 TEM observation of GaAs/$(GaAs)_5(AlAs)_5$ QWRs structure

In order to confirm the precise structures of the corrugated AlAs-on-GaAs interface and the flat GaAs-on-AlAs interface in a GaAs/AlAs QW using cross-sectional TEM observation, a GaAs/$(GaAs)_5(AlAs)_5$ QW structure with an average well width of 3 nm was grown on the (775)B GaAs substrate. First, a 10-period (30-nm-thick) $(GaAs)_5(AlAs)_5$ short-period superlattice (SPS) barrier layer was grown on a GaAs(50 nm)/AlAs(50 nm) superlattice buffer layer (500-nm thickness in total). Then, a 0.6-nm-thick GaAs layer as a part of a 3-nm-thick GaAs QW layer was grown on the top AlAs layer of the SPS barrier to prevent surface contamination of the AlAs layer during growth interruption. Then, T_s was raised from 550°C to 640°C, and a 2.4-nm-thick GaAs QW layer was grown. Finally, an upper $(GaAs)_5(AlAs)_5$ SPS barrier was grown at T_s=550°C. Figure 4.5 shows (a) a TEM micrograph of the ($\bar{1}$10) cross section of the GaAs/$(GaAs)_5(AlAs)_5$ QW and (b) its schematic illustration. It is clearly observed that the AlAs-on-GaAs interface of the 3-nm-thick QW grown at T_s=640°C is corrugated. The lateral period and step heights of the interface corrugation are 12 nm and 1.2 nm, respectively, which are the same as those for the 5-nm-thick GaAs well layer presented in Chapter 3. On the other hand, AlAs-on-GaAs interfaces and GaAs-on-AlAs interfaces in the SPS barriers grown at T_s=550°C are flat.

Figure 4.6 shows an AFM image (top view) of the (775)B corrugated surface of a 2.4-nm-thick GaAs layer grown at T_s=640°C. This AFM image is consistent with the TEM results discussed above.

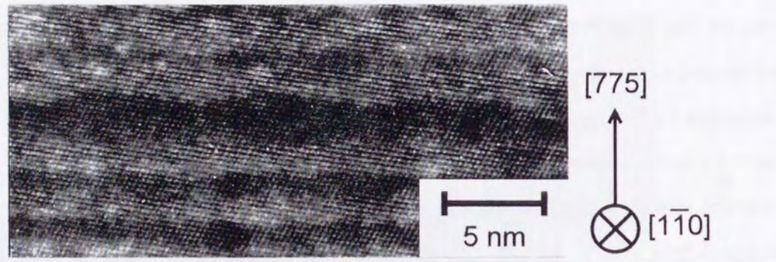

(a)

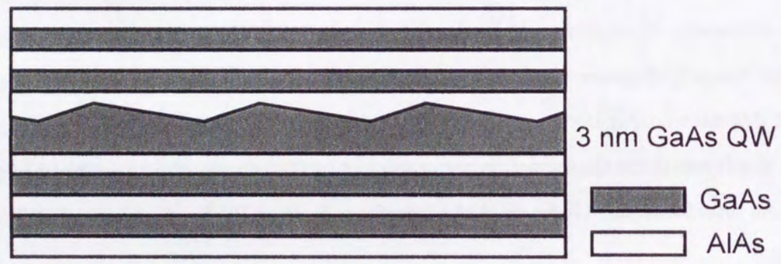

(b)

Figure 4.5: (a) TEM micrograph of the ($\bar{1}$10) cross section of GaAs/$(GaAs)_5(AlAs)_5$ QWRs formed in an average 3.0-nm-thick GaAs/$(GaAs)_5(AlAs)_5$ QW grown on a (775)B GaAs substrate by MBE. (b) Schematic illustration of GaAs/$(GaAs)_5(AlAs)_5$ QWRs.

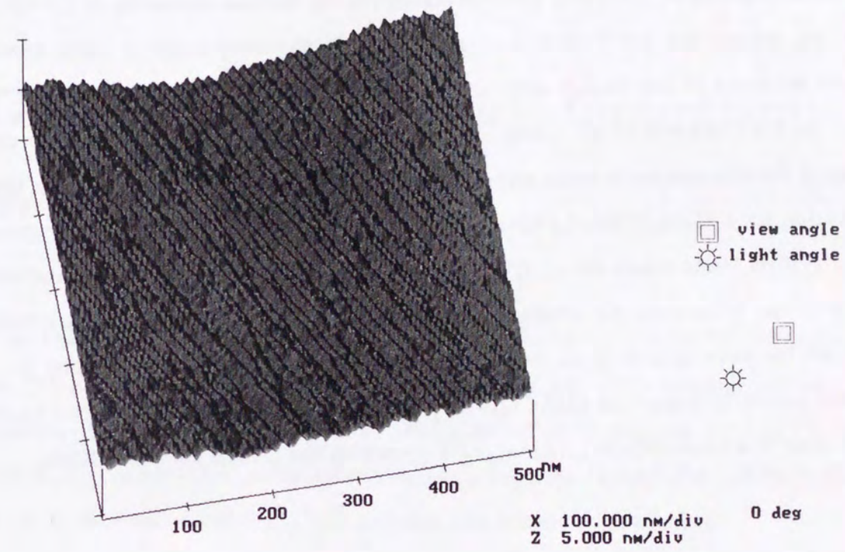

Figure 4.6: AFM image (top view) of the (775)B corrugated surface of a 2.4-nm-thick GaAs layer grown at T_s=640°C.

4.3 Summary

Surface morphologies of GaAs and AlAs layers grown on (775)B GaAs substrates by MBE were studied using AFM. The GaAs surface is flat for $T_s \leq 580$°C, however, it is corrugated for $T_s \geq 640$°C in contrast with the flat surface observed for AlAs layers. The flat GaAs surface grown at T_s=550°C becomes corrugated by thermal annealing at T_s=640°C under As_4 atmosphere (10^{-6} Torr) for one minute. In the early stage of GaAs growth (a layer thickness of less than 5 nm), shapes of the surface corrugation are almost the same. As the thickness of the GaAs layer increases, both the lateral period and step heights of the corrugation increase and saturate for $d_{GaAs} \geq 200$ nm. Cross-sectional TEM observation for a GaAs/$(GaAs)_5(AlAs)_5$ QW with a 3-nm-thick GaAs QW layer grown on the (775)B GaAs substrate at T_s=640°C indicates that the lateral period and step heights of the AlAs-on-GaAs interface corrugation are 12 nm and 1.2 nm, respectively, which are the same sizes to those for the GaAs/AlAs QWRs presented in Chapter 3.

These results indicate that GaAs QWRs just like the GaAs/AlAs QWRs can be obtained even in a GaAs/$(GaAs)_m(AlAs)_n$ QW grown on the (775)B GaAs substrate.

Chapter 5

GaAs/$(GaAs)_2(AlAs)_2$ Quantum Wires

In this chapter, it is presented about formation of GaAs/$(GaAs)_2(AlAs)_2$ QWRs on (775)B GaAs substrates, which was grown by the same method as the GaAs/$(GaAs)_5(AlAs)_5$ QWRs structure for TEM observation in Chapter 4. The PL properties showed much enhanced one-dimensionality than the GaAs/AlAs QWRs in Chapter 3 due to decreasing well width and avoiding the X-band edge problem.

5.1 Sample structure

Samples used in this chapter were grown under a condition as follows. The V/III pressure ratio was 9 (14) for GaAs (AlAs), and growth rates of GaAs and AlAs were 1.0 μm/h. Substrates were thermally cleaned at a substrate temperature (T_s) of 650°C for 15 minutes in As_4 atmosphere (10^{-6} Torr) just before MBE growth.

It should be noted that the surface of GaAs grown on the (775)B GaAs substrate can be changed between a flat surface and a corrugated surface by controlling the substrate temperature as reported in Chapter 4. The surface of GaAs becomes flat for T_s=540-580°C and corrugated above T_s=640°C (see Chapter 4). While, the surface of AlAs is always flat above T_s=540°C.

Figure 5.1 shows a schematic illustration of a GaAs/$(GaAs)_2(AlAs)_2$ QWRs struc-

ture grown on the (775)B GaAs substrate. The GaAs/$(GaAs)_2(AlAs)_2$ QWRs structure on the (775)B substrate was fabricated as follows. First, a 25-period (30-nm-thick) $(GaAs)_2(AlAs)_2$ short-period superlattice (SPS) barrier layer was grown on a 800-nm-thick GaAs/AlAs buffer layer at T_s=580°C [Fig. 5.2 (a)]. Second, a substrate temperature was raised to 640°C, and a GaAs QW (QWRs) layer was grown on the structure at T_s=640°C [Fig. 5.2 (b)]. Regular corrugation with very straight step edges in the $[1\bar{1}0]$ direction is formed. The lateral period and vertical amplitude of the corrugation is 12 nm and 1.2 nm, respectively. Third, the $(GaAs)_2(AlAs)_2$ SPS barrier was grown after reducing the substrate temperature from 640°C to 580°C. The surface turned to be flat again [Fig. 5.2 (c)]. The corrugated interface results in a periodic modulation of the well width in the QW. Therefore, lateral confinement effect of carriers arises, and QWRs are naturally formed at the thick parts in the GaAs/$(GaAs)_2(AlAs)_2$ QW grown on the (775)B substrate. After repeating second and third processes with changing QW layer thickness (L_w), a 20-nm-thick GaAs cap layer was grown on the structure finally. Hence, high-density GaAs/$(GaAs)_2(AlAs)_2$ QWRs were fabricated using the interesting MBE growth characteristics of GaAs and AlAs on the (775)B GaAs substrate. Average well widths were 2.1, 3.0, 4.2, 6.6 and 12 nm, respectively.

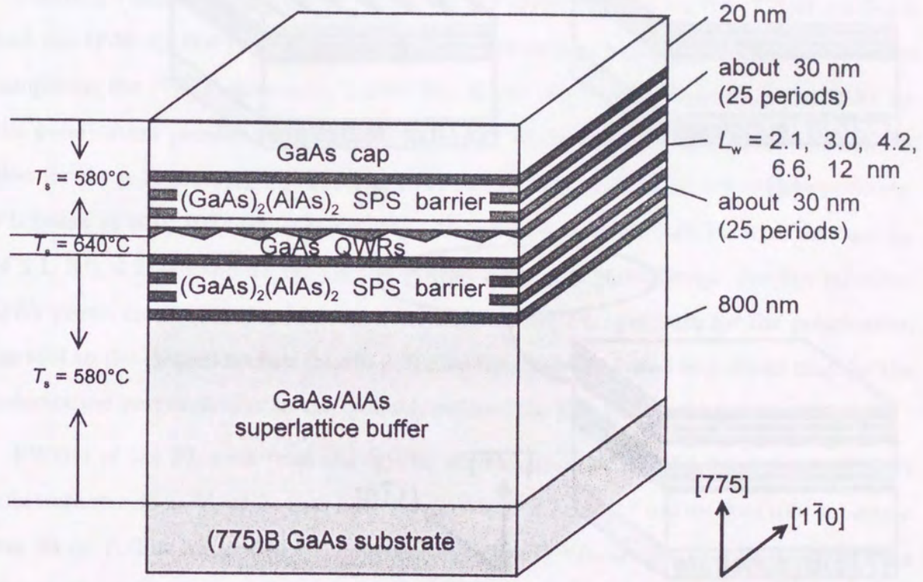

Figure 5.1: Schematic illustration of GaAs/$(GaAs)_2(AlAs)_2$ QWRs grown on the (775)B GaAs substrate.

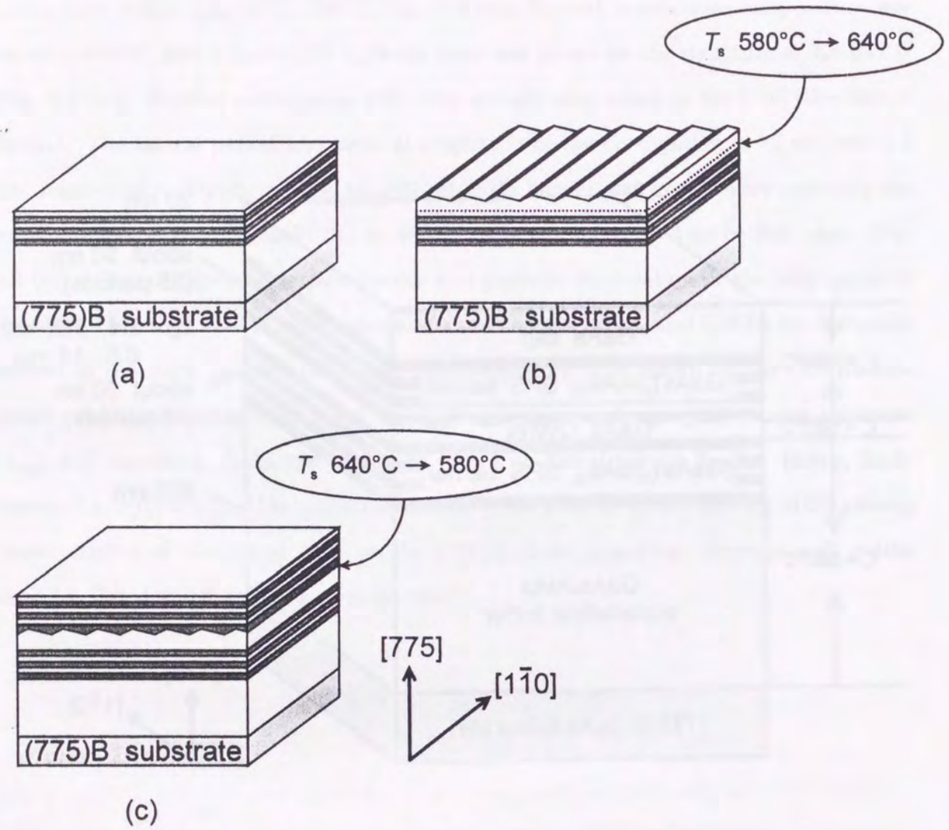

Figure 5.2: Fabrication process of GaAs/$(GaAs)_2(AlAs)_2$ QWRs grown on the (775)B GaAs substrate.

5.2 PL properties

PL spectra were measured at 14 K not only from the GaAs/$(GaAs)_2(AlAs)_2$ QWs (including QWRs) grown on the (775)B GaAs substrate but also from GaAs/$(GaAs)_2(AlAs)_2$ QWs grown on a (100) GaAs substrate at T_s=640°C without any growth interruptions. The samples were excited by a He-Cd laser beam with a power of 2 mW and a beam diameter of about 200 μm.

Figure 5.3 shows PL spectra at 14 K from the QWs (QWRs) on the (775)B substrate and the QWs on the (100) substrate for two different polarization directions. For the sample on the (775)B substrate, a solid line shows the PL spectrum from the QWs for the polarization parallel to the QWRs (the [1 $\bar{1}$ 0] direction), and a dotted line shows that for the polarization perpendicular to the QWRs (the [5 5 $\overline{14}$] direction), respectively. PL peaks at 670, 707, 741, 776 and 804 nm correspond to the QWRs with average L_w of 2.1, 3.0, 4.2, 6.6 and 12 nm on the (775)B substrate, respectively. For the reference QWs grown on the (100) substrate, a solid line shows PL spectrum for the polarization parallel to the cleaved surface (the [0 1 1] direction), and a dotted line shows that for the polarization perpendicular to the cleaved surface (the [0 $\bar{1}$ 1] direction), respectively.

FWHM of the PL peak from the QWRs with an average L_w of 2.1 nm on the (775)B substrate was 30 meV, while that from the QW with a L_w of 2.1 nm on the (100) substrate was 20 meV. The integrated PL intensity from the QWRs on the (775)B substrate was almost the same as that from the QW on the (100) substrate. These results indicate that the GaAs/$(GaAs)_2(AlAs)_2$ QWRs grown on the (775)B substrate had high optical quality.

Polarization degrees P of PL peaks from the GaAs/$(GaAs)_2(AlAs)_2$ QWs (QWRs) on the (775)B substrate, the GaAs/$(GaAs)_2(AlAs)_2$ QWs on the (100) substrate and the GaAs/AlAs QWs (QWRs) grown on the (775)B substrate presented in Chapter 3 are plotted as a function of L_w in Fig. 5.4. With decreasing L_w from 12 nm to 2.1 nm, the polarization anisotropies of PL from the GaAs/$(GaAs)_2(AlAs)_2$ and the GaAs/AlAs QWs (QWRs) on the (775)B substrates monotonically increase. The PL peak from the GaAs/$(GaAs)_2(AlAs)_2$ QWRs with the average L_w of 2.1 nm on the (775)B substrate

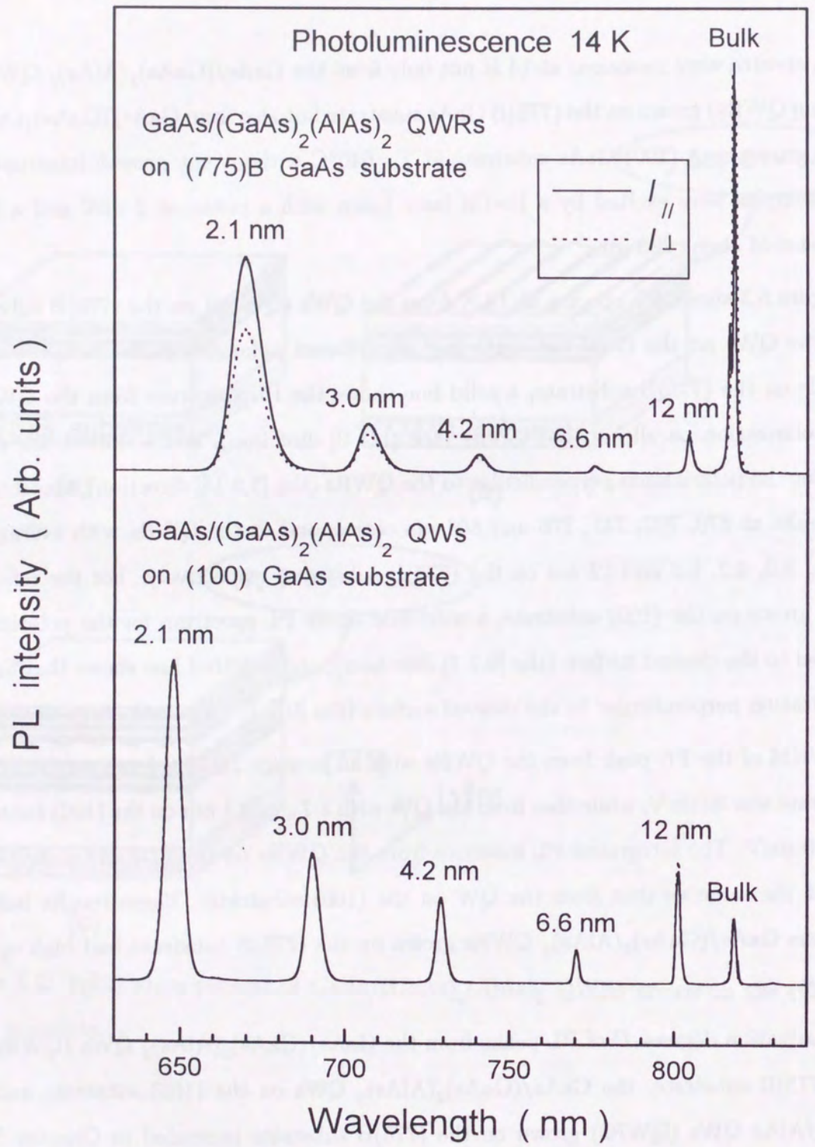

Figure 5.3: Polarized PL spectra (14 K) from $GaAs/(GaAs)_2(AlAs)_2$ QWs (including QWRs) grown on the (775)B GaAs substrate and conventional $GaAs/(GaAs)_2(AlAs)_2$ QWs grown on the (100) GaAs substrate.

exhibits the strongest polarization dependence ($P = 0.21$). On the other hand, the polarization dependence is constantly almost zero for the QWs on the (100) substrate. These results are in good agreement with theoretical investigations that PL from a QWR is polarized parallel to the wire direction (see *Appendix B*). The polarization degree of PL from the QWRs with the average L_w of 2.1 nm on the (775)B substrate was about twice as large as that ($P = 0.11$) from the GaAs/AlAs QWRs with an average L_w of 3.3 nm in Chapter 3. These results indicate that lateral confinement effect of carriers due to the corrugated interface is actually much enhanced by decreasing L_w from 3.3 nm to 2.1 nm, and high-density $GaAs/(GaAs)_2(AlAs)_2$ QWRs with a considerably strong one-dimensional confinement of carriers are realized on the (775)B substrate by MBE.

The high-density QWRs can be formed in a $GaAs/(GaAs)_2(AlAs)_2$ N-multi-layer structure grown on the (775)B substrate, then they are expected to be applied to semiconductor lasers with extremely high-density QWRs ($8N\times10^5$ QWRs/cm).

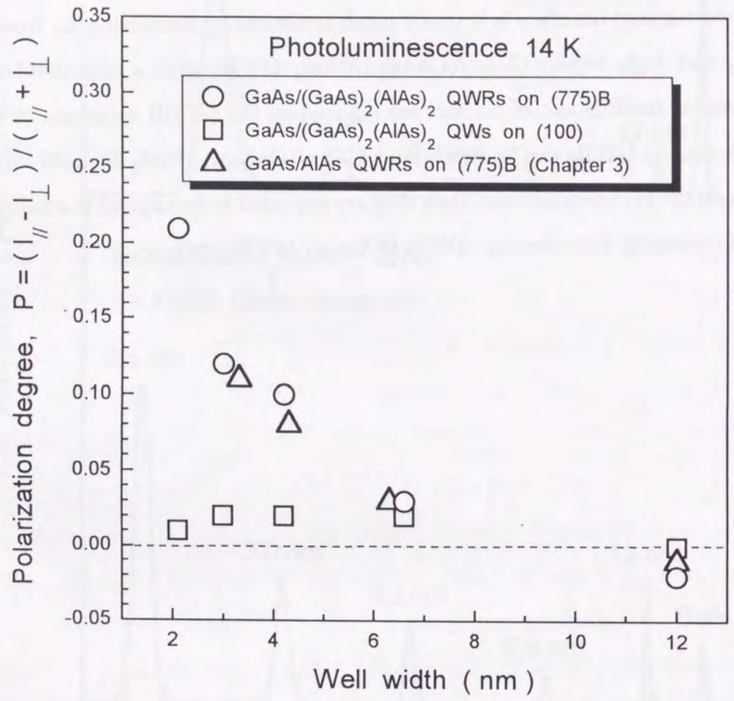

Figure 5.4: Polarization degrees, $P \equiv [(I_{\parallel} - I_{\perp})/(I_{\parallel} + I_{\perp})]$, for GaAs/$(GaAs)_2(AlAs)_2$ QWs (QWRs) grown on the (775)B GaAs substrate, GaAs/$(GaAs)_2(AlAs)_2$ QWs grown on the (100) GaAs substrate and the GaAs/AlAs QWs (QWRs) grown on the (775)B GaAs substrate (see Chapter 3) as a function of average well width L_w.

5.3 Theoretical analysis

Theoretical calculation and analysis in this section were done by Assoc. Prof. M. Ogawa in Kobe University under the collaboration with us, and the calculated results have been reported[36]. Optical properties and valence subbands of the GaAs/$(GaAs)_2(AlAs)_2$ QWs (QWRs) on the (775)B GaAs substrate were analyzed using the finite element method (FEM) based on the multi-band effective mass theory, where effects of the orientation of the crystal, the valence-band mixing, continuity of the probability-current densities and the finite-potential confinement of carriers in the QWR were rigorously treated in the k-dependent multiband space[37].

Figure 5.5 shows the valence subband structures of the GaAs/$(GaAs)_2(AlAs)_2$ QWRs with an average L_w of 2.1 nm. Each subband shows non-degeneracy since the confinement potential is not symmetric in the direction perpendicular to the QWRs in the (775)B plane (the $[5\,5\,\overline{14}]$ direction). Energy separation between the ground state (H1,1') and the first excited state (H2,2') in the valence band is as large as 60 meV at the zone center (k_y=0, k_y: the wave vector in the parallel direction to the QWRs), which is more than twice as large as k_BT at room temperature, and the energy separation is the largest for QWRs ever reported. This result is desirable for application to lasers, because the optical transition would occur between the ground states of the conduction and the valence bands.

Figure 5.6 shows the gain coefficients of the QWRs with (a) an average L_w of 2.1 nm and (b) an average L_w of 6.6 nm as a function of injected carrier concentration in two polarized directions parallel and perpendicular to QWRs (the $[1\,\overline{1}\,0]$ and the $[5\,5\,\overline{14}]$ directions, respectively). The calculated gain peaks for the average 2.1-nm-width QWRs are much larger than those for the average 6.6-nm-width QWRs. Furthermore, the polarization dependence is more conspicuous for the 2.1-nm QWRs than for the 6.6-nm QWRs. This result indicates the stronger one-dimensional carrier confinement effect of the 2.1-nm QWRs than that of the 6.6-nm QWRs, and it also confirms that the confinement effect becomes stronger with decreasing the average well width.

Figure 5.7 shows calculated polarized PL spectra from the (775)B GaAs/$(GaAs)_2(AlAs)_2$ QWRs at T=14 K. The calculated spectra are consistent with the exper-

imental result in Fig 5.3 qualitatively. This result supports a good one-dimensionality of the (775)B GaAs/$(GaAs)_2(AlAs)_2$ QWRs for the smallest average L_w=2.1 nm theoretically.

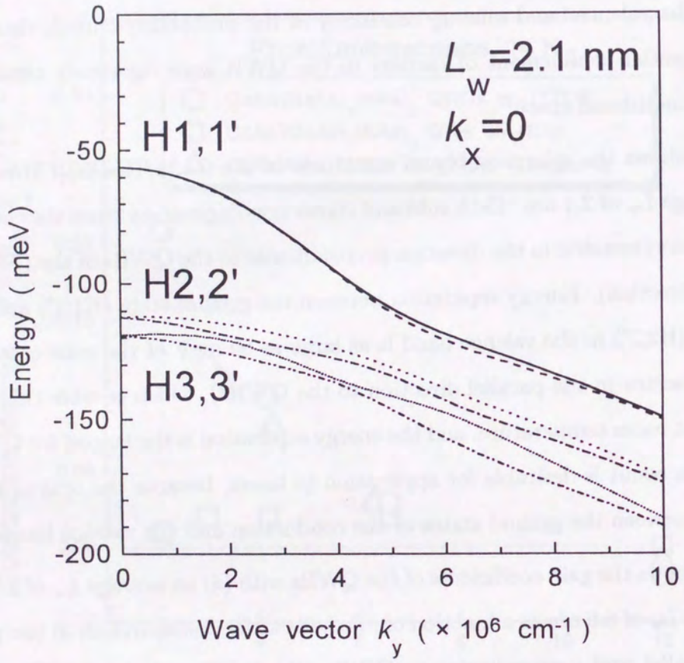

Figure 5.5: $E-k_y$ dispersion relations for the (775)B GaAs/$(GaAs)_2(AlAs)_2$ QWRs with an average L_w of 2.1 nm. The origin of energy is at the valence band top.

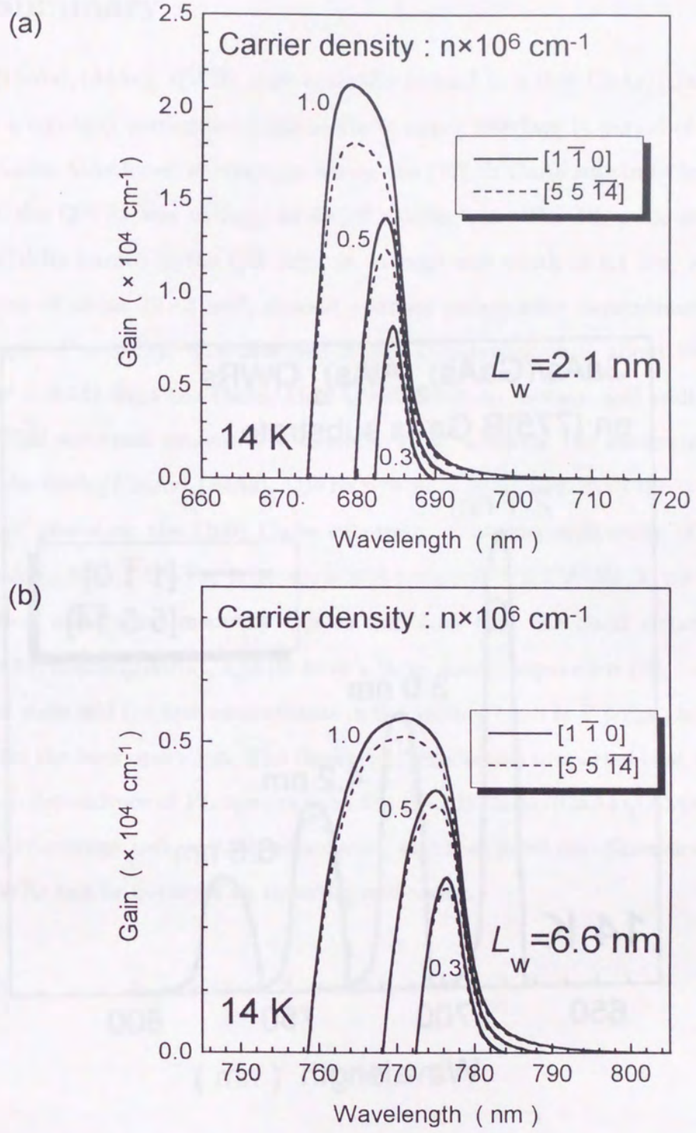

Figure 5.6: Calculated optical gain spectra of the GaAs/$(GaAs)_2(AlAs)_2$ QWs (QWRs) grown on the (775)B GaAs substrate for two different average well widths; (a) L_w=2.1 nm and (b) L_w=6.6 nm. Solid lines are for the parallel polarization (the [1 $\bar{1}$ 0] direction, parallel to the QWRs), and dashed lines are for the perpendicular polarization (the [5 5 $\bar{14}$] direction, perpendicular to the QWRs in the (775)B plane).

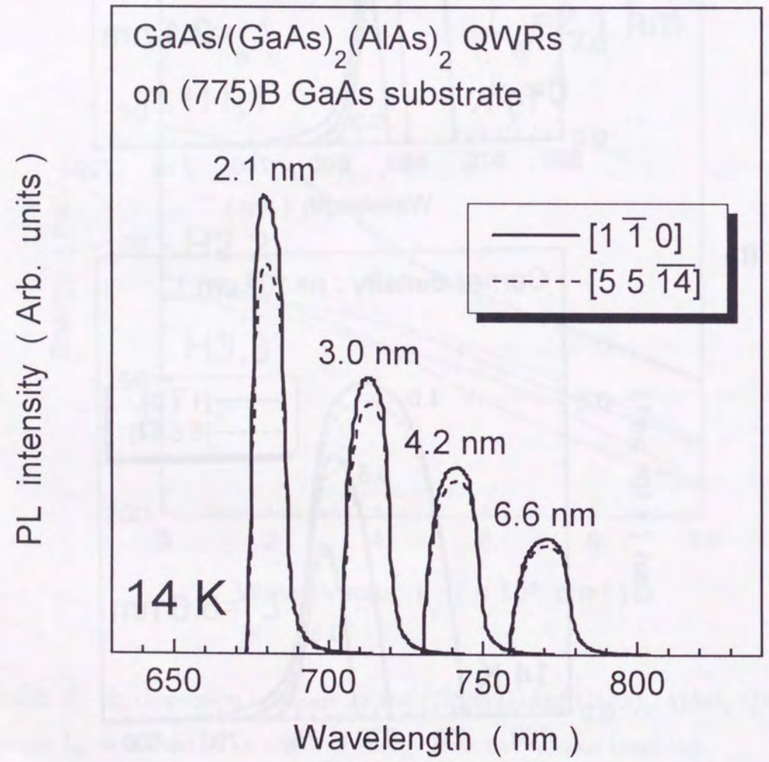

Figure 5.7: Calculated polarized PL spectra at 14 K from the (775)B GaAs/$(GaAs)_2(AlAs)_2$ QWs (QWRs) with average well widths of L_w=2.1, 3.0, 4.2 and 6.6 nm.

5.4 Summary

$GaAs/(GaAs)_2(AlAs)_2$ QWRs were naturally formed in a thin $GaAs/(GaAs)_2(AlAs)_2$ QW with a regularly corrugated AlAs-on-GaAs upper interface (a period of 12 nm) and a flat GaAs-on-AlAs lower interface grown on the (775)B GaAs substrate by MBE. The density of the QWRs was as high as 8×10^5 QWRs/cm. The PL peak at λ=670 nm from the QWRs formed in the QW with an average well width of 2.1 nm, which have a cross section of about 12×2 nm^2, showed a strong polarization dependence (the polarization degree $P = 0.21$). The observed degree of polarization is about twice as large as that ($P = 0.11$) from the GaAs/AlAs QWRs with an average well width of 3.3 nm on the (775)B substrate presented in Chapter 3. In addition, the integrated PL intensity from the $GaAs/(GaAs)_2(AlAs)_2$ QWRs was as large as that from the corresponding 2.1-nm QW grown on the (100) GaAs substrate. The size uniformity of the (775)B $GaAs/(GaAs)_2(AlAs)_2$ QWRs, however, is still not good (PL FWHM 30 meV).

Theoretical calculation made by Ogawa indicated that the band structures of the (775)B $GaAs/(GaAs)_2(AlAs)_2$ QWRs have a large energy separation (60 meV) between the ground state and the first excited state in the valence band at Γ point (k=0), which is favorable for the laser operation. The theoretical results also supported that the observed polarization dependence of PL spectra from the (775)B $GaAs/(GaAs)_2(AlAs)_2$ QWRs as a function of average well width is reasonable, and that good one-dimensionality of the (775)B QWRs can be obtained by reducing well width.

Chapter 6

$GaAs/(GaAs)_4(AlAs)_2$ Quantum Wires

In this chapter, high-density $GaAs/(GaAs)_4(AlAs)_2$ QWRs self-organized in a thin $GaAs/(GaAs)_4(AlAs)_2$ QW and their PL properties observed by various methods are reported. The $GaAs/(GaAs)_4(AlAs)_2$ QWRs were improved at the point of size uniformity drastically by a new MBE process, as a result, they showed not only high one-dimensionality and high optical quality but also high uniformity which has been a most important problem in case of self-organized QWRs.

6.1 Sample structure

Figure 6.1 is a schematic illustration of a $GaAs/(GaAs)_4(AlAs)_2$ QWRs structure grown on a (775)B GaAs substrate, which has more suitable barrier height for QWR laser applications than the $GaAs/(GaAs)_2(AlAs)_2$ QWRs presented in Chapter 5. Two samples of the $GaAs/(GaAs)_4(AlAs)_2$ QWRs were grown on the (775)B GaAs substrates by an improved MBE process and a previous MBE process. Both samples have the same structure fundamentally. In the improved process, a 27-nm-thick $(GaAs)_4(AlAs)_2$ short-period superlattice (SPS) barrier layer and a 0.6-nm-thick GaAs layer [a part of a GaAs QW (QWRs) layer with an average well width (L_w) of 2.1 nm] were grown on a 780-nm-thick GaAs/AlAs superlattice buffer layer at T_s=580°C. The surface of the top GaAs layer of

this structure was flat. Then, the substrate temperature was raised from 580°C to 650°C during a growth interruption of 1.5 minutes under As_4 atmosphere, and a 1.5-nm-thick GaAs layer [a rest part of the QW (QWRs) layer] and a 0.6-nm-thick $(AlAs)_2$ layer [the first layer of the upper $(GaAs)_4(AlAs)_2$ SPS barrier layer] were grown continuously at T_s=650°C. At this stage, the top AlAs-on-GaAs interface turned to be regularly corrugated with very straight edges in the $[1\bar{1}0]$ direction (see Chapter 4). Then, the substrate temperature was reduced from 650°C to 580°C during a growth interruption of 30 seconds, and a rest part of 15-period $(GaAs)_4(AlAs)_2$ SPS barrier layer and a 30-nm-thick GaAs cap layer were grown at T_s=580°C. On the other hand, in the previous process, the MBE growth was interrupted after the growth of the GaAs QW (QWRs) layer at T_s=650°C to decrease the substrate temperature to 580°C, and a whole $(GaAs)_4(AlAs)_2$ SPS barrier layer was grown at T_s=580°C on the corrugated GaAs surface, which was the same way as the GaAs/$(GaAs)_2(AlAs)_2$ QWRs reported in Chapter 5. Effect on the QWRs structure by the improved MBE process is described later. In both cases, a corrugated AlAs-on-GaAs upper interface and a flat GaAs-on-AlAs lower interface were formed in the GaAs/$(GaAs)_4(AlAs)_2$ QW with an average L_w of 2.1 nm on the (775)B GaAs substrate. The corrugated upper interface results in periodic modulation of the well width. Thick and thin parts in the GaAs/$(GaAs)_4(AlAs)_2$ QW are 2.7-nm thick and 1.5-nm thick, respectively, and carriers in the QW are localized at the thick parts. The lateral period of the corrugation is as small as 12 nm, and QWRs are formed just side-by-side, which results in the highest density of QWRs (8.3×10^5 QWRs/cm) to the author's knowledge. A conventional GaAs/$(GaAs)_4(AlAs)_2$ QW structure (L_w=2.1 nm) was also grown simultaneously on a (001) GaAs substrate for comparison.

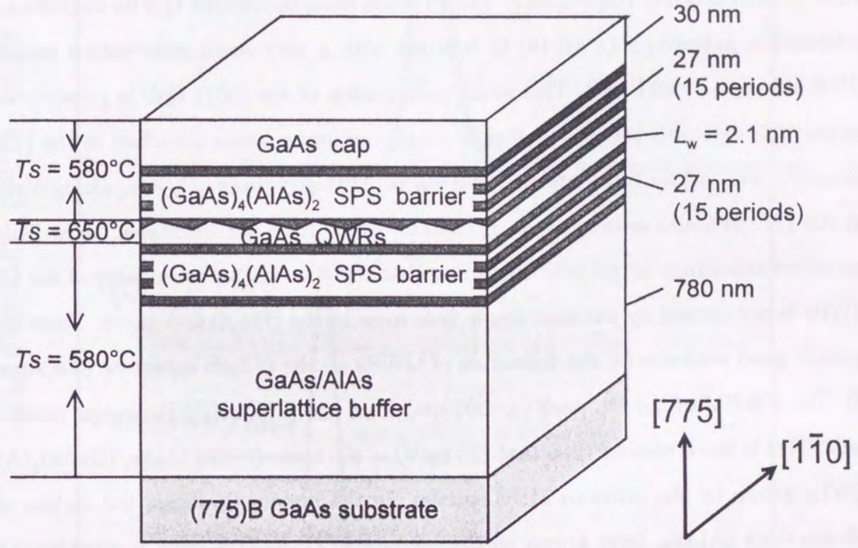

Figure 6.1: Schematic illustration of a GaAs/$(GaAs)_4(AlAs)_2$ QWRs structure grown on (775)B GaAs substrates. Two different samples were grown by two MBE process, however, both samples had the same structure basically.

6.2 PL properties at low temperature

Figure 6.2 shows polarized PL spectra measured at 14 K from the GaAs /$(GaAs)_4(AlAs)_2$ QW (QWRs) on the (775)B and the (001) GaAs substrates. PL peaks at λ=692 nm and 675 nm correspond to luminescence from the (775)B QWRs and the (001) QW, respectively. For both samples, a solid line and a broken one indicate PL spectra with polarizations parallel and perpendicular to the [1$\bar{1}$0] direction [the direction of the (775)B QWRs], respectively. The PL peak from the (775)B QWRs exhibits a large polarization anisotropy (P=0.19) in contrast with a very small polarization anisotropy (P=0.05) of the (001) QW. This small polarization of the (001) QW is possibly due to asymmetric exicitons trapped at locally energy-minimum areas stretched in the [1$\bar{1}$0] direction[42]. The author has confirmed that GaAs/AlAs and GaAs/$Al_{0.3}Ga_{0.7}As$ QWs grown on the (775)B GaAs substrates at T_s=580°C, which have flat interfaces, show little polarization anisotropy ($P \leq 0.06$), suggesting that the polarization anisotropy of the (775)B QWRs is not caused by the anisotropic hole mass in the (775)B QW layer. These results provide good evidence for the formation of QWRs on the (775)B substrate (see *Appendix B*). The FWHM of the PL peak (λ=692 nm) from the (775)B QWRs was as small as 15 meV. This is much smaller than that (25 meV) of the same (775)B GaAs/$(GaAs)_4(AlAs)_2$ QWRs grown by the previous MBE process. In the previous process, the surface of the 0.6-nm-thick $(AlAs)_2$ layer grown on the corrugated GaAs QW layer is considered to be microscopically rough since surface migration of Al atoms during the continuous growth is very small [Fig. 6.3 (a)]. Hence, the thickness of the $(AlAs)_2$ layer is considered to be irregularly fluctuated, which results in rather large lateral fluctuation of the potential height of the upper SPS barrier and leads to the broad PL line. On the other hand, in the improved process, the surface of the 0.6-nm-thick $(AlAs)_2$ layer is expected to be smoothed out due to more enhanced surface migration of Al atoms during the growth interruption as schematically illustrated in Fig. 6.3 (b). The PL intensity from the (775)B QWRs was almost the same as that from the (001) QW, indicating that the (775)B QWRs have high optical quality as that of the (001) QW.

In Fig. 6.4, FWHM values of PL peaks at 14 K for the GaAs/$(GaAs)_4(AlAs)_2$ QWRs

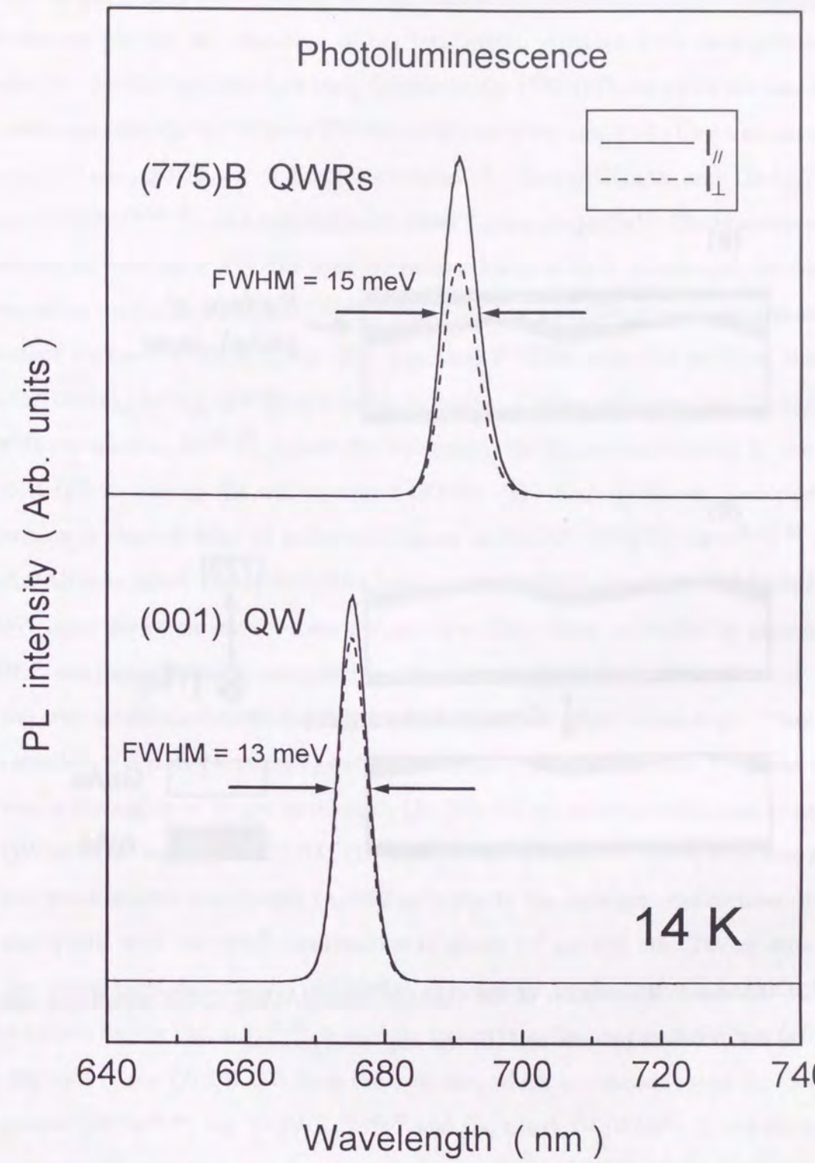

Figure 6.2: Polarized PL spectra (14 K) from the GaAs/$(GaAs)_4(AlAs)_2$ QWRs grown on the (775)B GaAs substrate and a GaAs/$(GaAs)_4(AlAs)_2$ QW simultaneously grown on the (001) GaAs substrate.

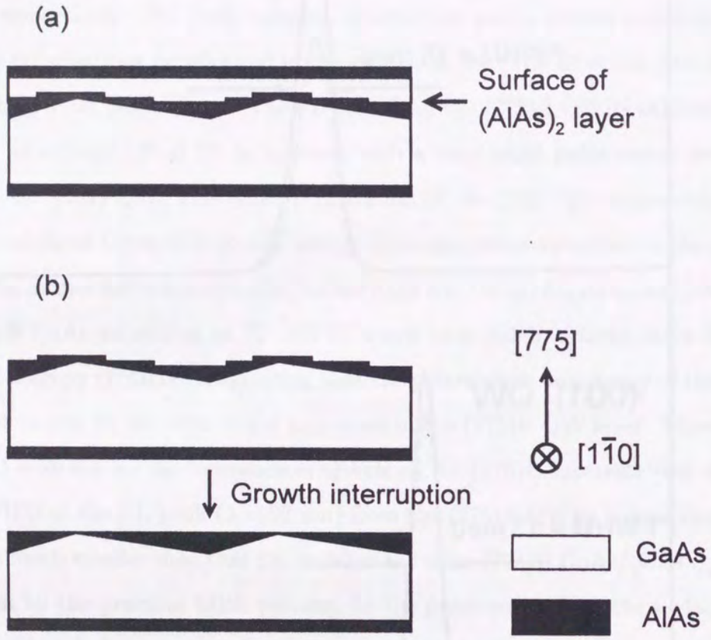

Figure 6.3: Schematic illustration of the GaAs/$(GaAs)_4(AlAs)_2$ QWR structures fabricated by (a) the previous process and (b) the improved process.

grown on the (775)B substrate by the improved MBE process and by the previous MBE process are plotted as a function of PL wavelength, together with data previously reported for the GaAs/$(GaAs)_2(AlAs)_2$ QWRs on the (775)B GaAs substrate (see Chapter 5), self-organized GaAs/AlGaAs QWRs on vicinal (110) and (001) GaAs substrates[31,32], GaAs/AlGaAs QWRs on V-shaped grooves[43,44], GaAs/AlGaAs and GaAs/AlAs T-shaped QWRs[28,45,46] and GaAs/AlGaAs tilted T-shaped QWRs[47]. There seems to be the tendency of increasing FWHM with decreasing luminescence wavelength, as commonly observed in the GaAs/AlGaAs QWs[34,48] (indicated by a broken line) due to the inevitable interface fluctuation of the QWs. The improved FWHM value (15 meV) of the (775)B GaAs/$(GaAs)_4(AlAs)_2$ QWRs is smaller than any of other self-organized GaAs/AlGaAs QWRs reported so far[31,32], apparently indicating the highest uniformity of the present (775)B QWRs among the self-organized QWRs. The GaAs/AlGaAs T-shaped QWRs grown on a cleaved edge of a GaAs/AlGaAs multi-QW (MQW) layer[28,45,46] and the GaAs/AlGaAs tilted T-shaped QWRs formed on a (111)B facet plane of a GaAs/AlGaAs MQW layer grown on reverse-mesa stripes on a (001) GaAs substrate by glancing-angle MBE[47] are most precisely controlled in size with the highest lateral uniformity because of the well established controllability and uniformity of MBE technology. They showed the smallest FWHMs (4–15 meV) for GaAs/AlGaAs QWRs, but their PL peaks were observed in the region of longer wavelength (λ=760–805 nm) due to their large cross section of QWRs. The very small FWHM (15 meV) of the present (775)B QWRs was achieved at the much shorter wavelength (λ=692 nm) due to the stronger confinement of carriers in the QWRs with the small cross section of about 2.7 nm×12 nm. Taking into account of the wavelength dependence of FWHM as observed in the best GaAs/AlGaAs QWs (the broken line in Fig. 6.4)[34,48], it is likely to say that the improved FWHM (15 meV at λ=692 nm) of the (775)B QWRs is the best one, which is comparable to the data of the V-groove QWRs[43,44], the T-QWRs[28,45,46] and the tilted T-QWRs[47]. In addition to this, the present PL was observed from very large number ($\sim 2\times10^4$) of the (775)B QWRs in the area of laser excitation of about 200 μm diameter in contrast with a small number (5–200 QWRs) for V-groove QWRs[43,44] and T-QWRs[28,45–47]. Hence, these results suggest that extremely high uniformity (probably the best uniformity) was achieved in the

self-organized and high-density GaAs/$(GaAs)_4(AlAs)_2$ QWRs grown on the (775)B GaAs substrate by MBE.

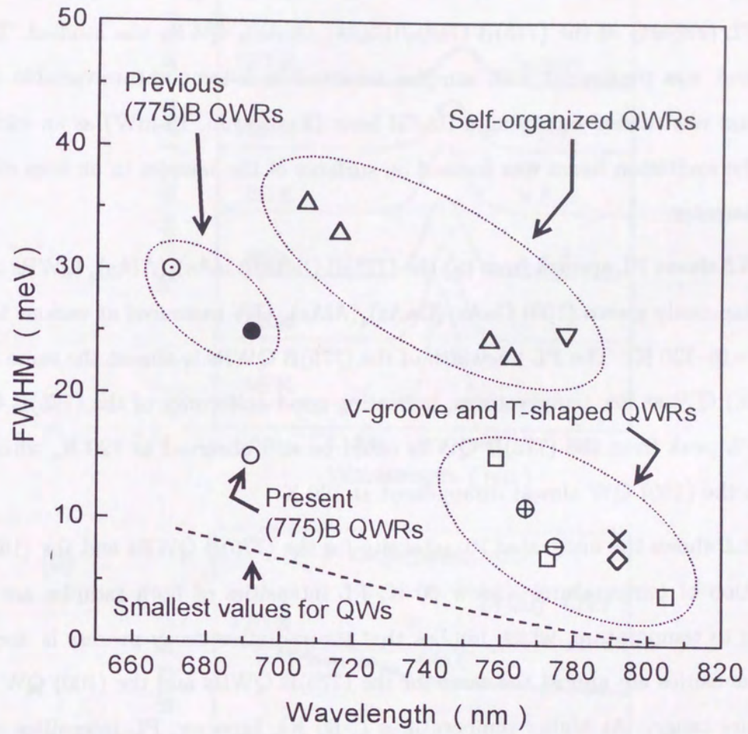

Figure 6.4: FWHMs of PL peaks from the GaAs/$(GaAs)_4(AlAs)_2$ QWRs grown on the (775)B GaAs substrate by the improved MBE process (○) and by the previous MBE process (●) as a function of wavelength. FWHMs reported so far for GaAs/AlGaAs QWRs are also plotted; GaAs/$(GaAs)_2(AlAs)_2$ QWRs on the (775)B GaAs substrate [⊙] (see Chapter 5), self-organized GaAs/AlGaAs QWRs on the vicinal (110) substrate [△][31], self-organized GaAs/AlGaAs QWRs on the vicinal (001) substrates [▽][32], GaAs/AlGaAs QWRs on V-grooves [⊕][43] [⊖][44], GaAs/AlGaAs and GaAs/AlAs T-shaped QWRs [◇][28] [□][45,46] and GaAs/AlGaAs tilted T-shaped QWRs [×][47]. The broken line indicates the smallest FWHMs reported for GaAs/$Al_xGa_{1-x}As$ QWs (x=0.3–1.0)[34,48].

6.3 Temperature dependence of PL properties

Following the PL measurement at a low temperature (14K), the temperature dependence of PL property of the (775)B GaAs/$(GaAs)_4(AlAs)_2$ QWRs was studied. The PL measurement was performed with samples mounted in a temperature-variable He gas cryostat and was carried out using a He-Cd laser (λ=325 nm, 10 mW) as an excitation source. The excitation beam was focused on surfaces of the samples in an area of about 200 μm diameter.

Figure 6.5 shows PL spectra from (a) the (775)B GaAs/$(GaAs)_4(AlAs)_2$ QWRs and (b) the simultaneously grown (100) GaAs/$(GaAs)_4(AlAs)_2$ QW measured at various temperatures (T=16–120 K). The PL linewidth of the (775)B QWRs is almost the same as that of the (100) QW at low temperatures, indicating good uniformity of the (775)B QWRs. A small PL peak from the (775)B QWRs could be still observed at 120 K, while a PL peak from the (100) QW almost disappeared at 120 K.

Figure 6.6 shows the integrated PL intensity for the (775)B QWRs and the (100) QW as a function of temperature. Below 60 K, PL intensities of both samples are rather insensitive to temperature, which implies that the radiative decay process is dominant, and PL intensities are almost the same for the (775)B QWRs and the (100) QW in this temperature range. At higher temperatures ($\geq$60 K), however, PL intensities of both samples decrease with increasing temperature because of an increase of the nonradiative decay process of exicitons. In this range, the PL intensity of the (775)B QWRs drops more slowly and is several times larger at each temperature compared with that of the (100) QW. These results indicate that the nonradiative decay process in the (775)B QWRs is more suppressed than in the (100) QW at elevated temperatures. It is likely to consider that a thermal quenching of the PL intensity for the (775)B QWRs is reduced due to their sharp one-dimensional density of states.

FWHMs of PL peaks from the (775)B QWRs and the (100) QW are plotted as a function of temperature in Fig. 6.7. The FWHM of the (775)B QWRs increases almost linearly with increasing temperature in the range of $T\leq$60 K, and it becomes almost constant at $T\geq$60 K. On the other hand, the FWHM of the (100) QW increases similarly with

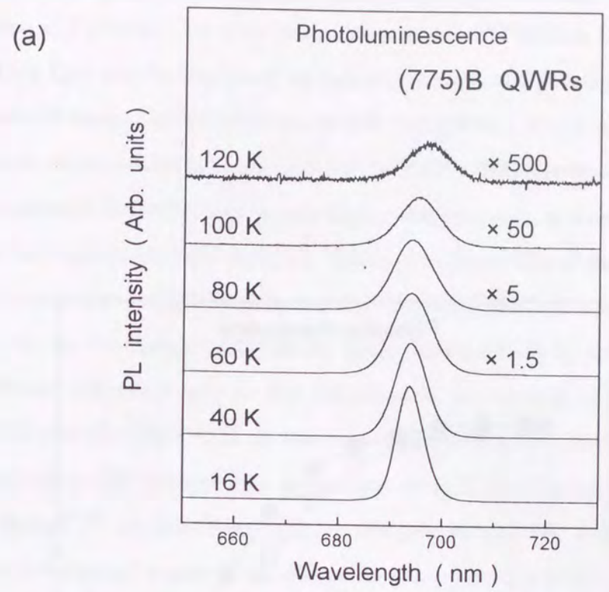

Figure 6.5: PL spectra from (a) the GaAs/$(GaAs)_4(AlAs)_2$ QWRs grown on the (775)B GaAs substrate and (b) a GaAs/$(GaAs)_4(AlAs)_2$ QW on the (100) GaAs substrate at various temperatures (T=16–120 K).

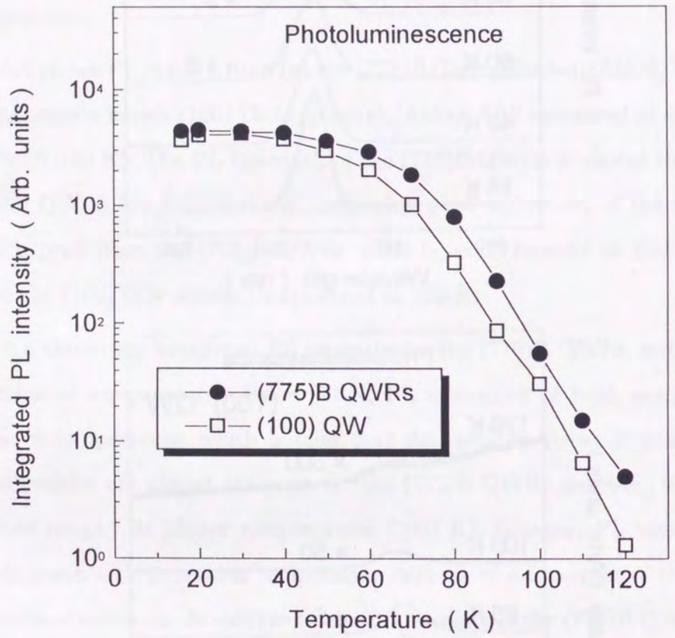

Figure 6.6: Integrated PL intensities for the (775)B GaAs/$(GaAs)_4(AlAs)_2$ QWRs and the (100) GaAs/$(GaAs)_4(AlAs)_2$ QW as a function of temperature.

increasing temperature in the range of $T \leq 50$ K, but it still increases linearly with slightly reduced slope at $T \geq 50$ K. This temperature dependence of FWHMs for the (775)B QWRs and the (100) QW can be explained as follows. At low temperatures, free carriers are trapped at local energy minimum areas in QW (or QWRs), which are formed by lateral fluctuations in thickness of the GaAs QW (or QWRs)[49]. When temperature increases, the carriers are released thermally and occupy higher energy states, as a result, they are widely distributed throughout the QW (QWRs). Hence, PL linewidths of the (100) QW and the (775) QWRs increase similarly with increasing temperature in the low-temperature range ($T \leq 50$–60 K). In the higher temperature range above 50–60 K, however, the FWHM showed different behaviors due to the difference of the density of states between the (775)B QWR and the (100) QW. It has been predicted theoretically that a FWHM of a PL peak from a QW increases in proportion to $k_B T$ because of its two-dimensional density of states[44,50], on the other hand, in the case of a QWR, a PL FWHM becomes almost constant against temperature due to its sharp one-dimensional density of states. The observed FWHM of the (100) QW increased in proportion to 1.19 ± 0.10 $k_B T$ above 50 K, and that of the (775)B QWRs was observed to be almost constant above 60 K (in proportion to 0.05 ± 0.04 $k_B T$). As a result, the PL linewidth of the (775)B QWRs became narrower than that of the (100) QW above 90 K, although the FWHM of the (775)B QWRs was about 2 meV larger than that of the (100) QW at 16 K. These results strongly suggest the one-dimensional characteristics of the (775)B QWRs compared with the (100) QW. Similar thermal broadening of PL linewidth from QWRs and a QW was also reported in the case of the GaAs/AlGaAs QWRs grown on a V-grooved GaAs substrate by MOCVD[44].

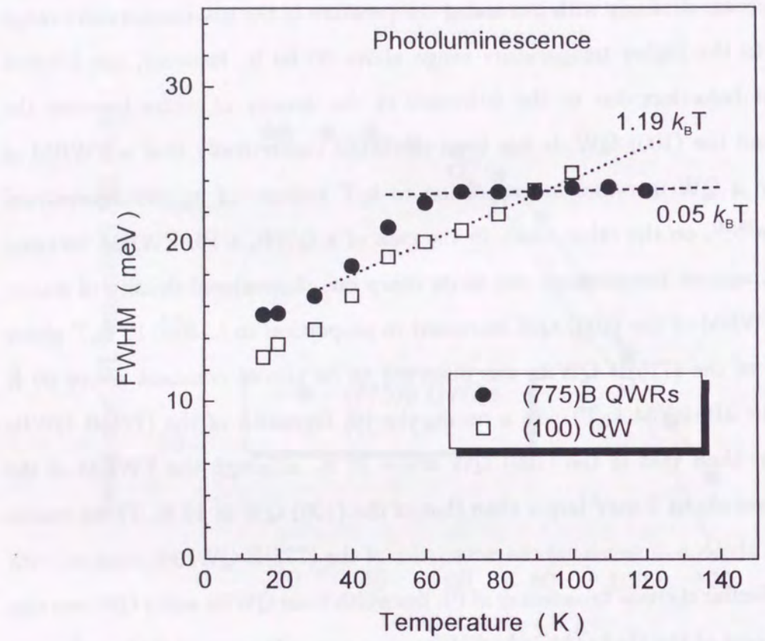

Figure 6.7: FWHMs of PL peaks from the (775)B GaAs/$(GaAs)_4(AlAs)_2$ QWRs and the (100) GaAs/$(GaAs)_4(AlAs)_2$ QW as a function of temperature.

6.4 Temperature dependence of exciton lifetime

Next, a time-resolved PL measurement was done on the (775)B GaAs/$(GaAs)_4(AlAs)_2$ QWRs to estimate exciton lifetimes. Figure 6.8 shows a block diagram of a time-resolved PL measurement system used in this work. The time-resolved PL measurement was carried out using a 2-ps-pulse light (λ=480 nm) with a repetition rate of 4 MHz. The excitation source was a frequency doubler (Spectra Physics model 3980), which supplies second harmonics of a light from a mode-locked Ti-Sapphire laser (Spectra Physics Tsunami system) synchronously pumped by an Ar^+ laser. The excitation beam was focused on a sample surface in an area of about 30 μm diameter by an optical microscope. PL from the sample was observed by a 25-cm-monochromator and a synchronous-scan streak camera with a time resolution of 5 ps.

Probability-density for electron in the ground state of the conduction band in the (775)B GaAs/$(GaAs)_4(AlAs)_2$ QWR structure was calculated by the finite element method. A contour map of the probability-density is shown in Fig. 6.9. The calculated result indicates that there is slight coupling between adjacent QWRs, and that the diameter of QWRs is almost the same as the well width, which is an important point to compare exciton lifetimes of QWRs with those of a QW[51].

Figure 6.10 shows the PL decay curves when samples were excited with the power of 30 μW (a) at 18 K and (b) at 50 K for the (775)B GaAs/$(GaAs)_4(AlAs)_2$ QWRs and the (100) GaAs/$(GaAs)_4(AlAs)_2$ QW. PL decay times were obtained using the single exponential decay model, and solid lines in Fig. 6.10 show the best fits to the data. The PL decay time of the (775)B QWRs at 18 K was 430 ps, which is about 20 % longer than that (360 ps) of the (100) QW, however, it (490 ps) became shorter than that (530 ps) of the (100) QW at 50 K. The excitation light created electron-hole pairs not only in the QWRs (or QW) layer but also in the $(GaAs)_4(AlAs)_2$ barrier layers. By assuming that the barrier layers absorbed 8 % of the incident photons, the number of excited carriers was supposed to be about 3×10^5 cm^{-1}.

The observed PL decay times for the (775)B QWRs and the (100) QW are shown as a function of temperature in Fig. 6.11. The decay time of the (775)B QWRs increases

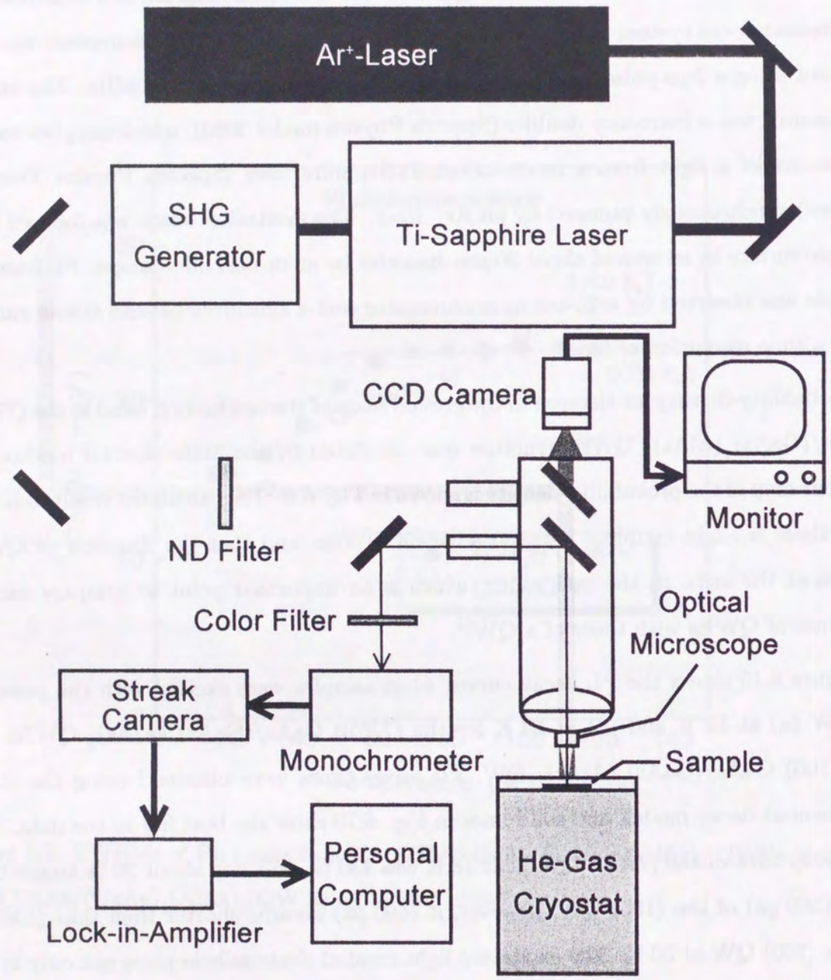

Figure 6.8: Block diagram of a time-resolved PL measurement system.

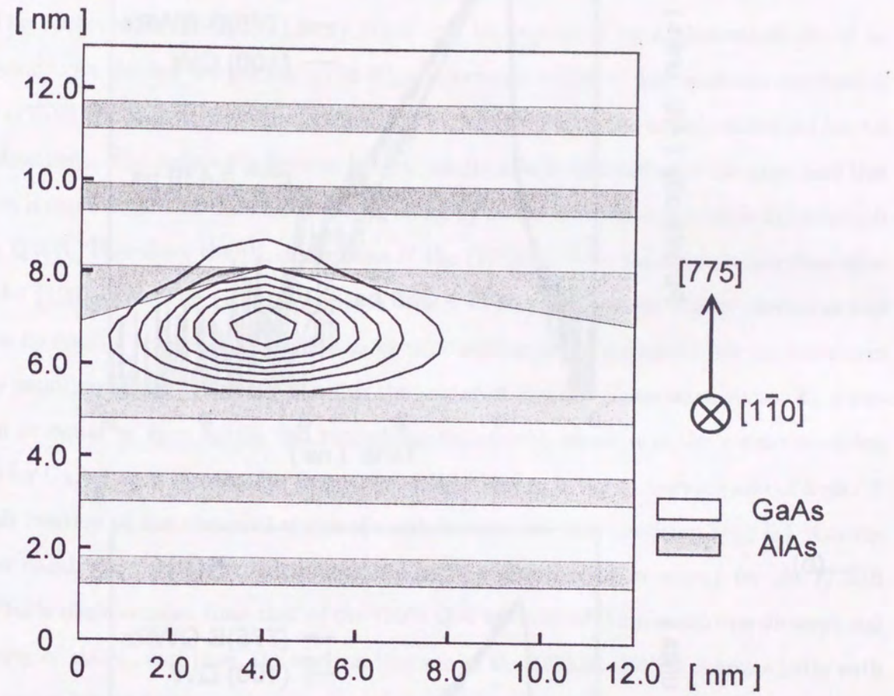

Figure 6.9: Contour map of probability-density $|\Psi|^2$ for electron in the ground state of the conduction band calculated for the (775)B QWR by the finite element method. The contours are lines of $|\Psi|^2 = 0.125,\ 0.25, \cdots,\ 0.875$.

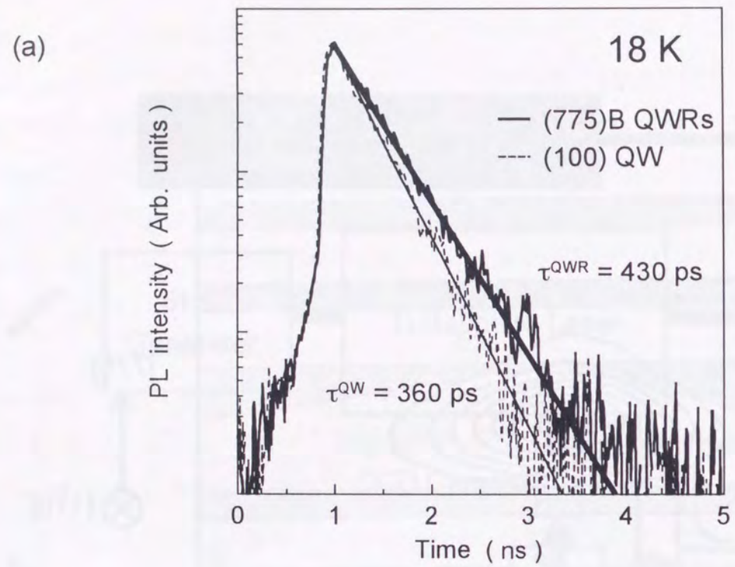

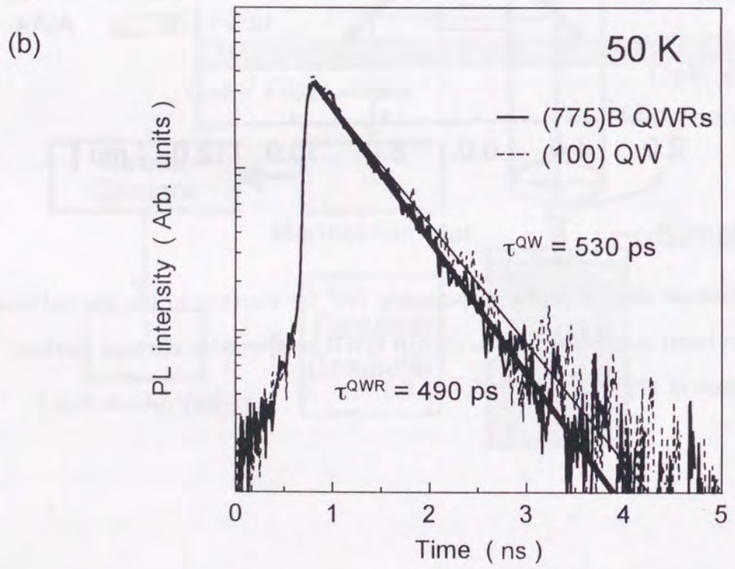

Figure 6.10: Time-resolved PL spectra from the (775)B QWRs and the (100) QW observed (a) at 18 K and (b) at 50 K.

more slowly with increasing temperature than that of the (100) QW in the range of 18 K$\leq T \leq$50 K. Similar results were reported for T-shaped QWRs fabricated by the cleaved-edge overgrowth method[52], ridge-QWRs fabricated on a patterned substrate[53] and serpentine superlattice QWR arrays[54].

The observed results of PL decay times can be explained by a theoretical model as follows[51]. At the low temperature (18 K), a coherence length of free excitons confined in the (775)B QWRs is more reduced than that in the (100) QW due to the additional lateral confinement. The reduced coherence length results in a longer radiative lifetime, and this effect is more dominant than a shortening effect by an enhancement of a oscillator strength in a QWR. Therefore, the PL decay time of the (775)B QWRs becomes longer than that of the (100) QW. The (100) QW has a longer exciton lifetime at higher temperatures since increasing temperature results in broad distribution in energy of free excitons and only small number of excitons of which the center-of-mass in-plane wave vector $k_{\parallel}$ is less than or equal to $k_0 = n\omega/c_0$ can recombine radiatively, where n is the refractive index (3.3 for GaAs), ω is the angular frequency of light and c_0 is the *in vacuo* speed of light. A small fraction of the occupied states of excitons satisfies this condition ($k_{\parallel} \leq k_0$). On the other hand, the thermal broadening of the exciton distribution in energy for the (775)B QWRs is much smaller than that of the (100) QW because of their sharp one-dimensional density of states, and thus, the exciton lifetime in the (775)B QWRs changes little with increasing temperature.

The temperature-dependent radiative lifetimes of free excitons in a QW $[\tau^{\mathrm{QW}}(T)]$[55,56] and in a QWR with cylindrical symmetry $[\tau^{\mathrm{QWR}}(T)]$[52,51] are theoretically obtained as

$$\tau^{\mathrm{QW}}(T) = \frac{3Mk_{\mathrm{B}}T}{\hbar^2 k_0^2}\tau_0^{\mathrm{QW}}, \tag{6.1}$$

$$\tau^{\mathrm{QWR}}(T) = \frac{5}{16}\sqrt{\frac{2\pi Mk_{\mathrm{B}}T}{\hbar^2 k_0^2}}\tau_0^{\mathrm{QWR}}, \tag{6.2}$$

where M is the exciton mass, τ_0^{QW} is the intrinsic radiative lifetime in a QW with $k_{\parallel} = 0$ and τ_0^{QWR} is the intrinsic radiative lifetime of excitons in a QWR with k_L=0 where k_L is the center-of-mass longitudinal wave vector. Eqs. (6.1) and (6.2) indicate that the PL decay time of a QWR increases in proportion to $\sqrt{T}$ and that of a QW increases in proportion to T, respectively. These theoretical expectations are in good agreement with

the temperature dependences of the observed decay times of the (775)B QWRs and the (100) QW as shown in Fig. 6.11. These results imply the good one-dimensional property of the (775)B QWRs. The observed radiative decay times in the range of 18–50 K for the (775)B QWRs and the (100) QW can be fitted by $\tau^{\mathrm{QWR}}(T) = (30\pm5)\,T^{1/2}+(290\pm30)$ [ps] and $\tau^{\mathrm{QW}}(T) = (6\pm1)\,T+(240\pm30)$ [ps], respectively. Using Eqs. (6.1) and (6.2) and a value of $M = 0.25\,m_0$ (m_0: the electron rest mass)[57], the intrinsic radiative lifetimes for the (775)B QWRs and the (100) QW are estimated to be $\tau_0^{\mathrm{QWR}} = 70$ ps and $\tau_0^{\mathrm{QW}} = 7$ ps, respectively. It is notable that these temperature dependences of radiative lifetimes for a QWR and a QW are conserved when excitons are localized by structural fluctuations[51].

Above 70 K, the nonradiative decay process becomes dominant, and the PL decay times for both the (775)B QWRs and the (100) QW decrease with increasing temperature, however, the decay time of the (775)B QWRs decreases more moderately than that of the (100) QW, probably because of the reduced nonradiative decay process due to their sharp one-dimensional density of states. It should be noted that the PL intensity of the (775)B QWRs decreases more slowly above 60 K and is several times larger compared with that of the (100) QW as shown in Fig. 6.6, which is consistent with the present results.

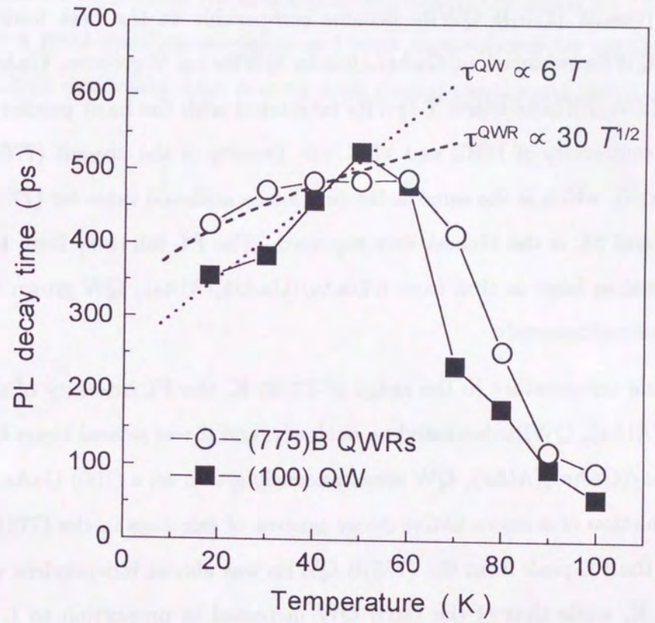

Figure 6.11: Temperature dependence of PL decay times of the (775)B QWRs and the (100) QW.

6.5 Summary

High-density GaAs/$(GaAs)_4(AlAs)_2$ QWRs with much improved uniformity were realized in a thin GaAs/$(GaAs)_4(AlAs)_2$ QW grown on a (775)B GaAs substrate by MBE. The PL peak from the QWRs at 14 K showed large polarization anisotropy ($P = 0.19$). FWHM of the PL peak was as small as 15 meV at the short wavelength of λ=692 nm, which is the smallest ever observed for self-organized GaAs/AlGaAs QWRs. Uniformity of the present (775)B QWRs became comparable to the best uniformity for GaAs/AlGaAs QWRs achieved in GaAs/AlGaAs QWRs on V-grooves, GaAs/AlGaAs T-QWRs and GaAs/AlGaAs tilted T-QWRs fabricated with the most precise controllability and high uniformity of MBE and MOCVD. Density of the present (775)B QWRs (8×10^5 QWRs/cm), which is the same as the previously achieved value for (775)B QWRs (see Chapter 3 and 5), is the highest ever reported. The PL intensity from the (775)B QWRs was almost as large as that from a GaAs/$(GaAs)_4(AlAs)_2$ QW grown on a (001) GaAs substrate simultaneously.

With increasing temperature in the range of $T\geq$60 K, the PL intensity of the (775)B GaAs/$(GaAs)_4(AlAs)_2$ QWRs decreased more slowly, and it was several times larger than that of the GaAs/$(GaAs)_4(AlAs)_2$ QW simultaneously grown on a (100) GaAs substrate, indicating a reduction of a nonradiative decay process of exicitons in the (775)B QWRs. The FWHM of the PL peak from the (775)B QWRs was almost independent of temperature above 60 K, while that of the (100) QW increased in proportion to 1.19 $k_{\rm B}$T in the range of $T\geq$50 K. These results are in good agreement with the theoretical expectation, that is, a FWHM of a PL peak from a QW increases in proportion to $k_{\rm B}T$ because of its two-dimensional density of states, while that of a QWR is almost independent of temperature due to its sharp one-dimensional density of states.

The PL decay time of the (775)B QWRs was 430 ps at 18 K, which was about 20 % longer than that (360 ps) of a GaAs/$(GaAs)_4(AlAs)_2$ QW simultaneously grown on a (100) GaAs substrate, indicating a more decreased coherence length of excitons in the (775)B QWRs than that in the (100) QW. The decay time of the (775)B QWRs, however, increased more slowly with increasing temperature, and it became shorter than that of

the (100) QW at 50 K, which is due to their sharp one-dimensional density of states of the (775)B QWRs. In the rage of 70–80 K, the decay time of the (775)B QWRs was longer than that of the (100) QW, implying that a nonradiative decay process of exicitons in the (775)B QWRs was more reduced than that in the (100) QW due to the one-dimensional density of states. Such apparently different behavior of the PL decay time of the (775)B QWRs compared with the (100) QW clearly suggests the good one-dimensional property of the (775)B QWRs.

These results indicate that the GaAs/$(GaAs)_4(AlAs)_2$ QWRs on the (775)B GaAs substrate have a good one-dimensionality and meet requirements for applications to QWR lasers, i.e., high uniformity, high density, high optical quality and simple fabrication process.

Chapter 7

Growth Mode of GaAs on High-Index GaAs Substrates around (775)B Plane

In this chapter, growth modes of GaAs layers grown on several high-index GaAs substrates around a (775)B plane are presented. This study was done to search the best surface orientation around a (775)B surface for fabrication of GaAs QWRs.

7.1 Surface AFM observation

Five kinds of GaAs substrates with different high-index surfaces were used, which were (776)B-, (775)B-, (332)B-, (553)B- and (221)B-oriented substrates. These surfaces correspond to 4°-, 8.5°-, 10°-, 12.3°- and 15.3°-off ones from the (111)B-oriented surface to the (110)-oriented surface (see Fig. 1.2).

Figure 7.1 shows a GaAs(4 nm)/AlAs(10 nm) superlattice (SL) structure grown on the high-index GaAs substrates for structural analysis by surface AFM observation. MBE growth conditions of these samples were as follows. Substrate temperatures (T_s) were 580 and 650°C, V/III pressure ratios for GaAs and AlAs were 7 and 12, respectively. The growth rate for GaAs and AlAs layers was 1 μm/h. Substrates were rotated during the MBE growth at a rate of 30 rpm.

Figure 7.2 shows surface AFM images of 4-nm-thick GaAs top layers of the GaAs(4 nm)/AlAs(10 nm) SL structures on the high-index GaAs substrates grown at (a) T_s=580°C and (b) T_s=650°C. In the case of T_s=580°C, a little difference was observed in surface morphologies due to the difference of surface orientation, and the vertical amplitudes of steps on all surfaces were only 1–2 monolayer at most, that is, all surfaces were flat. On the other hand, two types of morphology were observed for T_s=650°C. Corrugated surfaces were seen for (776)B, (775)B and (332)B substrates, and flat surfaces were obtained for (553)B and (221)B substrates. Among corrugated surfaces, corrugation on the (332)B surface was just like that on the (775)B surface. In the both samples, the lateral period was approximately 12 nm, and the vertical amplitude was approximately 1.2 nm. The lateral period and vertical amplitude of the (776)B corrugation were a little larger than those of the (775)B and the (332)B corrugations, which were approximately 20 nm and 2 nm, respectively.

These results imply that GaAs QWRs like the (775)B ones reported in Chapters 3, 5 and 6 can be grown not only on (775) GaAs substrates but also on (776)B and (332)B GaAs substrates.

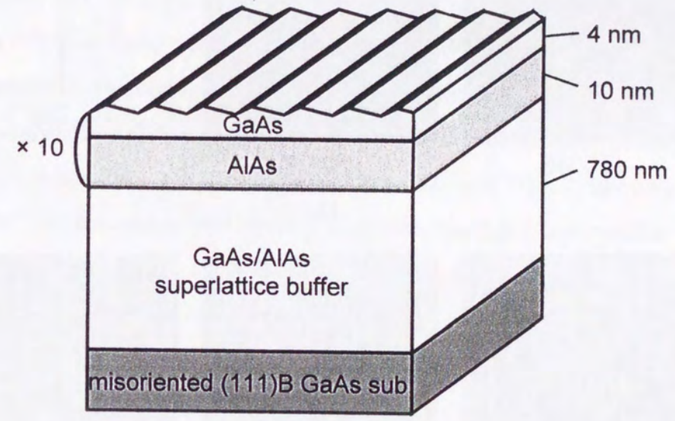

Figure 7.1: Schematic illustration of a GaAs(4 nm)/AlAs(10 nm) superlattice structure grown on high-index GaAs substrates around a (775)B plane.

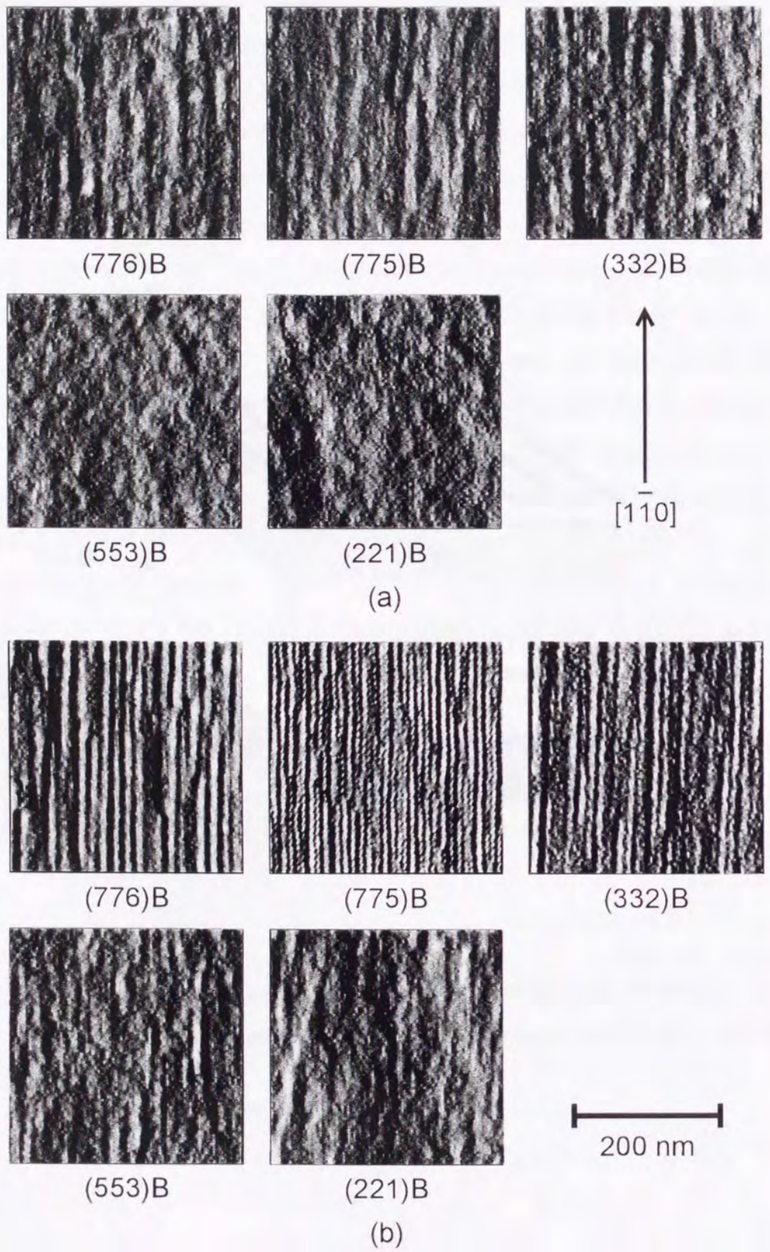

Figure 7.2: Surface AFM images of 4-nm-thick GaAs layers of the GaAs(4 nm)/AlAs(10 nm) superlattice structures on high-index GaAs substrates grown at (a) T_s=580°C and (b) T_s=650°C.

7.2 PL properties

Figure 7.3 shows a GaAs/$(GaAs)_4(AlAs)_2$ QWs (QWRs) structure with well widths of L_w=2.1, 3.0 and 4.2 nm grown on the high-index GaAs substrates for optical analysis by PL measurements. The growth procedure of this structure was the same to that of the improved GaAs/$(GaAs)_4(AlAs)_2$ QWRs grown on the (775)B substrate in Chapter 6. $(GaAs)_4(AlAs)_2$ short-period superlattice (SPS) barrier layers and buffer layers were grown at T_s=580°C, and QW (QWRs) layers and $(AlAs)_2$ layers which were the bottom parts of upper SPS barriers were grown at T_s=650°C. The V/III pressure ratio was 7 (12) for GaAs (AlAs), and the growth rate for GaAs and AlAs layers was 1.0 μm/h.

PL spectra from the GaAs/$(GaAs)_4(AlAs)_2$ QWs (QWRs) with well widths of 2.1, 3.0 and 4.2 nm grown on the high-index GaAs substrates are shown in Fig. 7.4. Three clear peaks from three kinds of QW are seen in the PL spectra for all samples, which correspond to the 2.1-nm, 3.0-nm and 4.2-nm QWs, respectively. There is little difference at the point of PL intensity for all samples, on the other hand, PL linewidths are various.

Figure 7.5 shows FWHMs of PL peaks from QWs grown on the high-index GaAs substrates as a function of well width. The result indicates that PL FWHMs of the (775)B QWs (QWRs) and the (221)B QWs are smallest, namely, the (775)B QWs (QWRs) and the (221)B QWs have the best uniformity of size among the samples. Hence, it was found that the (775)B substrate is the most suitable for fabrication of GaAs QWRs.

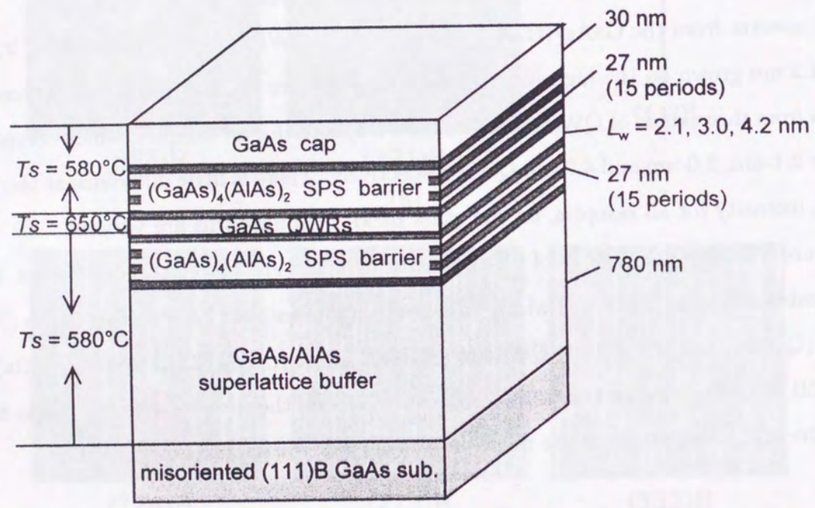

Figure 7.3: Schematic illustration of a GaAs/(GaAs)$_4$(GaAs)$_2$ QWs (QWRs) structure grown on high-index GaAs substrates.

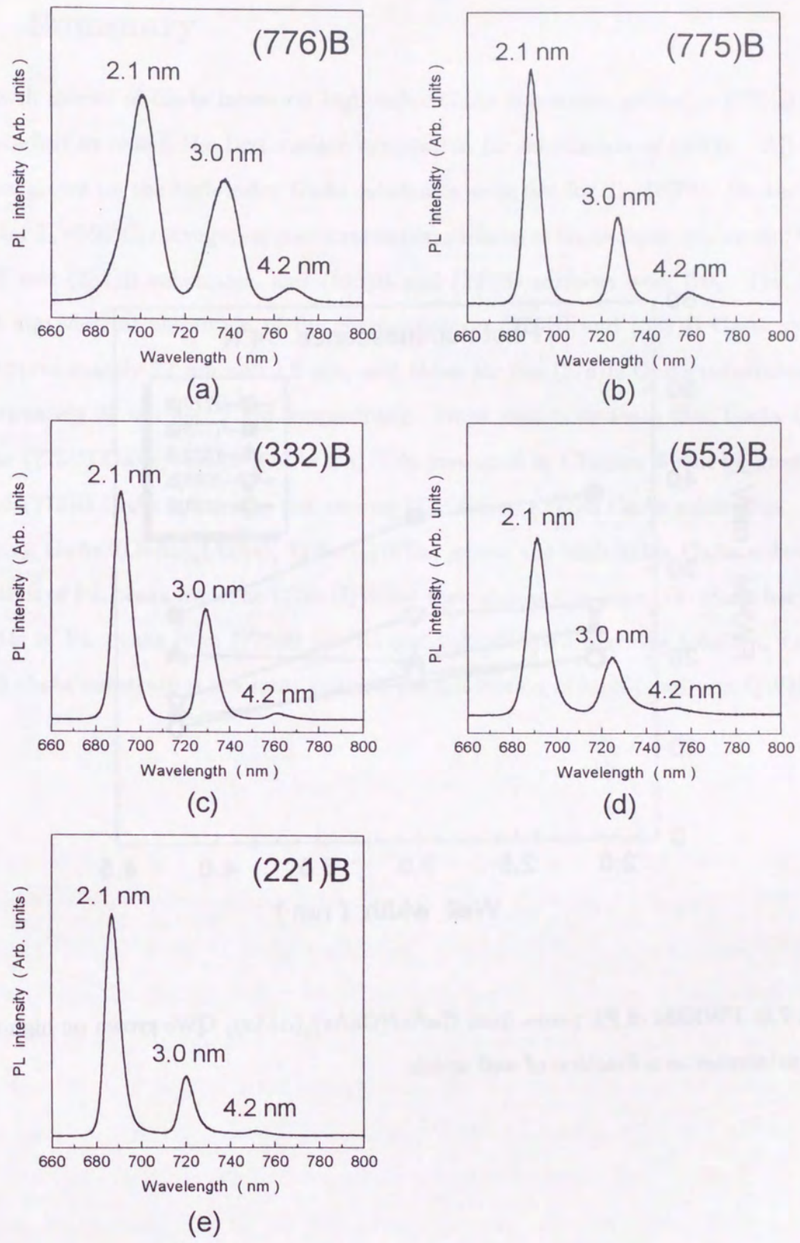

Figure 7.4: PL spectra from GaAs/(GaAs)$_4$(AlAs)$_2$ QWs (QWRs) with well widths of 2.1, 3.0 and 4.2 nm grown on high-index GaAs substrates of (a) (776)B, (b) (775)B, (c) (332)B, (d) (553)B and (e) (221)B.

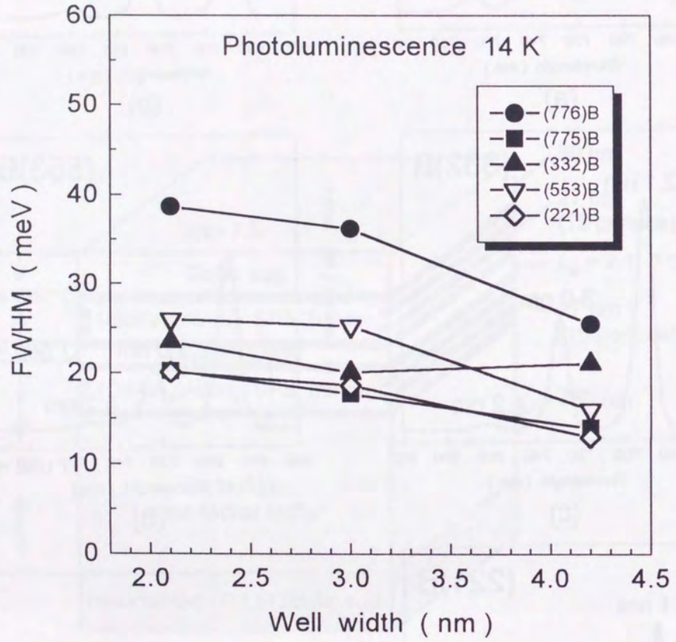

Figure 7.5: FWHMs of PL peaks from GaAs/$(GaAs)_4(AlAs)_2$ QWs grown on high-index GaAs substrates as a function of well width.

7.3 Summary

Growth modes of GaAs layers on high-index GaAs substrates around a (775)B plane were studied to search the best surface orientation for fabrication of QWRs. All GaAs surfaces grown on the high-index GaAs substrates were flat for T_s=580°C. On the other hand, for T_s=650°C, corrugation was observed on surfaces of GaAs layers grown on (776)B, (775)B and (332)B substrates, and (553)B and (221)B surfaces were flat. The lateral period and vertical amplitude of the corrugation on (775)B and (332)B GaAs surfaces were approximately 12 nm and 1.2 nm, and those for the (776)B GaAs substrates were approximately 20 nm and 2 nm, respectively. These results indicate that GaAs QWRs like the (775)B GaAs/$(GaAs)_4(AlAs)_2$ QWRs presented in Chapter 6 can be grown not only on (775)B GaAs substrates but also on (776)B and (332)B GaAs substrates.

Among GaAs/$(GaAs)_4(AlAs)_2$ QWs (QWRs) grown the high-index GaAs substrates, intensities of PL peaks from the QWs (QWRs) were almost the same. On the other hand, FWHMs of PL peaks from (775)B QWRs and (221)B QWs were the smallest, i.e., the (775)B GaAs substrate is the most suitable for fabrication of highly uniform QWRs.

Chapter 8

$GaAs/(GaAs)_4(AlAs)_2$ Quantum Wire Laser

Fabrication of stripe-geometry $GaAs/(GaAs)_4(AlAs)_2$ graded refractive index separate confinement heterostructure (GRIN-SCH) QWR lasers grown on (775)B GaAs substrates and their device characteristics are described.

8.1 Si and Be doping properties

In case of high-index GaAs substrates such as (311)A and (411)A GaAs substrates, doping properties of epitaxial layers are not the same as those for conventional (100) GaAs substrates[58–60]. In order to confirm doping properties of GaAs layers grown on (775)B GaAs substrates, Si- and Be-doped GaAs layers (1.5-μm-thick) were simultaneously grown on (775)B, (100) and (111)B GaAs substrates as a function of Si and Be effusion cell temperatures. The substrate temperature was 580°C, the V/III pressure ratio was 10, and the growth rate was 1 μm/h, respectively. Carrier concentration and mobility were determined by *van der Pauw* Hall measurements with a current of 10–100 nA.

Figure 8.1 shows Si and Be effusion cell temperature dependences at 77 K and room temperature (RT) of carrier concentrations in GaAs layers grown on (775)B, (100) and (111)B GaAs substrates. There is little difference in carrier concentration between (775)B samples and reference samples for both Si- and Be-doped GaAs layers.

Figure 8.2 shows surface morphologies of Si- and Be-doped GaAs layers grown on (775)B, (100) and (111)B GaAs substrates observed by a Normarski optical microscopy. Surfaces of (775)B and (100) samples are flat regardless of doping concentration, on the other hand, surfaces of all (111)B samples are rough.

Figure 8.3 shows electron and hole mobilities at 77 K and RT in Si- and Be-doped GaAs layers grown on (775)B, (111)B and (100) GaAs substrates as a function of carrier concentration. Electron and hole mobilities for (775)B samples are almost the same as those for (100) samples, however, those for (111)B samples alone are smaller. It can be considered that this result is due to poor crystal quality of GaAs layers grown on (111)B GaAs substrates. The (111)-oriented surfaces are very attractive because of its superior properties, such as high optical gain[61–63], second-harmonic generation[64,65] and piezo-electric effect. However, it is very difficult to obtain flat surfaces of GaAs layers grown on both (111)A and (111)B GaAs substrates[66–69]. The (775)B surface is of only 8.5°-off from the (111)B surface, thus the superior properties expected for the (111)B surface are also expected for the (775)B surface, in addition to the easy growth of high-quality epitaxial layers on the (775)B surface.

These results indicate that (775)B GaAs substrates can be treated just like conventional (100) GaAs substrates in respect of Si and Be doping into GaAs epitaxial layers.

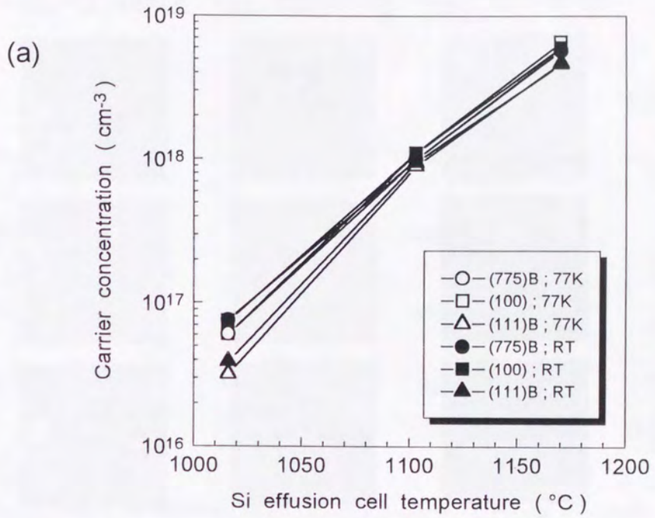

Figure 8.1: Si and Be effusion cell temperature dependences at 77 K and room temperature (RT) of carrier concentrations in GaAs layers grown on (775)B, (100) and (111)B GaAs substrates; (a) Si doping at 77 K, (b) Si doping at RT, (c) Be doping at 77 K and (d) Be doping at RT.

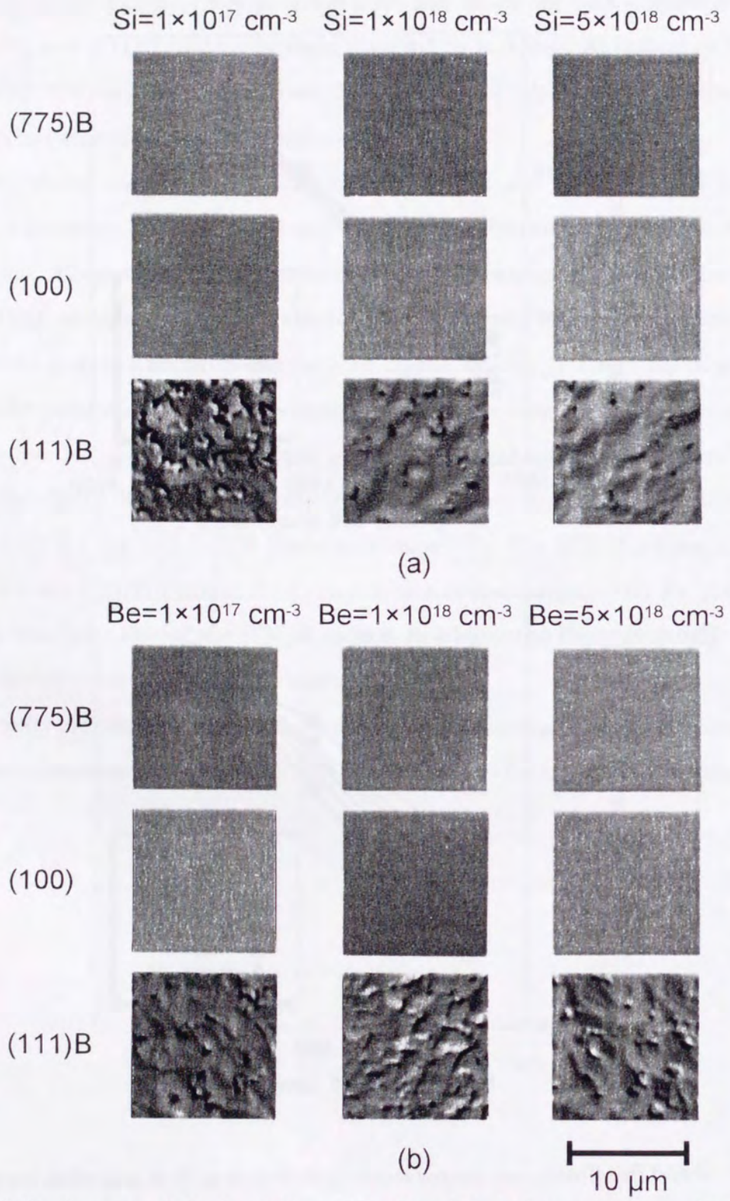

Figure 8.2: Surface morphologies of Si- and Be-doped GaAs layers grown on (775)B, (100) and (111)B GaAs substrates observed by a Normarski optical microscopy; (a) Si-doped GaAs layers and (b) Be-doped GaAs layers.

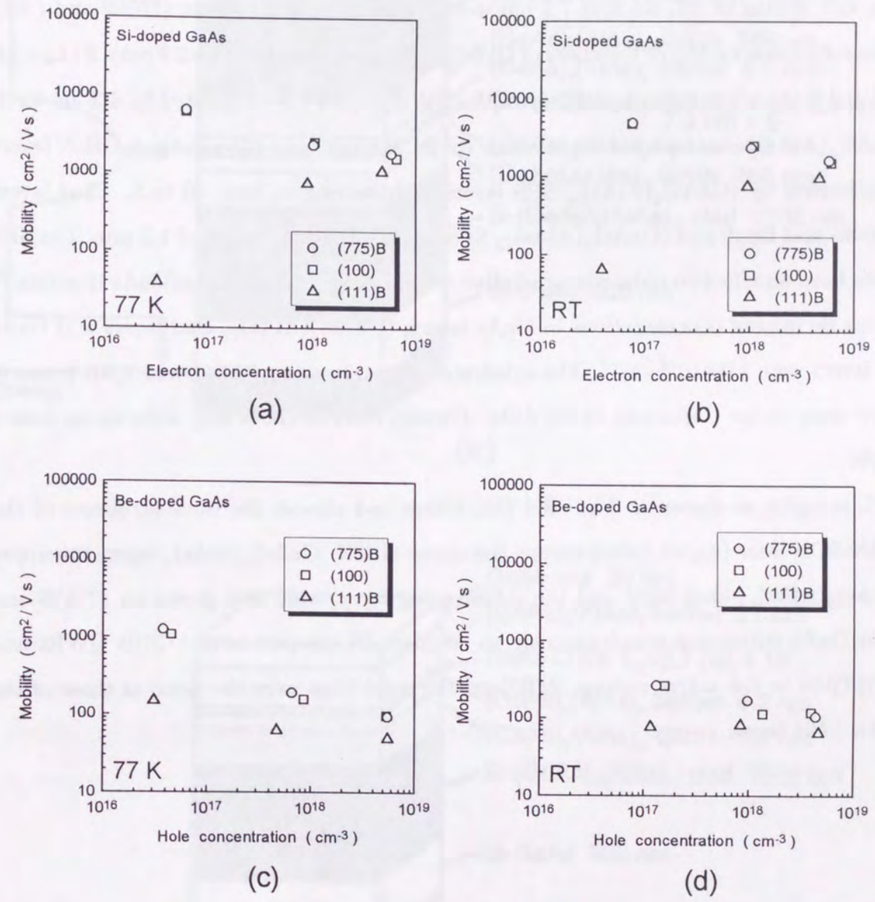

Figure 8.3: Mobilities of electron and hole at 77 K and RT in Si- and Be-doped GaAs layers grown on (775)B, (111)B and (100) GaAs substrates as a function of carrier concentration; (a) Si-doped GaAs at 77 K, (b) Si-doped GaAs at RT, (c) Be-doped GaAs at 77 K and (d) Be-doped GaAs at RT.

8.2 Sample structure

Figure 8.4 (a) shows a schematic illustration of a GaAs/$(GaAs)_4(AlAs)_2$ GRIN-SCH QW (QWR) laser structure and its energy band diagram. Three kinds of laser structure with well widths of 2.7, 3.6 and 7.2 nm were simultaneously grown on (775)B and (100) GaAs substrates by MBE. Numbers of QW (QWR) layer were 10 (L_w=2.7 nm), 8 (L_w=3.6 nm) and 5 (L_w=7.2 nm), respectively. QW (QWR) layers were separated by 4.2-nm-thick $(GaAs)_4(AlAs)_2$ short-period superlattice (SPS) barriers, and 168-nm-thick GRIN layers were formed by $(GaAs)_4(AlAs)_m$ SPS layers with varying m from 10 to 2. Clad layers were Si- and Be-doped $(GaAs)_4(AlAs)_{12}$ SPS layers with a thickness of 1.5 μm. The SPS layers have an effect to reduce nonradiative recombination at the AlAs/GaAs interface[70]. Si and Be doping concentrations in GaAs layers, $(GaAs)_4(AlAs)_{12}$ clad layers and GaAs cap layers were 2.0×10^{18} cm^{-3}. The substrate temperature was 700°C, and V/III pressure ratios were 12 for GaAs and 19 for AlAs. Growth rates of GaAs and AlAs layers were 1 μm/h.

PL samples as shown in Fig. 8.4 (b), which had almost the same structure of the GRIN-SCH laser (L_w=2.7 nm) except the upper GRIN $(GaAs)_4(AlAs)_n$ layer, the upper $(GaAs)_4(AlAs)_{12}$ clad layer and the p-GaAs cap layer, were also grown on (775)B and (100) GaAs substrates simultaneously to estimate PL properties of (775)B QWRs and (100) QWs in the active regions. MBE growth conditions were the same as those of the GRIN-SCH lasers.

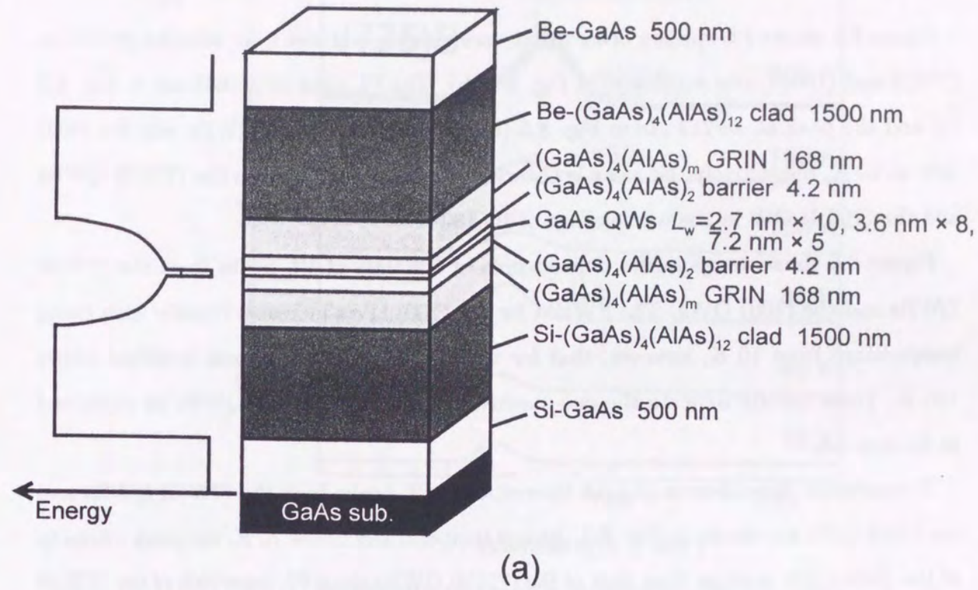

Figure 8.4: Schematic illustrations of (a) a GaAs/$(GaAs)_4(AlAs)_2$ GRIN-SCH QWR (QW) laser structure and (b) a GaAs/$(GaAs)_4(AlAs)_2$ QWR (QW) structure for PL observation grown on (775)B and (100) GaAs substrates by MBE.

8.3 PL properties

Figure 8.5 shows PL spectra observed at various temperatures from samples grown on (775)B and (100) GaAs substrates in Fig. 8.4 (b). The PL peak at λ=688 nm in Fig. 8.5 (a) and the peak at λ=714 nm in Fig. 8.5 (b) are from the (775)B QWRs and the (100) QW at 10 K, respectively. No peak is observed except the peaks from the (775)B QWRs and the (100)B QW in the whole range of 10–180 K.

Figure 8.6 shows temperature dependences of FWHMs of PL peaks from the (775)B QWRs and the (100) QWs. The FWHM for the (100) QWs increases lineally with rising temperature from 10 K, however, that for the (775)B QWRs is almost constant above 120 K. These results indicate the one-dimensionality of the (775)B QWRs as explained in Section 6.3.

Temperature dependences of peak intensities of PL peaks from the (775)B QWRs and the (100) QWs are shown in Fig. 8.7. At low temperatures below 70 K, the peak intensity of the (100) QWs is larger than that of the (775)B QWRs since PL linewidth of the (775)B QWRs is much larger than that of the (100) QWs as shown in Fig. 8.5. However, the PL peak intensity of the (100) QWs is almost the same as that of the (775)B QWRs in the range of 70–150 K, and the (775)B QWRs excel the (100) QWs above 160 K. These results are also explained by the difference of the density of states between the (775)B QWRs and the (100) QWs (see Section 6.3). Moreover, PL peak intensity is connected with a threshold current of laser directly, thus it should be noted that these PL results for the (775)B QWRs and the (100) QWs above 160 K are very important for the operation of lasers at RT.

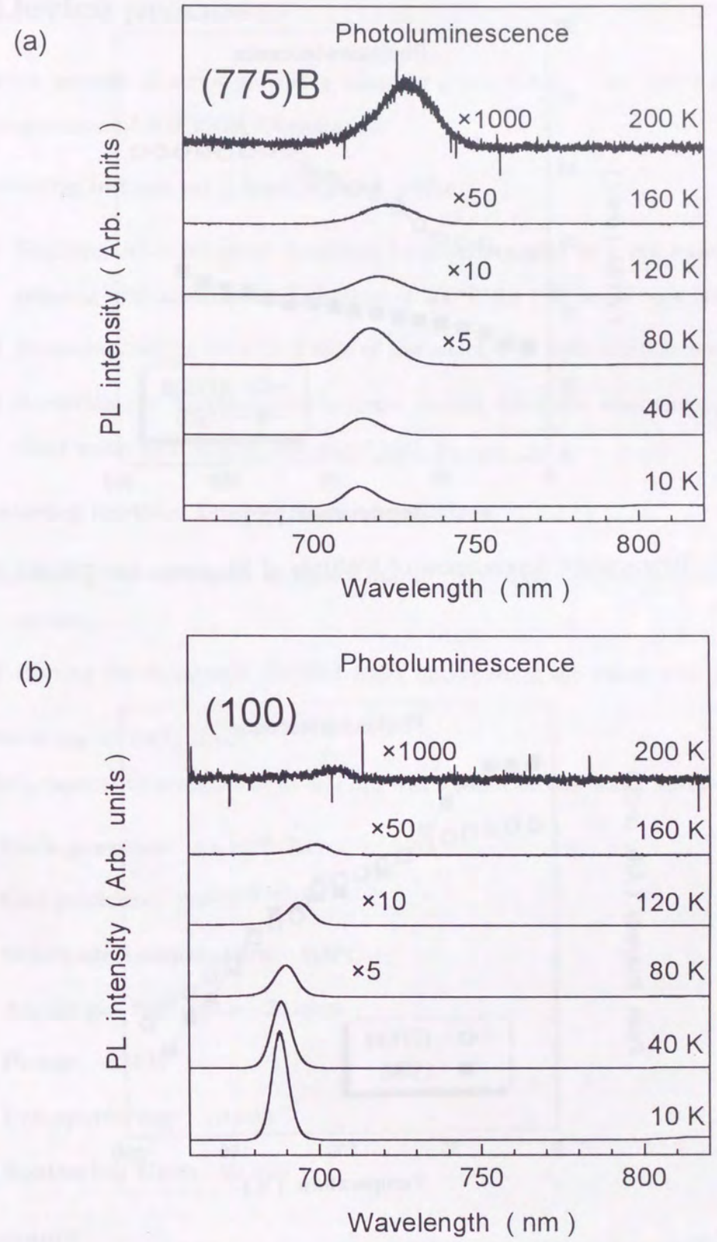

Figure 8.5: PL spectra from (a) (775)B QWRs and (b) (100) QWs observed at various temperatures.

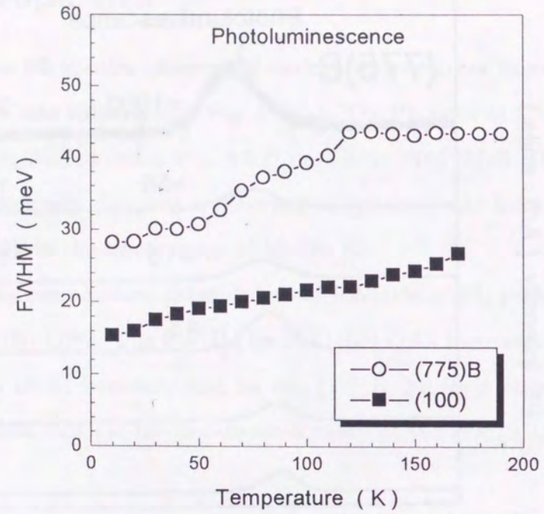

Figure 8.6: Temperature dependences of FWHMs of PL peaks for (775)B QWRs and (100) QWs.

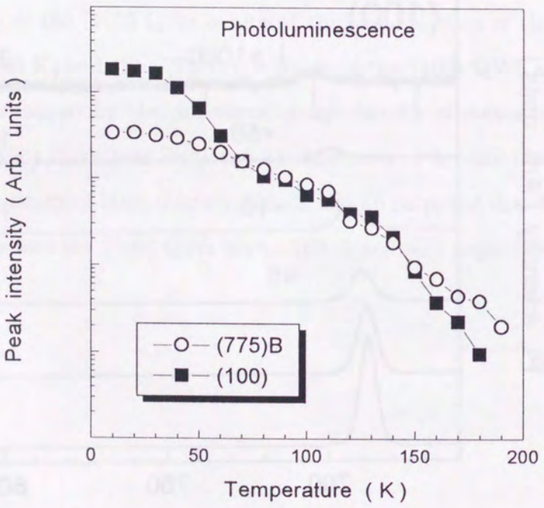

Figure 8.7: Temperature dependences of peak intensities of PL peaks for (775)B QWRs and (100) QWs.

8.4 Device process

Fabrication process of stripe-geometry lasers is given below. The lasers were made under a cooperation of KUBOTA Corporation.

1. **Removing indium on a back side of wafer**

   (a) Applying AZ-2000 resist (positive) to a surface side of a epi-wafer after degreasing with acetone and baking it at 200°C for 1–2 hours on a hot plate.

   (b) Removing indium on a back side of the wafer with hydrochloric acid (HCl).

   (c) Removing the AZ resist with acetone, baking the wafer after rinsing with distilled water and blowing the water with N_2 gas.

2. **Removing oxidized film on the wafer surface**

   (a) Etching the wafer with HCl for 3 min to remove an oxidized film on the wafer surface.

   (b) Rinsing the wafer with distilled water and blowing the water with N_2 gas.

3. **Spattering of SiO_2 film**

   A SiO_2 layer with a thickness of 400 nm was formed on the wafer surface.

   Back pressure: 5×10^{-6} Torr

   Gas pressure: 5×10^{-3} Torr

   Substrate temperature: 200°C

   Argon gas flow rate: 20 sccm

   Power: 300 W

   Pre-spattering: 10 min

   Spattering time: 10 min

4. **Exposure**

   (a) Baking the wafer at 120°C for 10 min on a hot plate. This process can be omitted when the wafer is just after spattering of a SiO_2 film.

(b) Applying OMR83-25cp (negative) resist to the surface side of the wafer with a rotation of 6000 rpm for 20 sec.

(c) Baking the wafer at 110°C for 2 min on a hot plate.

(d) Setting a photo-mask for making stripes on the wafer surface and exposing with ultraviolet ray (15 mW, 6 sec).

(e) Developing the wafer with exclusive developer at RT for 1 min.

(f) Rinsing the wafer with exclusive rinse at RT for 1 min.

(g) Baking the wafer at 150°C for 30 min in an oven.

5. **Etching SiO_2 film**

(a) Etching the SiO_2 film with buffered hydrofluoric acid for 4–5 min.

(b) Rinsing the wafer with distilled water and blowing the water with N_2 gas.

(c) Removing the OMR resist in an ozonizer.

6. **Removing oxidized film on the wafer surface**

(a) Etching the wafer with HCl for 3 min.

(b) Rinsing the wafer with distilled water and blowing the water with N_2 gas.

7. **Forming electrode on the surface side**

(a) Applying OFPR80-200cp (positive) resist to the surface side of the wafer with a rotation of 4000 rpm for 20 sec.

(b) Pre-Baking the wafer at 60°C for 2 min on a hot plate.

(c) Setting a photo-mask for electrodes on the wafer surface and exposing with ultraviolet ray (15 mW, 75 sec).

(d) Developing the wafer with exclusive developer at RT for 1 min, rinsing the wafer with distilled water and blowing the water with N_2 gas.

(e) Post-baking the wafer at 60 °C for 20 min on a hot plate.

(f) Evaporating Cr (5 nm), Au (10 nm), Au-Zn (100 nm) at a background pressure of 5×10^{-6} Torr and a substrate temperature of 150°C in a vacuum evaporating equipment.

(g) Removing the OFPR resist from the wafer surface by acetone in an ultrasonic bath (lift-off), rinsing it by isopropyl alcohol (IPA), methanol and distilled water and blowing the water with N_2 gas.

(h) Alloying the wafer at 450°C for 10 min in N_2 gas atmosphere.

8. **Grinding**

(a) Pasting the surface side of the wafer on a glass holder with heated electron wax.

(b) Removing the wax on the glass holder and the back side of the wafer with acetone-absorbed swabs.

(c) Grinding a substrate part of the wafer by a rapping disk to a thickness of about 100 μm.

(d) Heating the glass holder and tearing the wafer from the glass holder.

(e) Cleaning the wafer with acetone, IPA, methanol and distilled water and blowing the water with N_2 gas.

9. **Forming electrode on the back side**

(a) Evaporating Au-Ge (100 nm) and Ni (30 nm) on the back side of the wafer at a back pressure of 5×10^{-6} Torr without heating the wafer.

(b) Alloying the wafer at 420°C for 10 min in N_2 gas atmosphere.

10. **Cleaving**

(a) Scribing the wafer surface by a diamond scriber to the size of the cavity length.

(b) Cleaving the wafer by hand with tweezers.

8.5 Laser characteristics

Device characteristics of GRIN-SCH QW (QWR) lasers grown on (775)B and (100) GaAs substrates were measured in a shape of bar before cutting them to tips as shown in Fig. 8.8 (a). Fabry-Perot mirrors of lasers were uncoated. The cavity length and stripe width of lasers were 250 μm and 10 μm, respectively. Samples were measured by clipping one laser in the bar between a metal probe and a metal plate as shown in Fig. 8.8 (b). Emission from the laser was detected by a Si photo-detector.

The light output versus current (I-L) curves were measured at RT under a condition of pulsed current for randomly selected ten GaAs/$(GaAs)_4(AlAs)_2$ GRIN-SCH QW (QWR) lasers (pulse duration: 400 ns). The I-L characteristics for the (775)B QWR and the (100) QW lasers are shown in Fig. 8.9. Average (minimum) threshold currents ($I_{\rm th}$) of (775)B QWR lasers were 77.4 (70.0), 73.7 (66.4) and 54.4 (51.6) mA for $L_{\rm w}$ of 2.7, 3.6 and 7.2 nm, respectively. On the other hand, those of the (100) QW lasers were 272.9 (254) and 82.4 (78.4) mA for $L_{\rm w}$ of 3.6 and 7.2 nm, respectively. The (100) QW laser with $L_{\rm w}$ of 2.7 nm did not oscillate in the range of 0–400 mA (400 mA is a maximum value of a measurement instrument used in this study). Figure 8.10 shows lasing spectra from the (775)B QWR and the (100) QW lasers at RT under a condition of current of $I_{\rm th}\times1.6$, and the lasing wavelengths were 761, 791 and 846 nm for the (775)B QWR lasers with $L_{\rm w}$ of 2.7, 3.6 and 7.2 nm, respectively, and those for the (100) QW lasers with $L_{\rm w}$ of 3.6 and 7.2 nm were 776 and 842 nm, respectively.

Figure 8.11 shows the well width dependence of $I_{\rm th}$ for the lasers grown on (775)B and (100) GaAs substrates. Increase of observed $I_{\rm th}$ with decreasing well width for the (100) QW lasers likely supports the theoretical model, where the nonradiative recombination of electrons from L valleys increases with decreasing well width[71]. On the other hand, $I_{\rm th}$ for the (775)B QWR lasers is almost constant, and thus, it indicates that all carriers injected into the active region contribute to the stimulated emission. This result admits of two interpretations. One interpretation is by the sharp one-dimensional density of states of the (775)B QWRs. In the case of the (775)B QWR lasers, the one-dimensionality of the (775)B QWRs in the active region is enhanced by decreasing the well width, as a result,

higher optical gain is achieved. The other one is by the (775)B-oriented surface itself. The (775)B surface is oriented only 8.5°-off from the (111)B surface, and it has been reported that optical gain of QW reaches maximum for the (111)-oriented surface[62,63]. Hence, it can be expected that the similar effect occurs for the (775)B QWR lasers. It can be considered that the significant improvement of $I_{\rm th}$ for the 2.7-nm and 3.6-nm (775)B QWR lasers is probably due to these two causes.

Some QWR lasers have been reported, e.g., the V-groove QWR laser[19,26], the T-shaped QWR laser[72], the fractional superlattice QWR laser[73]. However, almost QWR lasers except the V-groove QWR laser[19,26] oscillated only at low temperatures below 200 K, not at RT. The V-groove QWR laser oscillated at RT under a condition of pulsed current, and the threshold current density ($J_{\rm th}$) was as low as 1 kA/cm^2, which is the best data for QWR lasers ever reported to the author's knowledge[19,26]. On the other hand, the (775)B QWR laser with $L_{\rm w}$ of 2.7 nm, which showed a good one-dimensionality in PL properties, was the first one for self-organized QWRs to oscillate at RT. The minimum $I_{\rm th}$ (70 mA) of the (775)B QWR laser with $L_{\rm w}$ of 2.7 nm is equal to $J_{\rm th}$ of 2.8 kA/cm^2, which was derived directly from the are of the electrode stripe (250 μm$\times$10 μm).

It should be noted that emissions from the (775)B QWR lasers would occur with the transition between the lowest electron subband and the lowest light-hole like subband due to the lateral confinement of carriers, because the stripe geometry was in the $[1\bar{1}0]$ direction. It is clear that this point reduced the performance of the (775)B QWR lasers a little (see the calculated results in Section 5.3). Hence, it can be considered that the performance of the (775)B QWR lasers will be further improved by changing the stripe geometry direction to be perpendicular to the QWRs. In this case, however, cleaved surfaces cannot be used as Fabry-Perot mirrors, and chemically etched mirrors should be used.

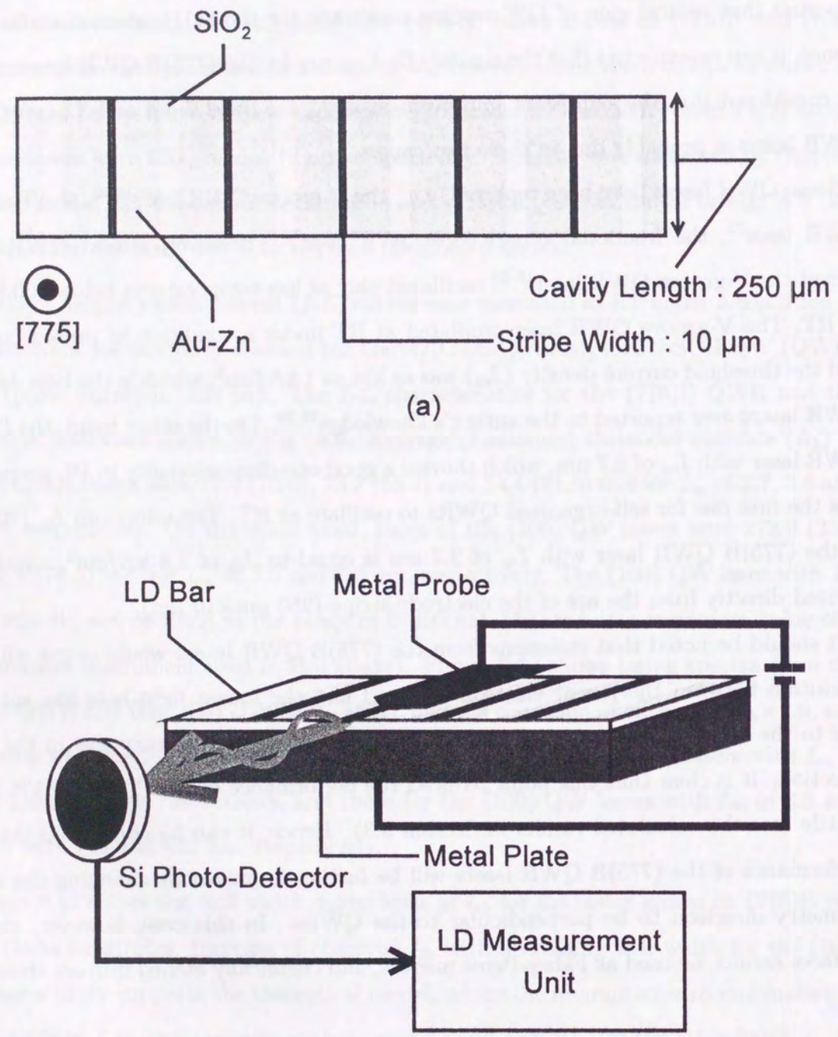

Figure 8.8: Schematic illustrations of (a) stripe-geometry GRIN-SCH lasers and (b) a measurement method. The bar contains several decades of laser tip.

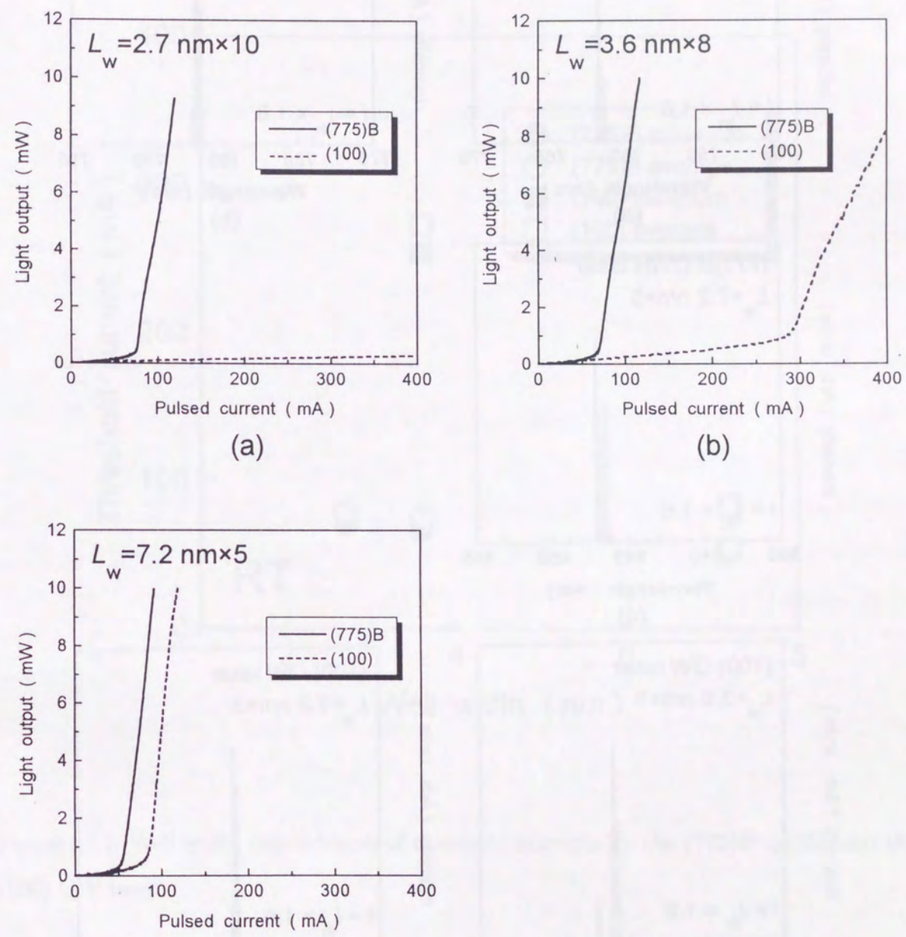

Figure 8.9: *I*-*L* curves of the (775)B QWR and the (100) QW GRIN-SCH lasers with (a) L_w=2.7 nm×10, (b) L_w=3.6 nm×8 and (c) L_w=7.2 nm×5.

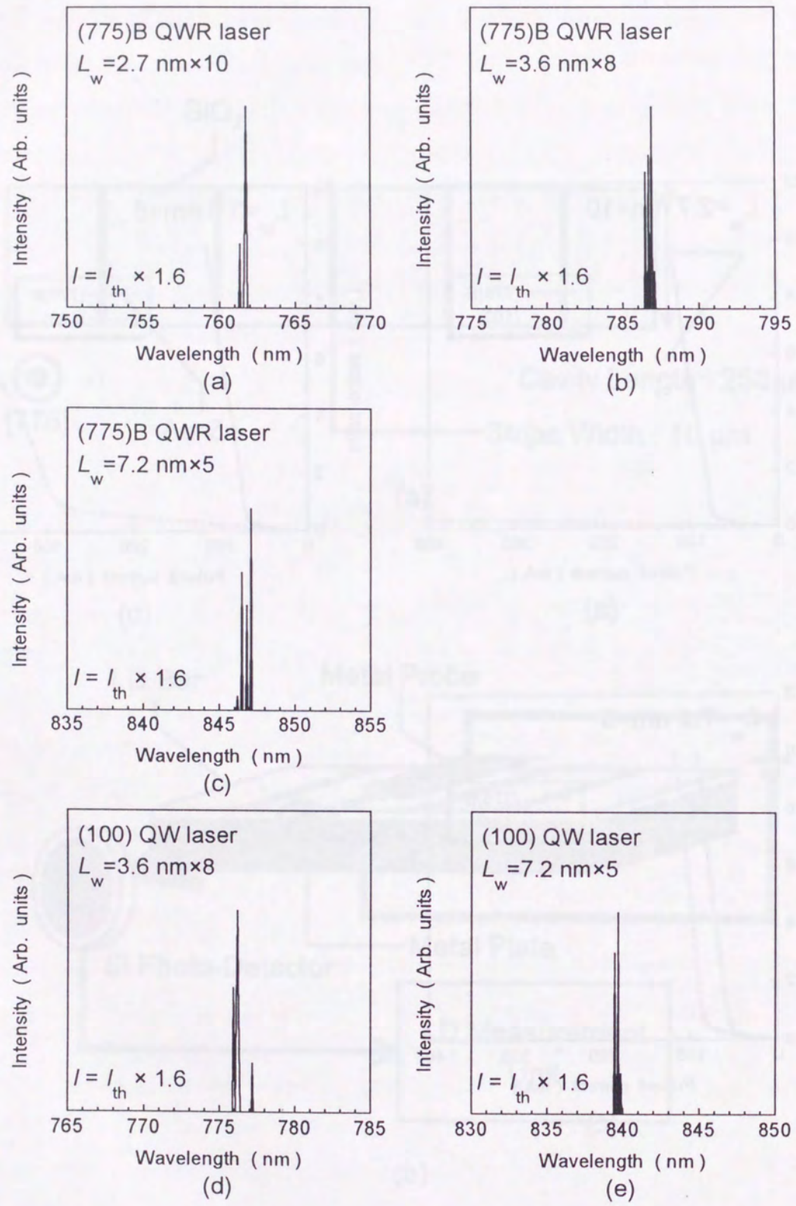

Figure 8.10: Lasing spectra from the (775)B QWR and the (100) QW lasers. (a) (775)B QWR laser; L_w=2.7 nm×10, (b) (775)B QWR laser; L_w=3.6 nm×8, (c) (775)B QWR laser; L_w=7.2 nm×5, (d) (100) QW laser; L_w=3.6 nm×8 and (e) (100) QW laser; L_w=7.2 nm×5.

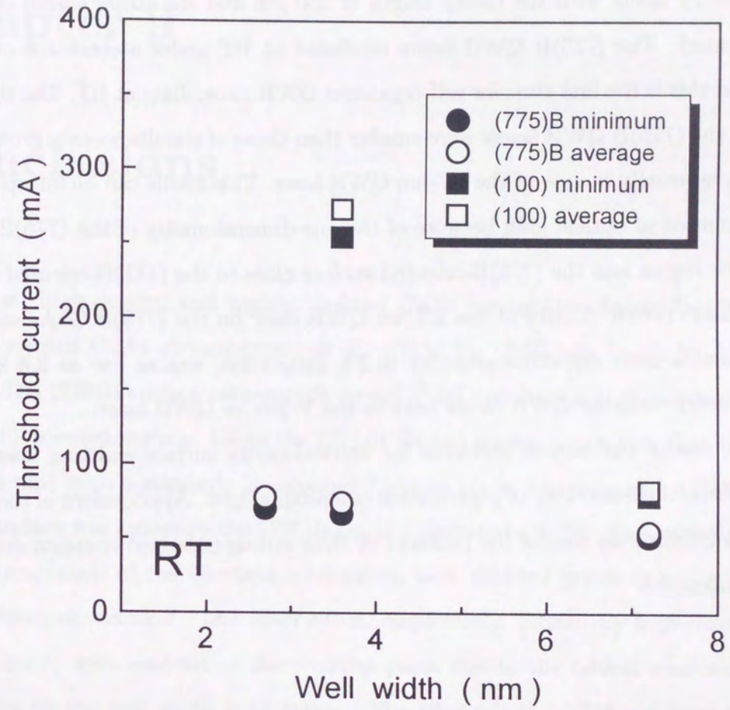

Figure 8.11: Well width dependences of threshold currents for the (775)B QWRs and the (100) QW lasers.

8.6 Summary

GaAs/$(GaAs)_4(AlAs)_2$ GRIN-SCH QWR (QW) laser structures with L_w of 2.7 nm×10, 3.6 nm×8 and 7.2 nm×5 were grown on (775)B and (100) GaAs substrates by MBE, and stripe-geometry lasers with the cavity length of 250 μm and the stripe length of 10 μm were fabricated. The (775)B QWR lasers oscillated at RT under a condition of pulsed current, and this is the first time for self-organized QWR to oscillate at RT. The threshold currents of the (775)B QWR lasers were smaller than those of simultaneously grown (100) QW lasers, especially in case of the 2.7-nm QWR laser. This result can be interpreted by the enhancement of optical gain because of the one-dimensionality of the (775)B QWRs in the active region and the (775)B-oriented surface close to the (111)B-oriented surface. The threshold current density of the 2.7-nm QWR laser on the (775)B GaAs substrate, which showed a good one-dimensionality in PL properties, was as low as 2.8 kA/cm^2, which is a good value for QWR lasers next to the V-groove QWR laser.

Recently, one of the largest problems for vertical-cavity surface emitting lasers (VCSELs) has been the instability of polarization of emitting light. Applications of the (775)B QWRs to VCSELs may resolve the problem by their strong polarized emission due to the lateral confinement.

Chapter 9

Conclusions

At first, high-density and highly uniform GaAs corrugation naturally formed on a (775)B-oriented GaAs surface grown at T_s=670°C by MBE was found by AFM observation. The (775)B surface corresponds to a 8.5°-off one from a (111)B-oriented surface to a (110)-oriented surface. Using the (775)B GaAs corrugation, a thin GaAs/AlAs QW (L_w=3.3 nm) with a regularly corrugated AlAs-on-GaAs interface and a flat GaAs-on-AlAs interface was grown on the (775)B GaAs substrate by MBE. The lateral period and vertical amplitude of the interface corrugation were decided precisely to be 12 nm and 1.2 nm by cross-sectional TEM observation, respectively. Extremely high-density QWRs (8×10^5 cm^{-1}) were realized at the roof-top parts due to the lateral confinement effect of carriers by the well width modulation. The PL peak at λ=715 nm from the (775)B GaAs/AlAs QWRs with a cross section of about 12×3 nm^2 showed a polarization degree of $P = (I_{\parallel} - I_{\perp})/(I_{\parallel} + I_{\perp})$=0.11 and a very small FWHM of 15 meV at 4.2 K.

Next, surface morphologies of GaAs and AlAs layers grown on (775)B GaAs substrates by MBE were studied in detail using AFM. It was found in this study that the (775)B GaAs surface is flat for $T_s \leq$580°C but is corrugated for $T_s \geq$640°C in contrast with a flat surface observed for AlAs layers grown at T_s=540–700°C. Furthermore, the flat GaAs surface grown at T_s=550°C becomes corrugated by thermal annealing at T_s=640°C under As_4 atmosphere (10^{-6} Torr) for one minute. In the early stage of GaAs growth (a layer thickness of less than 5 nm), shapes of the surface corrugation are almost the same. As the thickness of the GaAs layer increases, both the lateral period and step heights of

the corrugation increase and saturate for $d_{GaAs} \geq 200$ nm. Using the corrugated GaAs surfaces grown at T_s=640°C and the flat GaAs and AlAs surfaces grown at T_s=580°C, the GaAs/$(GaAs)_5(AlAs)_5$ QW with a corrugated AlAs-on-GaAs interface and a flat AlAs-on-GaAs lower interface like the GaAs/AlAs QWRs was grown on the (775)B GaAs substrate. Cross-sectional TEM observation indicated that the lateral period and step heights of the AlAs-on-GaAs interface corrugation were 12 nm and 1.2 nm, respectively, and that GaAs QWRs can be fabricated even with the modification of barrier layers from AlAs to $(GaAs)_5(AlAs)_5$ short-period superlattice.

Following the GaAs/$(GaAs)_5(AlAs)_5$ QWRs, GaAs/$(GaAs)_2(AlAs)_2$ QWRs naturally formed in a thin GaAs/$(GaAs)_2(AlAs)_2$ QW with a regularly corrugated AlAs-on-GaAs upper interface were grown on the (775)B GaAs substrate by MBE for optical investigation. The PL peak at λ=670 nm from the QWRs formed in the QW with an average well width of 2.1 nm, which had a cross section of about 12×2 nm^2, showed a strong polarization dependence ($P = 0.21$). The observed degree of polarization was about twice as large as that ($P = 0.11$) from the GaAs/AlAs QWRs, indicating much enhancement of one-dimensionality of the GaAs/$(GaAs)_2(AlAs)_2$ QWRs. Moreover, theoretical analysis was done about optical properties of the (775)B GaAs/$(GaAs)_2(AlAs)_2$ QWRs by the finite element method under the collaboration of Assoc. Prof. M. Ogawa in Kobe University. The calculated results were in good agreement with the experimental results and suggested high performance of the (775)B QWR lasers.

The GaAs/$(GaAs)_2(AlAs)_2$ QWRs had two problems, which were (1) large PL FWHM, that is, low uniformity in size and (2) too high barrier potential for laser application. Then, GaAs/$(GaAs)_4(AlAs)_2$ QWRs formed in a thin GaAs/$(GaAs)_4(AlAs)_2$ QW with a L_w of 2.1 nm were grown, which had suitable barrier height for lasers. The uniformity was much improved by the new growth technique using growth interruption. The PL peak from the QWRs at 14 K showed large polarization anisotropy ($P = 0.19$). FWHM of the PL peak was as small as 15 meV at the short wavelength of λ=692 nm, which is the smallest ever reported for self-organized GaAs/AlGaAs QWRs. Uniformity of the present (775)B QWRs became comparable to the best uniformity for GaAs/AlGaAs QWRs on V-grooves[43, 44], GaAs/AlGaAs T-QWRs[28, 45, 46] and GaAs/AlGaAs tilted T-QWRs[47] fabricated with the

most precise controllability and high uniformity of MBE and MOCVD. The PL intensity from the (775)B QWRs was almost as large as that from a GaAs/$(GaAs)_4(AlAs)_2$ QW grown on a (100) GaAs substrate simultaneously. Then, the one-dimensionality of the GaAs/$(GaAs)_4(AlAs)_2$ QWRs was confirmed not only by the PL polarization dependence but also by other PL results. With increasing temperature in the range of $T \geq 60$ K, the PL intensity of the (775)B GaAs/$(GaAs)_4(AlAs)_2$ QWRs decreased more slowly, and it was several times larger than that of the GaAs/$(GaAs)_4(AlAs)_2$ QW simultaneously grown on the (100) GaAs substrate, indicating the reduction of the nonradiative decay process of exicitons in the (775)B QWRs. The FWHM of the PL peak from the (775)B QWRs was almost independent of temperature above 60 K, while that of the (100) QW increased in proportion to 1.19 k_BT in the range of $T \geq 50$ K. These results are in good agreement with the theoretical expectation that a FWHM of a PL peak from a QW increases in proportion to k_BT because of its two-dimensional density of states, while that of a QWR is almost independent of temperature due to its sharp one-dimensional density of states. Moreover, the temperature dependence of PL decay time was studied. The PL decay time of the (775)B QWRs was 430 ps at 18 K, which was about 20 % longer than that (360 ps) of the (100) QW, indicating the more decreased coherence length of excitons in the (775)B QWRs than that in the (100) QW. The decay time of the (775)B QWRs, however, increased more slowly with increasing temperature, and it became shorter than that of the (100) QW at 50 K, which is due to their sharp one-dimensional density of states of the (775)B QWRs. In the range of 70–80 K, the decay time of the (775)B QWRs was longer than that of the (100) QW, implying that the nonradiative decay process of exicitons in the (775)B QWRs was more reduced than that in the (100) QW due to the one-dimensional density of states. Such apparently different behavior of the PL decay time of the (775)B QWRs compared with the (100) QW also suggests good one-dimensional properties of the (775)B QWRs. These PL results prove that the GaAs/$(GaAs)_4(AlAs)_2$ QWRs on the (775)B GaAs substrate meet requirements for applications to QWR lasers, i.e., high one-dimensionality, high uniformity, high density, high optical quality and simple fabrication process.

Growth modes of GaAs layers on high-index GaAs substrates around a (775)B plane

were studied to search the best substrate orientation for the fabrication of QWRs. Surfaces of GaAs layers grown on all high-index GaAs substrates were flat for T_s=580°C. At T_s=650°C, corrugation was observed on surfaces of GaAs layers grown on (776)B, (775)B and (332)B substrates, and (553)B and (221)B surfaces were flat. These results indicate that GaAs QWRs like the (775)B GaAs/$(GaAs)_4(AlAs)_2$ QWRs can also be grown on (776)B and (332)B GaAs substrates. Among GaAs/$(GaAs)_4(AlAs)_2$ QWs (QWRs) grown on the high-index GaAs substrates, PL FWHMs of (775)B QWRs and (221)B QWs showed the smallest value. Therefore, (775)B GaAs substrates is concluded to be the most suitable for fabrication of QWRs in the point of uniformity.

Finally, GaAs/$(GaAs)_4(AlAs)_2$ GRIN-SCH QWR lasers were grown on (775)B GaAs substrates by MBE, and stripe-geometry lasers with the cavity length of 250 μm and the stripe length of 10 μm were fabricated. The (775)B QWR lasers oscillated at room temperature (RT) under a condition of pulsed current, and laser operation at RT has been achieved for the first time in this study of the (775)B GaAs/$(GaAs)_4(AlAs)_2$ QWRs for self-organized QWRs. The threshold currents of the (775)B QWR lasers were smaller than those of the (100) QW lasers, especially in case of the 2.7-nm lasers. This result can be interpreted by the enhancement of optical gain because of the one-dimensionality of the (775)B QWRs in the active region and the (775)B surface close to the (111)B surface. The threshold current density of the (775)B QWR laser with a L_w of 2.7 nm which had a good one-dimensionality was as low as 2.8 kA/cm^2, which is a good result for QWR lasers next to the V-groove QWR laser[19,26].

It was succeeded to fabricate high-density and highly uniform GaAs QWRs on (775)B GaAs substrates by MBE. The (775)B QWRs are considered to have extremely high potential for applications to optical devices.

Acknowledgement

The author would like to express the sincerest gratitude to Professor Satoshi Hiyamizu for the thoughtful guidance, the encouragement, helpful discussions, critical reading, and amendment of manuscripts. He would like to express his deep thanks to Associate Professor Satoshi Shimomura and Dr. Nobuyuki Tomita for the helpful discussions and the warm encouragement. He also would like to express his thanks to Mr. Takahiro Kitada for the discussions.

Contribution of Mr. Masanori Yamamoto was especially indispensable to accomplish this work, hence the author would like to express special thanks to him. His thanks are also given to all collaborators, Mr. Hidenori Morimoto, Mr. Ryouhei Kuriyama and Mr. Yasuhide Ohno in Hiyamizu Laboratory for their assistance on experiments, and Mr. Takahiro Higuchi, Mr. Yasuhiro Morimoto and Ms. Masami Honda in Kwansei-Gakuin University for their cooperation on the TEM observation.

All members in Hiyamizu Laboratory are thanked for their help and supportive atmosphere. Especially, he wishes to thank Mr. Keisuke Shinohara for the interesting discussions. He also would like to express his deep thanks to Mrs. Ikuko Uchida for her various supports and to friends in Department of Material Physics for their kind encouragement.

He would like to express his special thanks to Professor Naokatsu Sano in Kwansei-Gakuin University for helpful discussions on the TEM measurements, and to Associate Professor Masato Ogawa and Professor Tanroku Miyoshi in Kobe University for their theoretical investigation and discussions. He is grateful to Mr. Yasunori Okamoto, Mr. Shin-ya Tsujikura and Mr. Seiji Ikawa in KUBOTA Corporation for permission to use a PL system and their cooperation to the fabrication process of QWR lasers. He is also

grateful to Dr. Kazuyoshi Kuroyanagi, Dr. Kazuhisa Fujita and Dr. Norihumi Egami in ATR Adaptive Communications Research Laboratories for permission to use a time-resolved PL system.

This work was supported in part by a Grant-in-Aid for Science Research on Priority Area, 'Quantum Coherent Electronics' from the Ministry of Education, Science, Sports and Culture, by The Mitsubishi Foundation and by a Grant-in-Aid for Scientific Research (B) from Ministry of Education, Science, Sports and Culture.

He wishes especially to thank Professor Hisao Nakashima and Professor Hiroshi Yoshida for their critical reading of the manuscript.

Finally, he would like to express thanks to his family.

References

[1] R. Dingle, H. L. Stormer, A. C. Gossard and W. Wiegmann, Appl. Phys. Lett. **33**, 665 (1978),

[2] T. Mimura, S. Hiyamizu, T. Fujii and K. Nanbu, Jpn. J. Appl. Phys., *Part 2* **19**, 225 (1980).

[3] L. L. Chang, L. Esaki and T. Tsu, Appl. Phys. Lett. **24**, 593 (1974).

[4] T. C. L. G. Sollner, W. D. Goodhue, P. E. Tannenwald, C. D. Parker and D. D. Peck, Appl. Phys. Lett. **43**, 588 (1983).

[5] J. P. van der Ziel, R. Dingle, R. C. Miller, W. Wiegmann and W. A. Nordland, Appl. Phys. Lett. **26**, 463 (1975).

[6] N. Holonyak, R. M. Koldas, R. D. Dupuis and P. D. Dapkus, IEEE J. Quantum Electron., 170 (1980).

[7] W. T. Tsang, Appl. Phys. Lett. **39**, 786 (1981).

[8] H. Sakaki, Jpn. J. Appl. Phys., *Part 2* **19**, 735 (1980).

[9] Y. Arakawa and H. Sakaki, Appl. Phys. Lett. **40**, 939 (1982).

[10] Y. Arakawa, K. Vahala and A. Yariv, Appl. Phys. Lett. **45**, 950 (1984).

[11] M. Asada, M. Miyamoto and Y. Suematsu, Jpn. J. Appl. Phys. *Part 2* **24**, 95 (1985).

[12] Y. Arakawa, K. Vahala and A. Yariv, Surf. Sci. **174**, 155 (1986).

[13] Y. Arakawa and A. Yariv, IEEE J. Quantum Electron., **QE-22**, 1887 (1986).

[14] A. Yariv, Appl. Phys. Lett. **53**, 1033 (1988).

[15] M. H. Degani and O. Hipolito, Phys. Rev. B **35**, 9345 (1987).

[16] L. Báyai, I. Galbaith, C. Ell, and Hang, Phys. Rev. B **36**, 6099 (1987).

[17] S. Schmitt-Rink, D. A. B. Miller, and D. S. Chemla, Phys. Rev. B **35**, 8113 (1987).

[18] K. Y. Lau, N. Bar-Chaim, I. Ury, C. Harder and A. Yariv, Appl. Phys. Lett. **43** 1 (1983).

[19] E. Kapon, OPTOELECTRONICS Devices and Technologies **8**, 429 (1993).

[20] P. M. Petroff, A. C. Gossard, R. A. Logan and W. Wiegmann, Appl. Phys. Lett. **41**, 635 (1984).

[21] A. C. Gossard, J. H. English, P. M. Petroff, J. Clibert, G. J. Dolan and S. J. Pearton, J. Cryst. Growth **81**, 101 (1987).

[22] Y. Nakamura, M. Tsuchiya, S. Koshiba, H. Noge, H. Kano and H. Sakaki, Jpn. J. Appl. Phys., *Part 1* **32**, 383 (1993).

[23] S. Koshiba, H. Noge, H. Akiyama, T. Inoshita, Y. Nakamura, A. Shimizu, Y. Nagamune, M. Tsuchiya, H. Kano, H. Sakaki and K. Wada, Appl. Phys. Lett. **64**, 363 (1994).

[24] Y. Liu, N. Yamamoto, Y. Nishimoto, N. Kamikubo, S. Shimomura, K. Gamo, K. Murase, N. Sano, A. Adachi, K. Fujita, T. Watanabe and S. Hiyamizu, J. Cryst. Growth **150**, 299 (1995).

[25] N. Tomita, T. Kishi, K. Takekawa, K. Fujita, T. Watanabe, A. Adachi, S. Shimomura and S. Hiyamizu, J. Cryst, Growth **175/176**, 809 (1997).

[26] E. Kapon, D. M. Hwang and R. Bhat, Phys. Rev. Lett. **63**, 430 (1989).

[27] X. L. Wang, M. Ogura and H. Matsuhata, Appl. Phys. Lett. **67**, 804 (1995).

[28] W. Wegscheider, L. N. Pfeiffer, M. M. Dignam, A. Pinczuk, K. W. West S. L. McCall and R. Hull, Phys. Rev. Lett. **71**, 4071 (1993).

[29] T. Fukui and H. Saito, J. Vac. Sci. Technol. **B6**, 1373 (1988).

[30] H. Weman, M. S. Miller, C. E. Pryor, Y. J. Li, P. Bergman, P. M. Petroff and L. J. Mertz, Phys. Rev. B **46**, 8047 (1993).

[31] M. Takeuchi, T. Takeuchi, Y. Inoue, T. Kato, K. Inoue, H. Nakashima, K. Maehashi, P. Fischer, J. Christen, M. Grundmann and D. Bimberg, Superlattices and Microstructures **22**, 43 (1997).

[32] S. Hara, J. Motohisa, T. Fukui and H. Hasegawa, Jpn. J. Appl. Phys., *Part 1* **34**, 4401 (1995).

[33] R. Nötzel, N. N. Ledentsov, L. Däweritz, K. Ploog and M. Hohenstein, Phys. Rev. B **45**, 3507 (1992).

[34] S. Shimomura, A. Wakejima, A. Adachi, Y. Okamoto, N. Sano, K. Murase and S. Hiyamizu, Jpn. J. Appl. Phys., *Part 2* **32**, 1728 (1993).

[35] S. Shimomura, K. Shinohara, T. Kitada, Y. Tsuda, A. Adachi, Y. Okamoto, N. Sano and S. Hiyamizu, J. Vac. Sci. Technol. **B13**, 696 (1995).

[36] M. Ogawa, S. Fukushima, M. Itoh, T. Miyoshi, M. Higashiwaki and S. Hiyamizu, to be published in Physica B (1998).

[37] M. Ogawa, M. Itoh and T. Miyoshi, Physica B **227**, 65 (1996).

[38] J. Ishizaki, K. Ohkuri and T. Fukui, Jpn. J. Appl. Phys., *Part 1* **35**, 1280 (1996).

[39] M. Kasu and T. Fukui, Jpn. J. Appl. Phys., *Part 1* **31**, 864 (1992).

[40] R. L. Schwoebel, J. Appl. Phys. **40**, 614 (1969).

[41] K. Ohkuri, J. Ishizaki, S. Hara and T. Fukui, J. Cryst. Growth **160**, 235 (1996).

[42] K. Brunner, G. Abstreiter, G. Böhm, G. Tränkle and G. Weimann, Appl. Phys, Lett. **64**, 3320 (1994).

[43] J. Christen, E. Kapon, E. Colas, D. M. Hwang, L. M. Schiavone, M. Grundmann and D. Bimberg, Surf. Sci. **267**, 257 (1992).

[44] X. L. Wang, M. Ogura and H. Matsuhata, Appl. Phys. Lett. **67**, 3629 (1995).

[45] T. Someya, H. Akiyama and H. Sakaki, Phys. Rev. Lett. **74**, 3664 (1995).

[46] T. Someya, H. Akiyama and H. Sakaki, Appl. Phys. Lett. **66**, 3672 (1995).

[47] N. Tomita, K. Takekawa, K. Ohta, K. Fujita, N. Egami, Y. Okamoto, S. Shimomura and S. Hiyamizu, to be published in J. Vac. Sci. Technol. B (1998).

[48] M. Tanaka, H. Sakaki, J. Yoshino and T. Furuta, Surf. Sci. **174**, 65 (1986).

[49] D. S. Jiang, H. Jung and K. Ploog, J. Appl. Phys. **64**, 1371 (1988).

[50] D. Moroni, J. P. Andre, E. P. Menu, Ph. Gentric and J. N. Patillon, J. Appl. Phys. **62**, 2003 (1987).

[51] D. S. Citrin, Phys. Rev. Lett. **69**, 3393 (1992).

[52] D. Gershoni, M. Katz, W. Wegscheider, L. N. Pfeiffer, R. A. Logan and K. West, Phys. Rev. B, **50**, 8930 (1994).

[53] H. Akiyama, S. Koshiba, T. Someya, K. Wada, Y. Nakayama, T. Inoshita, A. Shimizu and H. Sakaki, Phys. Rev. Lett. **72**, 924 (1994).

[54] H. Weman, C. I. Harris, J. P. Bergman, M. S. Miller, J. C. Yi, and J. L. Merz, Superlattices and Microstructures **17**, 61 (1995).

[55] L. C. Andreani, Solid State Commun. **77**, 641 (1991).

[56] D. S. Citrin, Solid State Commun. **84**, 281 (1992); Phys. Rev. B, **47**, 3832 (1993).

[57] L. C. Andreani and F. Bassani, Phys. Rev. B **41**, 7536 (1990).

[58] M. Shigeta, Y. Okano, H. Seto, H. Katahama, S. Nishine and K. Kobayashi, J. Cryst. Growth **111**, 284 (1991).

[59] K. Agawa, Y. Hashimoto, K. Hirakawa, N. Sakamoto and T. Ikoma, IEICE Trans. Electron. **E77-C9**, 1408 (1994).

[60] K. Shinohara, T. Motokawa, K. Kasahara, S. Shimomura, N. Sano, A. Adachi, and S. Hiyamizu, Semicond. Sci. & Technol. **11**, 125 (1996).

[61] T. Ohtoshi, T. Kuroda, A. Niwa and S. Tsuji, Appl. Phys. Lett. **65**, 1886 (1994).

[62] T. Hayakawa, K. Takahashi, M. Kondo, T. Suyama, S. Yamamoto and T. Hijikata, Phys. Rev. Lett. **60**, 349, (1988).

[63] T. Hayakawa, T. Suyama, K. Takahashi, M. Kondo, S. Yamamoto and T. Hijikata, Appl. Phys. Lett. **52**, 339 (1988).

[64] D. Vakhshoori, J. Appl. Phys. **70**, 5205 (1991).

[65] D. Vakhshoori, R. J. Fischer, M. Hong, D. L. Sivco, G. J. Zydzik, G. N. S. Chu and A. Y. Cho, Appl. Phys. Lett. **59**, 896 (1991).

[66] H. Imamoto, F. Sato, K. Imanaka and M. Shimura, Appl. Phys. Lett. **55**, 115 (1989).

[67] D. K. Biegelsen, R. D. Bringans, J. E. Northrup and L. E. Swartz, Phys. Rev. Lett. **65**, 452 (1990).

[68] T. Hayakawa, M. Morishima, M. Nagai, H. Horie and K. Matsumoto, Surf. Sci. **267**, 8 (1992).

[69] T. Yamamoto, M. Inai, T. Takabe, M. Fujii and K. Kobayashi, J. Cryst. Growth **127**, 865 (1993).

[70] H. Iwata, H. Yokoyama, M. Sugimoto and H. Hamao, Appl. Phys. Lett. **54**, 2427 (1989).

[71] A. Sugimura, IEEE J. Quantum Electron. **QE-20**, 336 (1984).

[72] W. Wegscheider, L. N. Pfeiffer, A. Pinczuk, K. W. West, M. M. Dignam, R. Hull and R. E. Leibenguth, J. Cryst. Growth **150**, 285 (1995).

[73] H. Saito, K. Uwai and N. Kobayashi, Jpn. J. Appl. Phys. **32**, 4440 (1993).

[74] C. Weisbuch, R. Dingle, A. C. Gossard and W. Wiegmann, Solid State Commun. **38**, 709 (1981).

[75] L. Goldstein, Y. Horikoshi, S. Tarucha and H. Okamoto, Jpn. J. Appl. Phys., *Part 1* **22**, 1489 (1983).

[76] M. Asada, A. Kameyama and Y. Suematsu, IEEE J. Quantum Electron. **QE-20**, 745 (1984).

[77] M. Yamanishi and I. Suemune, Jpn. J. Appl. Phys. **23**, 35 (1984).

[78] C. R. McIntyre and L. J. Sham, Phys. Rev. B **45**, 9443 (1992).

[79] E. O. Kane, J. Phys. Chem. Solids **1**, 82 (1956).

[80] E. O. Kane, J. Phys. Chem. Solids **1**, 249 (1957).

Publication list

Publications

[1] "Low temperature etching of GaAs-substrates and improved morphology of GaAs grown by MOMBE using TDMAAs and TEG."
D. Marx, H. Asahi, X. F. Liu, M. Higashiwaki, A. B. Villaflor, K. Miki, K. Yamamoto, S. Gonda, S. Shimomura and S. Hiyamizu
Journal of Crystal Growth **150**, 551 (1995).

[2] "High-density GaAs/AlAs quantum wires grown on (775)B-oriented GaAs substrates by molecular beam epitaxy."
M. Higashiwaki, M. Yamamoto, T. Higuchi, S. Shimomura, Y. Okamoto, N. Sano and S. Hiyamizu,
Japanese Journal of Applied Physics, *Part 2* **35**, 606 (1996).

[3] "High-density GaAs/$(GaAs)_2(AlAs)_2$ quantum wires naturally formed on (775)B-oriented GaAs substrates by molecular beam epitaxy."
M. Higashiwaki, M. Yamamoto, S. Shimomura and S. Hiyamizu,
Journal of Crystal Growth **175/176**, 814 (1997).

[4] "Highly uniform and high-density GaAs/$(GaAs)_4(AlAs)_2$ quantum wires grown on (775)B-oriented GaAs substrates by molecular beam epitaxy."
M. Higashiwaki, M. Yamamoto, S. Shimomura and S. Hiyamizu,
Applied Physics Letters **71**, 2005 (1997).

[5] "Surface corrugation of GaAs layers grown on (775)B-oriented GaAs substrates by molecular beam epitaxy."
M. Yamamoto, M. Higashiwaki, S. Shimomura, N. Sano and S. Hiyamizu,
Japanese Journal of Applied Physics, *Part 1* **36**, 6285 (1997).

[6] "High-density $In_{0.14}Ga_{0.86}As/(GaAs)_5(AlAs)_5$ quantum wires naturally formed on (775)B-oriented GaAs substrates by molecular beam epitaxy."
S. Hiyamizu, M. Higashiwaki, M. Yamamoto and S. Shimomura,
to be published in Materials Science and Engineering B (1998).

[7] "Temperature dependence of photoluminescence from high-density $GaAs/(GaAs)_4(AlAs)_2$ quantum wires grown on (775)B-oriented GaAs substrates by molecular beam epitaxy."
M. Higashiwaki, S. Shimomura and S. Hiyamizu,
to be published in Physica B (1998).

[8] "Temperature dependence of exciton lifetimes in high-density $GaAs/(GaAs)_4(AlAs)_2$ quantum wires grown on (775)B-oriented GaAs substrates by molecular beam epitaxy"
M. Higashiwaki, K. Kuroyanagi, K. Fujita, N. Egami, S. Shimomura and S. Hiyamizu,
to be published in Solid State Electronics (1998).

[9] "Analysis of optical properties of corrugated quantum wire structure fabricated on (775)B GaAs surface."
M. Ogawa, S. Fukushima, M. Itoh, T. Miyoshi, M. Higashiwaki and S. Hiyamizu,
to be published in Physica B (1998).

International conferences and workshops

[1] "Low temperature etching of GaAs-substrates and improved morphology of GaAs grown by MOMBE using TDMAAs and TEG."
D. Marx, H. Asahi, X. F. Liu, M. Higashiwaki, A. B. Villaflor, K. Miki, K. Yamamoto, S. Gonda, S. Shimomura and S. Hiyamizu
8th International Conference on Molecular Beam Epitaxy (MBE-VIII),
Osaka, JAPAN, August (1994).

[2] "High-density $GaAs/(GaAs)_2(AlAs)_2$ quantum wires naturally formed on (775)B-oriented GaAs substrates by molecular beam epitaxy."
M. Higashiwaki, M. Yamamoto, S. Shimomura and S. Hiyamizu,
9th International Conference on Molecular Beam Epitaxy (MBE-IX),
Malibu, USA, August (1996).

[3] "High-density $In_{0.14}Ga_{0.86}As/(GaAs)_5(AlAs)_5$ quantum wires naturally formed on (775)B-oriented GaAs substrates by molecular beam epitaxy."
S. Hiyamizu, M. Higashiwaki, M. Yamamoto and S. Shimomura,
2nd International Conference on Low Dimensional Structures and Devices (LDSD97),
Lisbon, PORTUGAL, May (1997).

[4] "Temperature dependence of photoluminescence from high-density $GaAs/(GaAs)_4(AlAs)_2$ quantum wires grown on (775)B-oriented GaAs substrates by molecular beam epitaxy."
M. Higashiwaki, S. Shimomura and S. Hiyamizu,
8th International Conferenece on Modulated Semiconductor Structures (MSS8),
Santa Barbara, USA, July (1997).

[5] "Temperature dependence of exciton lifetimes in high-density $GaAs/(GaAs)_4(AlAs)_2$ quantum wires grown on (775)B-oriented GaAs substrates by molecular beam epitaxy"
M. Higashiwaki, K. Kuroyanagi, K. Fujita, N. Egami, S. Shimomura and S. Hiyamizu,
International Workshop on Nano-Physics and Electronics (NPE97),
Tokyo, JAPAN, September (1997).

[6] "Analysis of optical properties of corrugated quantum wire structure fabricated on (775)B GaAs surface."
M. Ogawa, S. Fukushima, M. Itoh, T. Miyoshi, M. Higashiwaki and S. Hiyamizu,
12th International Conference on Electronic Properties of Two-Dimensional Systems (EP2DS-12),
Tokyo, JAPAN, September (1997).

Appendix A

Detection of size fluctuation from PL linewidth

In practical heterostructures grown by MBE, it is impossible to fabricate flat interfaces perfectly, that is, the interfaces involve fluctuations in the scale of one or a few monolayer (ML). These fluctuations influence PL spectra[74, 75]. In case of GaAs/AlGaAs heterostructures, the thickness of 1 ML is equivalent to 2.8 Å since the lattice constant a is 5.6 Å, hence the width of QW corresponds to integer times of $a/2$. If there is unevenness points with the height of ΔL_z in a QW with an average well width of L_z, there is an energy distribution in the energy of the subband, which is expressed as,

$$\frac{\pi^2\hbar^2}{\mu}\left(\frac{\Delta L_z}{L_z^3}\right).$$

In case that a size of unevenness is larger than *de Brogie* wavelength of electron, which corresponds to a situation in a QW with growth interruption, some peaks appear in a PL spectrum due to fluctuation of energy as shown in Fig. A.1 (a). On the other hand, in case that the size is smaller than the *de Brogie* wavelength, which corresponds to a situation in a QW without growth interruption, a PL spectrum turns to be a wide one with one peak as shown in Fig. A.1 (b).

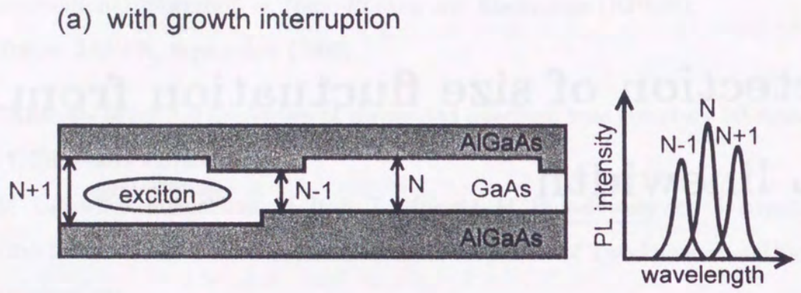

Figure A.1: Effect of interface fluctuation on PL linewidth of QW (a) with and (b) without growth interruption.

Appendix B

Polarization of luminescence from QWR

Here, theoretical studies about polarization of luminescence from a cleaved surface of QW by Asada et al.[76] and Yamanishi et al.[77] are presented. The polarization dependence of luminescence from a QWR surface is the same basically[78].

From the $\boldsymbol{k}\cdot\boldsymbol{p}$ theory, the Bloch base functions $u(\boldsymbol{r})$ for the conduction band and the valence band can be expressed by the s-orbit function $|s\rangle$, the p-orbit functions $|X\rangle$, $|Y\rangle$, $|Z\rangle$ and the spin functions $|\uparrow\rangle$, $|\downarrow\rangle$ as follows[79,80],

$$
\begin{aligned}
&\text{Conduction band} && |s\rangle|\uparrow\rangle, \text{ or } |s\rangle|\downarrow\rangle \\
&\text{Heavy hole band} && \frac{1}{\sqrt{2}}\{|X\rangle + i|Y\rangle\}|\uparrow\rangle \\
& && \frac{1}{\sqrt{2}}\{|X\rangle - i|Y\rangle\}|\downarrow\rangle \\
&\text{Light hole band} && \frac{1}{\sqrt{6}}[\{|X\rangle + i|Y\rangle\}|\downarrow\rangle - 2|Z\rangle|\uparrow\rangle] \\
& && \frac{1}{\sqrt{6}}[\{|X\rangle - i|Y\rangle\}|\uparrow\rangle - 2|Z\rangle|\downarrow\rangle] \ .
\end{aligned}
$$

For the transition between the conduction band and the heavy hole band, the matrix element $\langle u_c^*|\boldsymbol{p}|u_v\rangle$, which is proportional to the matrix element of the dipole moment, is obtained as,

x direction $\quad \dfrac{\sqrt{3}M}{\sqrt{2}}$

y direction $\quad \pm\, i\dfrac{\sqrt{3}M}{\sqrt{2}}$

z direction $\quad 0$,

where

$$\sqrt{3}M = \langle S|p_x|X\rangle = \langle S|p_y|Y\rangle = \langle S|p_z|Z\rangle = \frac{m}{2}\left[\frac{E_g(E_g+\Delta_0)}{m_e^*(E_g+\frac{2}{3}\Delta_0)}\right] .$$

$\sqrt{3}$ is a coefficient to be decided to make a value of the matrix element on the average in all directions of the $\boldsymbol{k}$ vector in bulk crystal equal to M. Here, m is the mass of free electron, m_e^* is the effective mass of electron in the conduction band, E_g is the energy of the band gap and Δ_0 is the energy of the spin-orbit split-off band. Hence, it is clear that the momentum matrix element between the conduction band and the heavy hole band rotates in the plane perpendicular to the $\boldsymbol{k}$ vector.

For the coordinate with the QW layer as the x-y plane and the growth direction as the z axis as shown in Fig. B.1 (a), x-, y- and z-components of the matrix element can be expressed as,

x-component $\quad \dfrac{\sqrt{3}M}{\sqrt{2}}(\cos\theta\cos\phi + i\sin\phi)$

y-component $\quad \dfrac{\sqrt{3}M}{\sqrt{2}}(\cos\theta\sin\phi \pm i\cos\phi)$

z-component $\quad -\left(\dfrac{\sqrt{3}M}{\sqrt{2}}\right)\sin\theta$,

where the $\boldsymbol{k}$ direction is expressed by the latitude θ and the longitude ϕ.

The transition matrix of the optical transition is derived from $\langle u_c^*|\boldsymbol{e}\cdot\boldsymbol{p}|u_v\rangle$, hence components parallel to the electric field vector of light $\boldsymbol{e}$ in the momentum matrix elements contribute to the optical transition. In case of bulk crystal, the factor of 1/3 is obtained as the average of contributions of the momentum matrix elements in all directions since the $\boldsymbol{k}$ vector can be taken in every direction. On the other hand, the range of the $\boldsymbol{k}$ vector in QW is different from that in the bulk crystal due to the quantum confinement, i.e., the component $k_{\|}$ of the $\boldsymbol{k}$ vector in the QW plane can be decided freely, however, the

component k_z in the growth direction can only be obtained as $k_z = (\pi/L_z)\cdot n$, [n=1, 2, 3, $\cdots$]. Therefore, it needs to calculate the average for all ϕ about one subband to obtain the average of the matrix elements concerning the one subband.

In case that the electric vector of light is parallel to the QW plane, the light parallel to the QW plane is called the TE polarized light. Then, the direction of the electric vector is defined as the y-direction, and the average of the second power of the y-component $(\sqrt{3}M/\sqrt{2})\cdot(\cos\theta\sin\phi \pm i\cos\phi)$ of the momentum matrix elements is derived as,

$$\begin{aligned}\langle M^2\rangle_{hh,TE} &= \frac{3M^2}{2}\,\frac{1}{2\pi}\int_0^{2\pi}(\cos^2\theta\sin^2\phi+\cos^2\phi)\,d\phi \\ &= \frac{3M^2}{4}\,(1+\cos^2\theta) \\ &= \frac{3M^2}{4}\,(1+\frac{k_z^2}{k^2}) \\ &= \frac{3M^2}{4}\,(1+\frac{E_{z,n}}{E_n}) ,\end{aligned}$$

where $E_{z,n}$ and E_n are the quantized energy and the whole energy in the subband n, respectively. At the edge of the subband, $E_{z,n}$ equals to E_n, hence,

$$\langle M^2\rangle_{hh,TE} = \frac{3M^2}{2} .$$

For the light with the electric vector perpendicular to the interface of the QW which is called the TM polarized light, as the electric vector is parallel to the z-direction, the average of the second power of y-components $-(\sqrt{3}M/\sqrt{2})\sin\theta$ of the momentum matrix elements is derived as,

$$\begin{aligned}\langle M^2\rangle_{hh,TM} &= \frac{3M^2}{2}\,(\sin^2\theta) \\ &= \frac{3M^2}{2}\,(1-\frac{k_z^2}{k^2}) \\ &= \frac{3M^2}{4}\,(1-\frac{E_{z,n}}{E_n}) .\end{aligned}$$

At the edge of the subband, $E_{z,n}$ equals to E_n, hence,

$$\langle M^2\rangle_{hh,TM} = 0 .$$

Namely, the heavy hole does not respond to the TM polarized light at the subband edge. This fact can be explained as follows. The second power of the base function of the heavy

hole is like a shape of donut as shown in Fig. B.1 (b), moreover, the donut plane is perpendicular to the $\boldsymbol{k}$ vector. Therefore, the donut plane is parallel to the interface of the QW at the subband edge. Hence, it responds to the TE polarized light, however, it does not respond to the TM polarized one.

In case of QWR, the light parallel and perpendicular to the QWR direction correspond to the TE polarized and the TM polarized lights in a QW, respectively, and polarization of luminescence from a QWR surface can be observed. However, it should be noted that there are some effects on QWR due to carrier confinement in two directions, e.g., effects of mixing between heavy hole and light hole bands, the orientation of the sample surface, finite-potential confinement. Therefore, it is not so easy in case of QWR like the case of QW mentioned above, however, the explanation about polarization fits QWR qualitatively, not quantitatively.

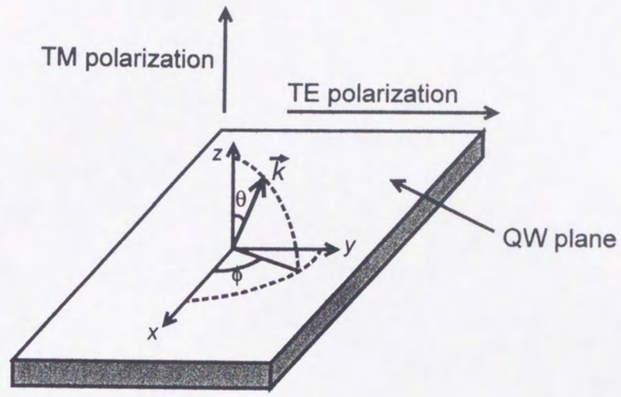

(a)

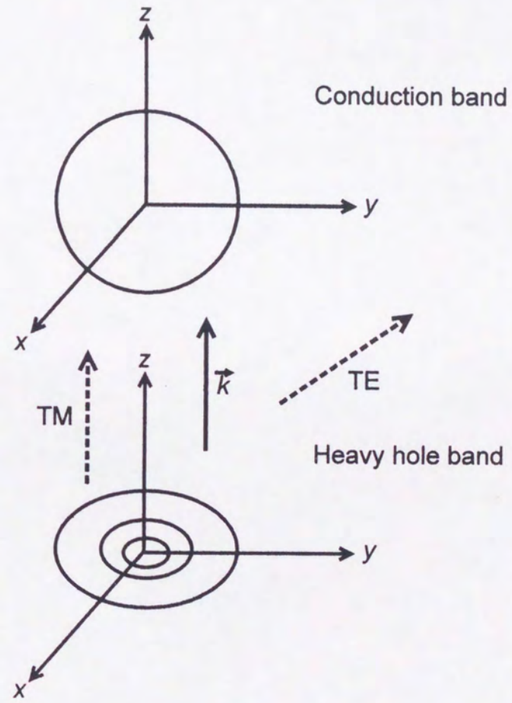

(b)

Figure B.1: (a) the coordinate for analysis of polarization dependence of luminescence and (b) the base wavefunctions.